



Gemini Plus

Research and Innovation Action (RIA)

This project has received funding from the European Union's Horizon 2020 research and innovation programme under grant agreement No 755478.

Start date : 2017-09-01 Duration : 36 Months
<http://gemini-initiative.eu/>



Core design calculations of GEMINI + system

Authors : Dr. Jim KUIJPER (NUCLIC), D. Muszynski (NCBJ)

Gemini Plus - Contract Number: 755478

Project officer: Dr. Panagiotis MANOLATOS

| | |
|---------------------|---|
| Document title | Core design calculations of GEMINI + system |
| Author(s) | Dr. Jim KUIJPER, D. Muszynski (NCBJ) |
| Number of pages | 106 |
| Document type | Deliverable |
| Work Package | WP2 |
| Document number | D2.8 |
| Issued by | NUCLIC |
| Date of completion | 2021-02-24 21:39:57 |
| Dissemination level | Confidential, only for members of the consortium (including the Commission Services). |

Summary

Literally at the heart of the Euratom Horizon 2020 project GEMINI+ are the core neutronics (design) calculations. For these calculations on a relatively small (180 MWth) prismatic HTGR with cylindrical core, the 3-D monte-carlo particle transport and depletion code SERPENT version 2 (VTT, Finland) was selected, the main reasons being the flexibility and versatility of this code. This enables the modelling of all relevant details of the reactor without unnecessary approximations. A particularly useful feature of the SERPENT code is the multi-physics input capability. This allows to map a temperature field over the defined geometry, enabling the calculation of converged power and temperature distribution by means of iteration and data exchange between SERPENT and a (steady-state) thermal- hydraulics code. In this particular case the SPECTRA code (NRG, The Netherlands) was used to provide the temperature distribution. 4 to 5 iterations are sufficient to reach simultaneously converged distributions for power and temperature. This report -Deliverable D2.8- consists of 4 more or less independent parts (A - D) on neutronics, depletion and activation calculations and an additional part (E) concerning review and update. Part A gives an overview of the performed analyses for the latest (June 2020) 11- core layer design of the GEMINI+ HTGR, and results thereof. Neutronics features seem quite promising, but further improvements and therefore further investigations would be desirable. Part B shows results of neutronics analyses of an earlier, 10-core layer version of the GEMINI+ HTGR. Part C provides some additional information concerning the (preliminary) fuel design. Part D concerns the activation of the replaceable and permanent reflectors, and the core barrel and pressure vessel, during some operation cycles of 550 days, but also during the 30 to 60 years lifetime of the reactor. Finally, Part E contains the responses from the authors to the review comments on the draft version of this report.

Approval

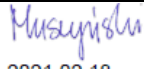
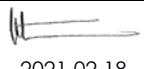
| Date | By |
|---------------------|----------------------------|
| 2021-02-24 22:26:06 | Dr. John LILLINGTON (AMEC) |
| 2021-02-25 03:06:08 | Mr. Janusz MALESA (NCBJ) |

Core design neutronics for the GEMINI+ HTGR

GEMINI+ Deliverable D2.8

J.C. Kuijper (NUCLIC)
D. Muszynski (NCBJ)

NUCLIC Report No. R20060 / JCK
Version 1.0 (Final)
Date 18 February 2021

| Version | Written by | Checked by | Approved/ Accepted/ Released by |
|--------------------|-----------------------|---|---|
| 0.0 | J.C. Kuijper (NUCLIC) | WP2, Task 2.4 participants | J. Lillington (Jacobs) |
| 1.0 | J.C. Kuijper (NUCLIC) | D. Muszynski (NCBJ) | J. Lillington (Jacobs) |
| Signature/ Date | |  2021.02.18 |  2021.02.18 |

This project has received funding from the Euratom research and training programme 2014-2018 under the grant agreement n°755478. The content of this deliverable reflects only the authors' views. The European Commission is not responsible for any use that may be made of the information it contains.

The high precision monte carlo calculations were carried out on the HPC cluster of the Swierk Computing Centre (CIS), National Centre for Nuclear Research (NCBJ), Poland.

NUCLIC

IEPENLAAN 129, 1741TD SCHAGEN, THE NETHERLANDS

T +31 (0)224 298 532

M +31 (0)6 4022 9728

W <https://www.nuclik.nl>

E contact@nuclik.nl

KvK / NL Chamber of Commerce registration no. 65669193



R20060/JCK

1 / 106

General introduction & Overview

This report is **Deliverable D2.8** of the Euratom Horizon 2020 project GEMINI+ [1]. It contains the results of core neutronics design analyses on a few design versions of the GEMINI+ HTGR, a small, 180 MW_{th}, prismatic **H**igh **T**emperature **G**as-cooled **R**eactor. Detailed information on the preliminary design can be found in GEMINI+ Deliverable D2.5 [2]. The report consists of 4 more or less independent parts (A – D) and an additional part (E) concerning review and update.

The results for the latest (June 2020) design version, with 11 layers of fuel blocks, are presented in **Part A**, the original version of which was also submitted as paper to HTR2021 [3]. The current report, however, is an extended version in which some additional (more recent) information (status December 2020) has been added.

Part B shows results of neutronics analyses of an earlier, 10-layer version, of the GEMINI+ HTGR, reported earlier internally within the GEMINI+ project as NUCLIC note N19060 version 02 [3].

Part C provides some additional information concerning the (preliminary) fuel design, and is an updated/extended version of NUCLIC note N19064 version 02 [4].

Part D concerns the activation of the replaceable and permanent reflectors, and the core barrel and pressure vessel, during some operation cycles of 550 days, but also during the 30 to 60 years lifetime of the reactor.

For the neutronics analyses presented in Part A, Part B and Part D the full power temperature distribution over the core in the BOL (Beginning Of Life) state was calculated by NRG using the SPECTRA code [6,7]. Further details are given in Part A and Part B, respectively.

Finally, **Part E** contains the responses from the authors to the review comments on the draft version [8] of this report, which was also reported in a separate note [9]. Addressing the comments also initiated some minor changes in Parts A and D to arrive at the current/final version of this report.

[1] “GEMINI+ - Research and development in support of the GEMINI Initiative“, Euratom Horizon 2020 project 755478, 1 September 2017 - 31 August 2020.

[2] B. Lindley, M. Davies (Jacobs), D. Hittner (LGI), M.M. Stempniewicz, E.A.R. de Geus (NRG), J. Kuijper (NUCLIC), G. Brinkmann, D. Vanvor (BriVaTech), “Final Description and Justification of the GEMINI+ System – GEMINI+ Deliverable D2.5”, Euratom Horizon 2020 project GEMINI+, contract no. 755478,

[3] Jim C. Kuijper, Dominik Muszynski, “Neutronics for the GEMINI+ HTR”, Proc. HTR 2021, Yogyakarta, Indonesia, June 3-5, 2021.

[4] J.C. Kuijper, D. Muszynski, “Initial SERPENT neutronics calculations on basic HTGR configuration A (no burnable poison) - GEMINI+, WP2, Task 4.2”, NUCLIC note N19060, version 02, 4 September 2019.

- [5] J.C. Kuijper, "Preliminary fuel specification for the GEMINI+ prismatic HTR (conceptual design stage) - Status: 16. December 2019", NUCLIC note N19064 version 0.2, 16 December 2019.
- [6] "SPECTRA - Sophisticated Plant Evaluation Code for Thermal-Hydraulic Response Assessment, Version 3.61, January 2020, Volume 1 – Program Description, Volume 2 – User's Guide, Volume 3 – Verification and Validation", NRG report K6223/20.166353 MSt-200130, Arnhem, January 2020, <https://www.nrg.eu/fileadmin/nrg/Documenten/Spectra-Vol1.pdf>
- [7] M.M. Stempniewicz, "Thermal-Hydraulic Model of the GEMINI+ HTR Plant - Safety Analysis, WP1.6", NRG report 24203/19.153415, 30 May 2019.
- [8] J.C. Kuijper, D. Muszynski, "Core design neutronics for the GEMINI+ HTGR – GEMINI+ Deliverable D2.8", NUCLIC report R20060, version 0.0, NUCLIC, Schagen, The Netherlands, 19 January 2021.
- [9] J.C. Kuijper, D. Muszynski, "Response to review comments D2.8 (Report R20060/version 0.0)", NUCLIC note N21060, NUCLIC, Schagen, The Netherlands, 17 February 2021.

Contents

| | |
|---|-----------|
| General introduction & Overview | 3 |
| Contents | 5 |
| Part A - Neutronics for the GEMINI+ HTGR | 9 |
| Abstract | 10 |
| I. INTRODUCTION | 10 |
| II. THE SERPENT Code | 13 |
| <i>II.A. Explicit coated particle modelling</i> | <i>13</i> |
| <i>II.B. Multiphysics input</i> | <i>13</i> |
| <i>II.C. Statistical uncertainties</i> | <i>13</i> |
| III. THE SERPENT NEUTRONICS MODEL | 14 |
| IV. k_{eff} HISTORY | 18 |
| V. CONTROL RODS | 20 |
| VI. POWER AND BURN-UP DISTRIBUTION | 23 |
| VII. TEMPERATURE COEFFICIENTS OF REACTIVITY | 28 |
| VIII. AXIAL XE-OSCILLATIONS? | 30 |
| IX. STEAM INGRESS | 31 |
| X. FLUX INSTRUMENTATION AND STARTUP SOURCE | 33 |
| XI. CONCLUSIONS | 35 |
| Acknowledgement | 35 |
| References | 35 |
| Part B - Initial SERPENT neutronics calculations on basic HTGR configuration A (no burnable poison) - GEMINI+, WP2, Task 4.2 | 37 |

| | |
|--|-----------|
| Introduction - Objectives | 38 |
| Initial neutronics focus | 38 |
| Main features of the configuration(s) | 40 |
| Fuel management/loading | 41 |
| Core burn-up modelling | 43 |
| SERPENT input parameter settings | 43 |
| Results & discussion | 43 |
| <i>Influence of Xe-135 and Sm-149 on k_{eff}/reactivity</i> | 44 |
| <i>Control rod worth at different values of the enrichment</i> | 44 |
| <i>Reactivity effect of cooling down from HFP to CZP state</i> | 44 |
| <i>Evolution of k_{eff} from BOL to EOL</i> | 44 |
| <i>Power distribution from BOL to EOL</i> | 45 |
| <i>Decay heat</i> | 46 |
| <i>Iteration of power and temperature distribution at BOL</i> | 46 |
| <i>Fast flux ($E > 1$ MeV) distribution in the pressure vessel</i> | 46 |
| <i>Maximum fast fluence ($E > 1$ MeV) in pressure vessel</i> | 48 |
| <i>Fast flux in reactor cavity</i> | 48 |
| Conclusions & recommendations | 48 |
| References | 49 |
| Part B - Appendix A - Influence of interchanged temperatures in the reflector | 69 |
| Part C - Preliminary fuel specification for the GEMINI+ prismatic HTR (conceptual design stage) | 73 |
| Introduction | 74 |
| 1. Dimensions and densities | 75 |
| 2. Enrichment and particle volume fraction in compact | 75 |
| 3. Temperature distribution and failure fraction | 76 |
| 4. Power and Burn up | 76 |

| | |
|---|------------|
| 6. Conclusions | 82 |
| References | 82 |
| Part D - Activation | 85 |
| I. INTRODUCTION | 86 |
| II. NITROGEN IN NBG17 GRAPHITE | 88 |
| III. SERPENT MODEL AND METHODOLOGY | 88 |
| IV. SERPENT depletion mode v. activation mode (comparison - one cycle example) | 90 |
| V. REPLACEABLE REFLECTOR 1ST AND 2ND RING | 93 |
| VI. STRUCTURES WITH LONG IRRADIATION TIME | 96 |
| <i>VI.A REACTOR PRESSURE VESSEL (STEEL A508)</i> | 96 |
| <i>VI.B CORE BARREL (STEEL 800H)</i> | 98 |
| <i>VI.C PERMANENT REFLECTOR (GRAPHITE NBG17)</i> | 99 |
| VII. CONCLUSIONS | 101 |
| References | 101 |
| Part E – Review and update | 103 |
| <i>Introduction</i> | 104 |
| <i>Response to review comments</i> | 104 |
| References | 106 |

Part A - Neutronics for the GEMINI+ HTGR

Part A contains the analyses on the current (June 2020) 11-layer design of the GEMINI+ HTGR, as presented in the paper submitted to HTR2021, September 2020 [1], extended with additional (more recent) information, reflecting the status of December 2020.

[1] Jim C. Kuijper, Dominik Muszynski, "Neutronics for the GEMINI+ HTR", Proc. HTR 2021, Yogyakarta, Indonesia, June 3-5, 2021.

Abstract

Literally at the heart of the Euratom Horizon 2020 project GEMINI+ are the core neutronics (design) calculations. For these calculations on a relatively small (180 MWth) prismatic HTGR with cylindrical core, the 3-D monte-carlo particle transport and depletion code SERPENT version 2 (VTT, Finland) was selected, the main reasons being the flexibility and versatility of this code. This enables the modelling of all relevant details of the reactor without unnecessary approximations. A particularly useful feature of the SERPENT code is the multi-physics input capability. This allows to map a temperature field over the defined geometry, enabling the calculation of converged power and temperature distribution by means of iteration and data exchange between SERPENT and a (steady-state) thermal- hydraulics code. In this particular case the SPECTRA code (NRG, The Netherlands) was used to provide the temperature distribution. 4 to 5 iterations are sufficient to reach simultaneously converged distributions for power and temperature. The paper gives an overview of the performed analyses for the current (June 2020) design of the GEMINI+ HTGR, and results thereof. Neutronics features seem quite promising, but further improvements and therefore further investigations would be desirable.

I. INTRODUCTION

The Euratom Horizon 2020 project GEMINI+ [1] is aiming at the (preliminary) design of a reactor system with a net power output of 165 MWth (gross thermal power of 180 MWth including house load), hereby maximising the convergence between European and NGNP Industry Alliance HTGR designs. The GEMINI+ system is currently designed to provide steam (230 t/h at 540 °C and 13.8 MPa) to industrial end users for use in electricity production and/or process heat. The current (June 2020) state of the design is described in [2].

The GEMINI+ reactor is a relatively small (180 MW thermal power) prismatic block type reactor HTGR. The reactor components (fuel blocks, reflector blocks, compacts, coated fuel particles) are very similar to those of existing designs (General Atomics GT-MHR and MHTGR [3,4], Framatome SC-HTGR [5]), although they are fully based on information available in the open literature.

In support of the design and (thermal hydraulic) safety analysis of the GEMINI+ HTGR, reactor (core) physics (neutronics) and depletion calculations have been performed on a limited number of design versions of this reactor. Some of the results will be presented in this report.

Main characteristics of the reactor (neutronics model) are listed in Table 1. An earlier design featured 10 layers of fuel blocks in the core and slightly different placement of control rod positions in core and (radial) reflector, in the sense that the blocks containing some of the control rod channels may have been rotated, compared to the current (June 2020) 11-layer design. This modification was necessary in view of limitations to the required penetrations of the pressure vessel head [2].

Table 1. Main configuration characteristics of the SERPENT model of the GEMINI+ prismatic block HTGR.

| Parameter | Value | Unit |
|---|--|------|
| Reactor/core configuration | - | - |
| # Radial rings of fuel blocks (ring around centre column is first ring) | 3 | - |
| # Fuel block columns | 25 | - |
| # Control block columns | 6 | - |
| # Axial fuel/control block layers | 11 | - |
| Distance between side faces of adjacent blocks | 0.2 | cm |
| Core height | 800 / 880 10 layers / 11 layers of blocks | cm |
| # Replaceable reflector rings | 2 | - |
| # Replaceable reflector columns | 54 | - |
| Bottom reflector (with coolant holes) | - | - |
| Reflector material | NBG-17 graphite [6] | - |
| Reflector thickness | 160 | cm |
| Top reflector (with coolant and control rod holes) | - | - |
| Reflector material | NBG-17 graphite [6] | - |
| Reflector thickness | 120 | cm |
| Core barrel | - | - |
| Core barrel inner radius | 199.1 | cm |
| Core barrel effective outer radius | 207.1 | cm |
| Core barrel material | Alloy 800H | - |
| Core barrel height (in SERPENT neutronics model) | 1080 / 1160 (10 / 11 layer core) | cm |
| Reactor Pressure Vessel | - | - |
| RPV inner radius | 234.1 | cm |
| RPV outer radius | 244.05 | cm |
| RPV material | Alloy SA508 | - |
| RPV height (in SERPENT neutronics model) | 1080 / 1160 (10 / 11 layer core) | cm |
| Fuel block configuration | - | - |
| Block height | 80 | cm |
| Hexagon flat-to-flat distance | 36 | cm |
| Block material | NBG-17 graphite [6] | - |
| Triangular pitch | 1.9 | cm |
| # channels with fuel compacts | 216 (w/o BP) 210 (with BP) | - |
| Compact channel diameter | 1.27 | cm |
| # small coolant channels | 6 | - |
| Small coolant channel diameter | 1.27 | cm |
| # large coolant channels | 102 | - |
| Large coolant channel diameter | 1.6 | cm |
| Control block configuration | - | - |
| Block height | 80 | cm |
| Hexagon flat-to-flat distance | 36 | cm |
| Block material | NBG-17 graphite [6] | - |
| Triangular pitch | 1.9 | cm |
| # channels with fuel compacts | 174 (w/o BP) 170 (with BP) | - |
| Compact channel diameter | 1.27 | cm |
| # small coolant channels | 5 | - |
| Small coolant channel diameter | 1.27 | cm |
| # large coolant channels | 102 | - |
| Large coolant channel diameter | 1.6 | cm |
| Control rod channel diameter | 13 | cm |

N.B. The (effective) inner and outer radius of the core barrel and the pressure vessel as stated here may slightly deviate from what is stated in [2]. This, however, does not significantly influence the neutronic characteristics of the core.

Table 1 (cont.). Main configuration characteristics of the SERPENT model of the GEMINI+ prismatic block HTGR.

| Parameter | Value | Unit |
|---|--|-------------------|
| Control rod configuration (model - simplified) | - | - |
| # core rods | 6 | - |
| # reflector rods | 18 | - |
| Rod geometry | Annular | - |
| Rod length | 800 / 880 (10 layer core / 11 layer core) | cm |
| Inner radius | 3.75 | cm |
| Outer radius | 5.25 | cm |
| Absorber material | B ₄ C | - |
| Absorber material density | 2.52 | g/cm ³ |
| Fuel compact configuration | - | - |
| Matrix material | C | - |
| Matrix material density | 1.75 | g/cm ³ |
| # coated particles per compact | 2500 *) | - |
| Compact cylinder height | 5.0 | cm |
| Compact cylinder radius | 0.625 | cm |
| Coated particle configuration | - | - |
| Kernel diameter | 500 | micron |
| Kernel material | UO ₂ | - |
| Kernel density | 10.4 | g/cm ³ |
| Buffer layer thickness | 95 | micron |
| Buffer layer material | C | - |
| Buffer layer density | 1.05 | g/cm ³ |
| Inner PyC layer thickness | 40 | micron |
| Inner PyC material | C | - |
| Inner PyC density | 1.90 | g/cm ³ |
| SiC layer thickness | 35 | micron |
| SiC material | SiC | - |
| SiC density | 3.18 | g/cm ³ |
| Outer PyC layer thickness | 40 | micron |
| Outer PyC material | C | - |
| Outer PyC density | 1.90 | g/cm ³ |
| Burnable poison (BP) configuration (see Figs. 3 and 4 for locations of the burnable poison cylinders in the fuel blocks). | | |
| Height | 75.0 | cm |
| Outer radius of annular graphite cylinder | 0.625 | cm |
| Material of annular cylinder | C | - |
| Density of annular cylinder | 1.75 | g/cm ³ |
| Burnable poison (BP) material mixture | B ₄ C in graphite | - |
| Fraction f_{BP} of B ₄ C in graphite | 0.0 - 1.0 ^{*)} | - |
| Density of B ₄ C in mixture | 2.52 | g/cm ³ |
| Density of C in mixture | 1.75 | |
| Outer radius R_{BP} of BP material mixture | 0.2 - 0.525 ^{*)} | cm |
| Subdivision of BP material for accurate depletion calculation - # concentric rings | 10 | - |
| ¹⁰ B content of boron in BP | 20 (natural boron) | % |

*) The number of coated particles per compact, as well as the fuel enrichment and the parameters of the burnable poison cylinders have been/are being varied in the neutronics studies, in order to arrive at an acceptable / optimised configuration (ongoing in August/September/October 2020).

Currently a single batch loading scheme and an operation cycle of 550 full power days is assumed. This may be replaced later by a multi-batch (typically 2 or 3) loading scheme, to improve utilization of the fuel, i.e. to increase the burn-up at final discharge. Furthermore, a single value of the enrichment is assumed. From initial studies, an enrichment of 12% in ^{235}U seemed to be most practical for now.

II. THE SERPENT Code

The main code employed for the core neutronics calculations is SERPENT version 2.1.31 in combination with JEFF 3.1.1 nuclear data [7]. SERPENT is a continuous energy monte carlo neutron (and photon) transport code, capable of modelling arbitrary geometry. The later includes the modelling of explicit coated particles in compacts. Integrated into the code is a detailed burn-up/depletion calculation method, featuring a semi-automatic subdivision to distinguish between cells that may initially contain the same material, but deviate during depletion due to differences in local flux (and -spectrum). Further features used in the GEMINI+ neutronics calculations are the following:

- Generation and use of explicit random particle distributions.
- Multiphysics input option.

II.A. Explicit coated particle modelling

SERPENT (versions 2.1.x) has the capability to generate random spatial distributions of spheres, e.g. in a cylinder. This was used to generate the random particle positions in a stack of 15 compacts in a fuel block, e.g. $15 \times 2500 = 37500$ coated particles per 15 compacts. Strictly speaking, a random distribution should be generated for a single (5 cm high) compact (no coated particles crossing the outer boundary of the compact), of which 15 should be put in a stack subsequently. However, the difference in k_{eff} between these two approaches is only a few pcm, so it was decided to use the simpler approach in further analyses, as described above. All compact channels of all fuel blocks are subsequently filled with the same distribution of coated particles in matrix material.

II.B. Multiphysics input

SERPENT has a “multi-physics” input option. This has been used to assign different temperature to different materials in different locations in the model, without the necessity to assign different material names to materials at different temperatures. This feature has been used to import the (steady state) temperature distributions for different materials (fuel kernel, coatings, matrix material of the compacts, block graphite, etc.) as calculated by the thermal hydraulics code SPECTRA for the corresponding thermal hydraulics model [2,8,9,10].

II.C. Statistical uncertainties

As SERPENT uses the (continuous energy) monte carlo method to simulate neutron (and photon) transport, all results come with a statistical uncertainty

that is dependent on the number of neutrons per calculation cycles and the number of cycles per calculation for a single point in time. (Most of) the monte carlo calculations were performed using a neutron population of 100000 (“fine” mode) or 400000 (“extra fine” mode), 1000 cycles with 20 or 100 inactive cycles, using around 350 cores, and a hybrid MPI/OpenMP parallelization.

III. THE SERPENT NEUTRONICS MODEL

The current (June 2020) neutronics model with 11 layers of fuel blocks in the core is shown in Fig. 1 (horizontal cross section) and Fig. 2 (vertical cross section). Also indicated are the identifiers of the control rods in the core (“CRx”) and radial reflector (“RR[x]x”), and 5 “representative” fuel columns (“C1” to “C5”). The neutronics model has been restricted to those elements that are of influence on the neutronics behaviour. Therefore, the upper and lower part of the pressure vessel (including the components within those sections) have not been included. Further information on materials and dimensions of the neutronics model is given in Table 1. Details of the fuel blocks with and without a control rod channel is shown in Figs. 3 and 4. Note that 6 out of 216 and 4 out of 174 compact channels have been replaced by burnable poison cylinders (see below for further explanation).

The initial version of the reactor featured 10 layers of fuel blocks in the core, with 25 full fuel blocks and 6 fuel blocks with a control rod channel per layer. No burnable poison (BP) was used in this version, which, however, exhibited a too high (> 1600 °C) maximum fuel temperature in a Depressurised Loss of Forced Cooling (DLOFC) accident [10]. Therefore, an extra layer of fuel blocks was added in order to lower the (average) power density, increasing the total height of the core, radial reflectors, core barrel and pressure vessel by 80.0 cm [11]. This promises a great improvement (i.e. much lower) in maximum fuel temperature during DLOFC, as was indicated by transient thermal-hydraulic calculations assuming a uniform power distribution [12]. A further assumption in this DLOFC simulation was a “radially flat” power profile.

In addition, burnable poison (B_4C in graphite) was introduced, as indicated in Figs. 3 and 4, for two purposes:

- To tailor the history of the (uncontrolled) k_{eff} from Beginning-of-Life (BOL; start of operation; ^{135}Xe -free) to End-of-Life (EOL; 550 full power days; equilibrium ^{135}Xe and ^{149}Sm). The main purpose of this is to ensure that the uncontrolled k_{eff} (i.e. the value for all rods out) is within the range that can actually be compensated by the control/shutdown rods in the reflector and the core, for all operational states of the reactor. See Sections V and VI.
- To improve the (radial) power distribution over the core, as additional measure in response to the too high maximum fuel temperature in the earlier design version with 10 layers of fuel blocks in the core, without BP.

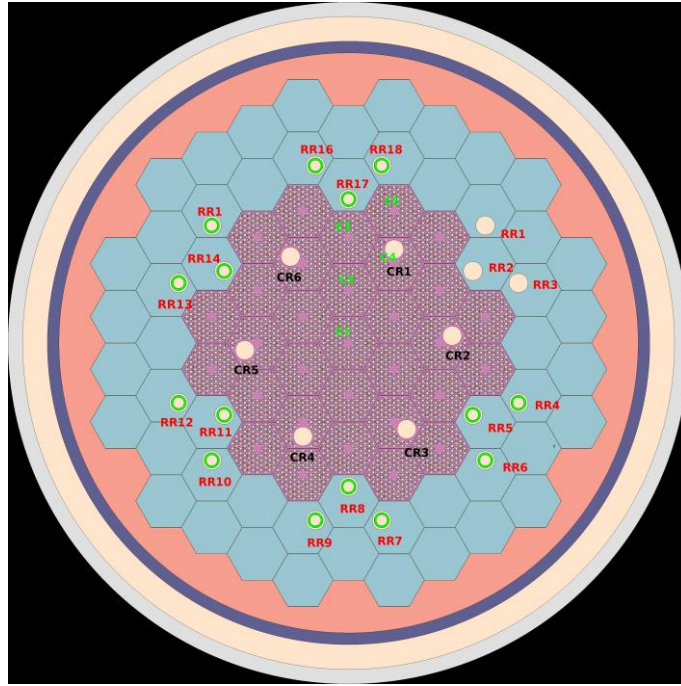


Fig. 1 Horizontal cross section ($z = 1000$ cm plane; near the top of the core) of the SERPENT neutronics model for the current (June 2020) version of the GEMINI+ reactor. Control rod identifiers are given. The outer (light grey) section is the pressure vessel. Dimensions are given in Table 1. Also indicated (in green) are 5 representative (due to symmetry; for C4 this is not exact, but in rather good approximation) core columns (C1 - C5).

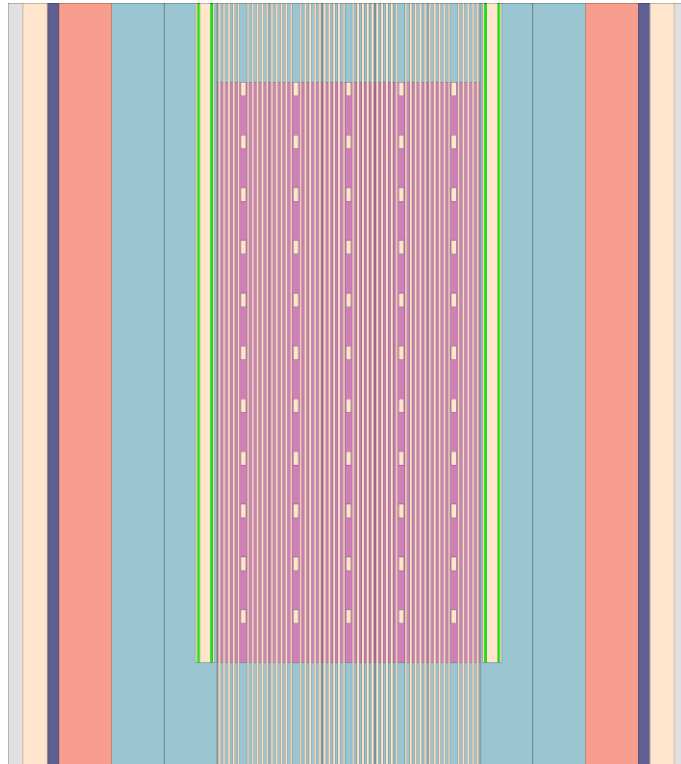


Fig. 2 Vertical cross section ($x = 0$ cm plane) of the SERPENT neutronics model for the current (June 2020) version of the GEMINI+ reactor (11 layers of fuel blocks in the core). Note that the visible reflector control rods (RR8 and RR17, in green) have been fully inserted in this case. Further note that the aspect ratio shown in the drawing is not entirely realistic. Actual dimensions are given in Table 1.

Efforts for the 2nd point are currently (August/September 2020) ongoing and have not yet been fully finalised. The aim is to flatten the (radial) power distribution (as this was the assumption in the DLOFC calculations that showed favourable characteristics with respect to peak fuel temperature [12]), or even to shift the maximum power density to the outer fuel blocks close to the radial reflector, mainly by optimising the (radial) distribution of burnable poison (and possibly the enrichment). See Section VI.

The temperature distribution over the 11-layer geometry in Hot Full Power (HFP) conditions originates from a steady state thermal hydraulics calculation by SPECTRA, assuming a “flat” radial power profile (i.e. the same axial power profile for all fuel columns) and a re-scaled 10-layer axial profile (i.e. from 10 to 11 layers) [2]. The latter originates from the iterative procedure between neutronics (SERPENT) and thermal hydraulics (SPECTRA) that was applied for the initial 10-layer configuration [9] (also see Part B). Only a few iterations already resulted in a converged solution for the temperature and power distribution, as is demonstrated in Fig. 5.

Note that the axial power profiles for iterations 3 and 4 already almost coincide for the representative fuel columns C1 to C5 (N.B. These representative fuel columns are designated “FA1” to “FA5”, respectively, in [9,10]).

Also note that this procedure **was only followed at BOL** and the resulting temperature distribution was kept unchanged during the entire operating cycle until EOL, as was envisaged from the start of the project [1]. However, in view of the considerable changes in power distribution during the operating cycle from BOL to EOL (see further sections in this paper), it would be advisable to revise this procedure, e.g. by introducing a simplified thermal-hydraulics feedback module running in conjunction with SERPENT, providing temperature distribution feedback for every time step.

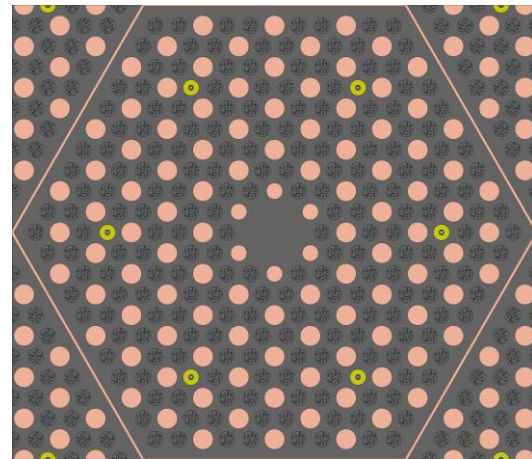


Fig. 3. Full fuel block without control rod channel. 6 compact stacks have been replaced by burnable poison cylinders.

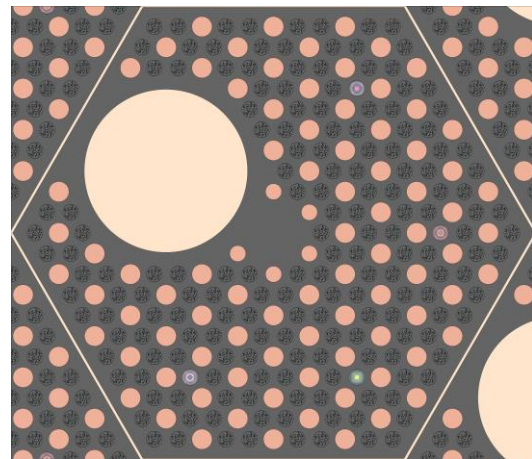


Fig. 4. Fuel block with control rod channel. 4 compact stacks have been replaced by burnable poison cylinders.

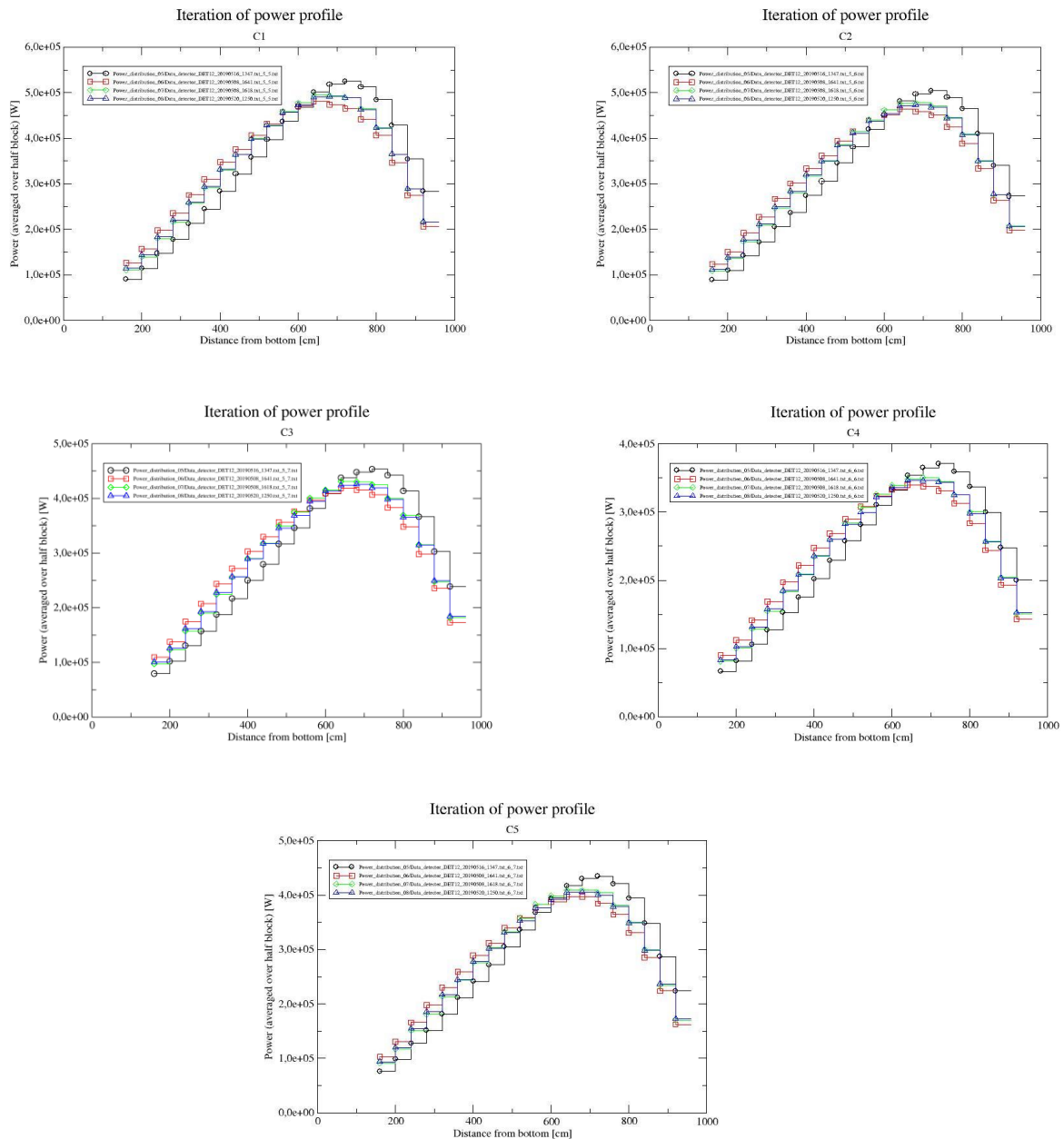


Fig. 5. Successive iterations of the axial distribution of the power in the representative fuel columns C1 to C5 at BOL (10-layer core; no burnable poison; see Part B). Starting with a cosine-shaped axial power distribution (not shown in the graphs) a corresponding temperature distribution was calculated by SPECTRA [10], based on which the power distribution for the next iteration was calculated. This was repeated 4 times, resulting in successive axial power distributions (indicated as “5” up to “8” in the graphs). Note that the power distributions of the 3rd and 4th iterations already nearly coincide, indicating convergence. Relative standard deviation of the power (per half block; half block is the meshing used for the calculation of the neutron flux and derived parameters, e.g. the power) in the results shown is 0.22 % for the peak values.

A specific remark concerns the number of coated particles in a compact. In the majority of the neutronics calculation this was assumed to be 2500. In the thermal hydraulics analyses [9, 10, 11, 12], however, it is assumed to be 3760. However, the actual number of coated particles in a compact does not significantly impact the maximum fuel temperature of the reactor in steady-state conditions or even in a (DLOFC - Depressurised Loss of Forced Cooling)

transient. The latter was shown by NCBJ by comparing the 2 DLOFC cases [13].

IV. k_{eff} HISTORY

The search for an optimised configuration (spatial distribution of burnable poison parameters: fraction f_{BP} of B_4C in graphite; radius R_{BP} of the cylinder containing B_4C in graphite; it is assumed that all burnable poison pins in a single fuel block are identical, initially) is executed in phases. In the first phase, which focusses on the optimisation of the (uncontrolled) k_{eff} history from BOL (Xe-free) to EOL, it is assumed that all burnable poison cylinders in the core are initially identical.

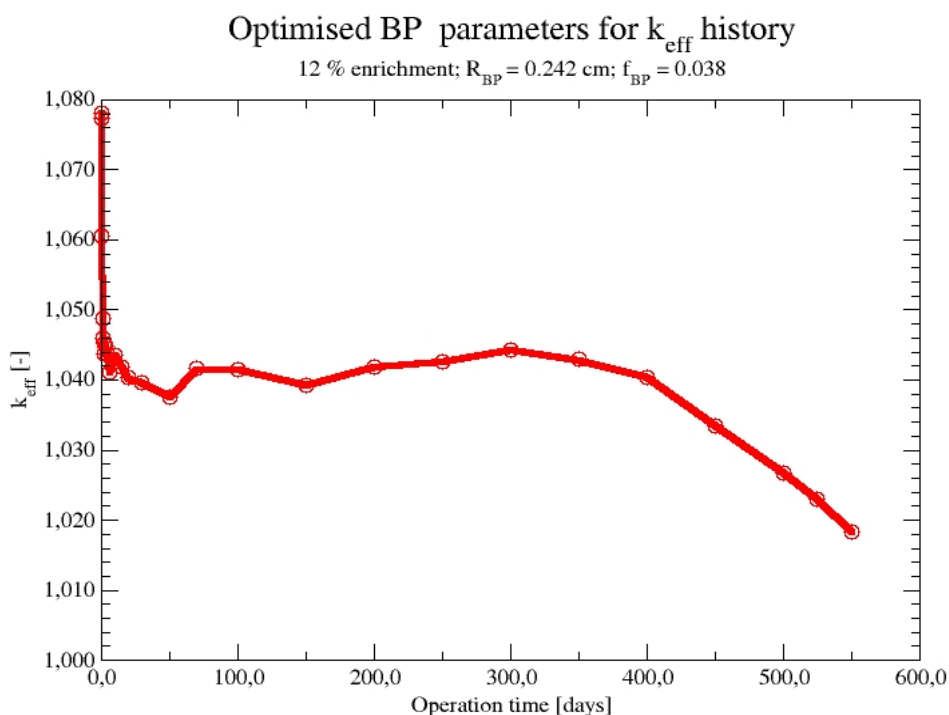


Fig. 6. Uncontrolled (i.e. all control rods out) k_{eff} versus operation time for a uniform enrichment of 12%, burnable poison cylinder radius $R_{BP} = 0.242$ cm and burnable poison fraction (B_4C in graphite) $f_{BP} = 0.038$. Note the equilibrium reactivity worth of ^{135}Xe is approximately -2840 pcm. k_{eff} varies between 1.078 (BOL, no Xe) and 1.018 (EOL, Xe-eq.). The relative standard deviation in k_{eff} is 12 to 13 pcm, which is consistent with the neutron population parameters: 100000 neutrons per cycle and 1000 cycles per point in time. In the calculation 26 non-equidistant time steps were used.

Several combinations of enrichment (12%, 13% and 15%) and burnable poison parameters (fraction f_{BP} and cylinder radius R_{BP} ; uniform values for all blocks in the core) have been investigated [13] and it was found that a uniform enrichment of 12%, burnable poison cylinder radius $R_{BP} = 0.242$ cm and burnable poison density (B_4C in graphite) $f_{BP} = 0.038$ provided an acceptable behaviour of the uncontrolled (i.e. all control rods out) of k_{eff} as function of time from Beginning of Life (BOL) to End of Life (EOL = 550 full power days), as is shown in Fig. 6. In this stage of the optimisation the main purpose of

introducing burnable poison is to minimise k_{eff} (but still with k_{eff} sufficiently above 1 until EOL), so that the control and shutdown rods can be effectively used for start-up and shutdown. Ideally, k_{eff} is approximately constant after reaching Xe-equilibrium (approx. 3 days) or slowly decreasing.

The k_{eff} at BOL is 1.078 (Xe-free), and 1.018 (Xe-equilibrium) at EOL. This BOL-to-EOL reactivity swing is well within the reactivity range of the reflector control rods (see Section V). It should be noted that, for 12 % enrichment without burnable poison, the k_{eff} (Xe-free) at BOL would have been above 1.40! A corresponding BOL-to-EOL reactivity swing of about -40% would be impossible to handle by the reflector rods.

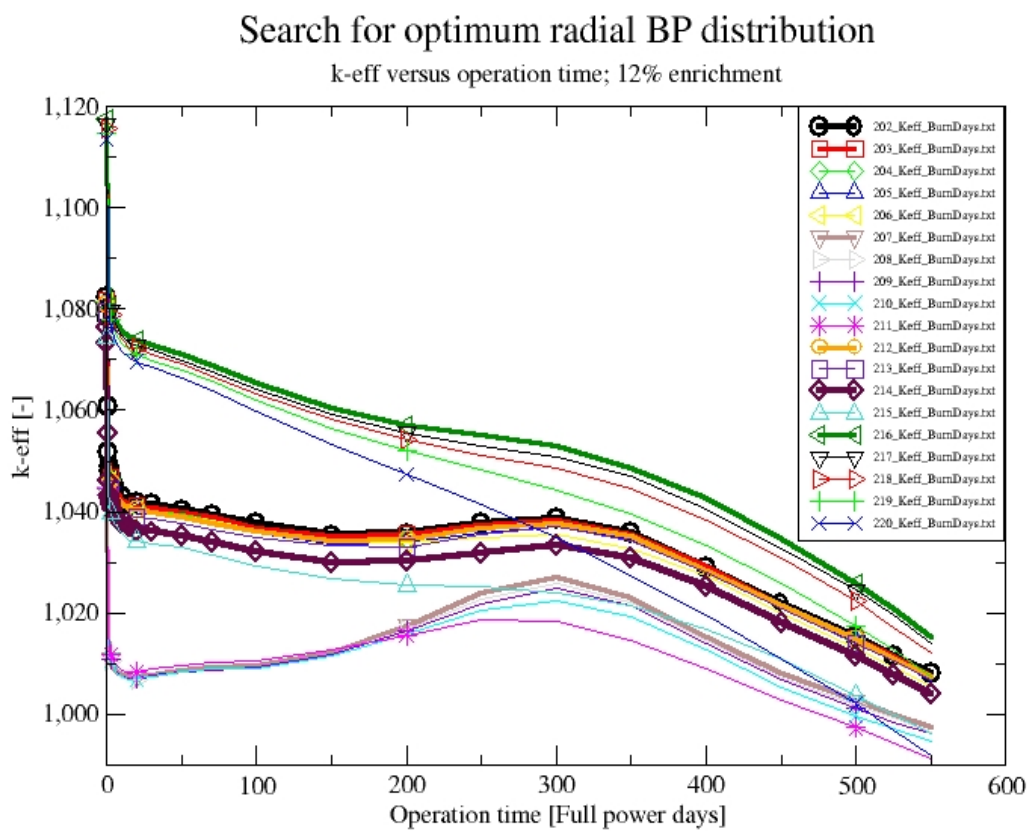


Fig. 7. Uncontrolled k_{eff} histories from calculations to improve the radial power distribution (see Section VI), by applying different burnable poison parameters for columns C1 and C2 on the one hand and C3, C4 and C5 on the other. Case 202 (bold "black circles") is the same as shown in Fig. 6 (uniform BP parameters). Case 214 (bold "purple diamonds") is the most favourable configuration so far. Neutron population parameters are the same as in Fig. 6, again yielding a relative standard deviation in k_{eff} of 12 to 13 pcm.

In the 2nd phase of the optimisation, the objective is to improve the radial power distribution (see Section VI), by modifying the radial distribution of the burnable poison parameters, to a lesser or larger extent deviating from the uniform distribution given above, keep the enrichment at 12 %. For simplicity only 2 sets of values (of R_{BP} and f_{BP}) were used for each of the cases: one set of values for the central fuel columns (C1 - C3) and one set for the peripheral

fuel columns (C4, C5). In the search for the optimal performance, the total amount of B_4C in the core (at BOL) was kept constant. Difference between central and peripheral columns was either in f_{BP} or R_{BP} .

Fig. 7 shows the k_{eff} history for several combinations of BP parameters for central and peripheral fuel columns. Case 102 is the case with uniform BP parameters (the same as in Fig. 6). Case 214 turned out to be the most favourable until now (September 2020) concerning the (radial) power distribution. (see Section VI), while it is also marginally superior to case 202 concerning the k_{eff} history (i.e. k_{eff} closer to 1.00). BP parameters for this case are given in Table 2.

Table 2. Burnable poison parameters for case 214.

| BP parameter | Columns C1, C2 | Columns C3, C4, C5 | Units |
|--------------|----------------|--------------------|-------|
| f_{BP} | 0.038 | 0.038 | [-] |
| R_{BP} | 0.290 | 0.227 | [cm] |

V. CONTROL RODS

The reactor configuration features 6 control rods in the core and 18 (6 clusters of 3 each) in the reflector, as shown in Fig. 1, Table 3a shows the k_{eff} for several control rod patterns (each rod is either fully in or fully out) for uniform initial enrichment of 12 % and uniform burnable poison parameters as in case 202, at Cold Zero Power (CZP; “room” temperature conditions: $T = 300$ K), BOL, Xe-free conditions.

Table 3a. k_{eff} for characteristic control rod configurations at CZP, BOL, Xe-free for 11 layer core, uniform 12 % initial enrichment and uniform burnable poison parameters (case 202). CR = Core Rods, RR = Reflector Rods.

| Rod positions | k_{eff} | Remarks |
|---|-----------------------|---|
| All CR in; all RR in | 9.14812E-01 (0.012%) | CZP state is subcritical with all rods in: OK |
| All CR in; all RR out | 1.00170E+00 (0.58%) | Core rods in only are not sufficient in this configuration in CZP state: not OK (at BOL) |
| All CR in; RR1/2/3 in; RR10/11/12 in | 9.65733E-01 (0.012%) | Core rods + some reflector rods are sufficient at BOL. This could be OK , as most RR are in anyway during first days of operation (see below). |
| CR1 out; RR1, RR2, RR3 out; other rods in | 9.77099E-01 (0.012%) | Approximately 60 degr. sector free of rods, to accommodate (re-) load: OK |
| CR1 out; RR1, RR2, RR3, RR16, RR17, RR18 out; other rods in | 1.018760E+00 (0.012%) | Slightly over 60 degr. sector free of rods, to accommodate (re-load): not OK |

It is clear that the core rods alone can **not** keep the reactor subcritical at BOL, CZP, Xe-free conditions. It is also **not** possible with only the reflector rods. However, it **is** possible to maintain subcriticality at BOL, CZP, Xe-free, by all core rods + 6 reflector rods inserted.

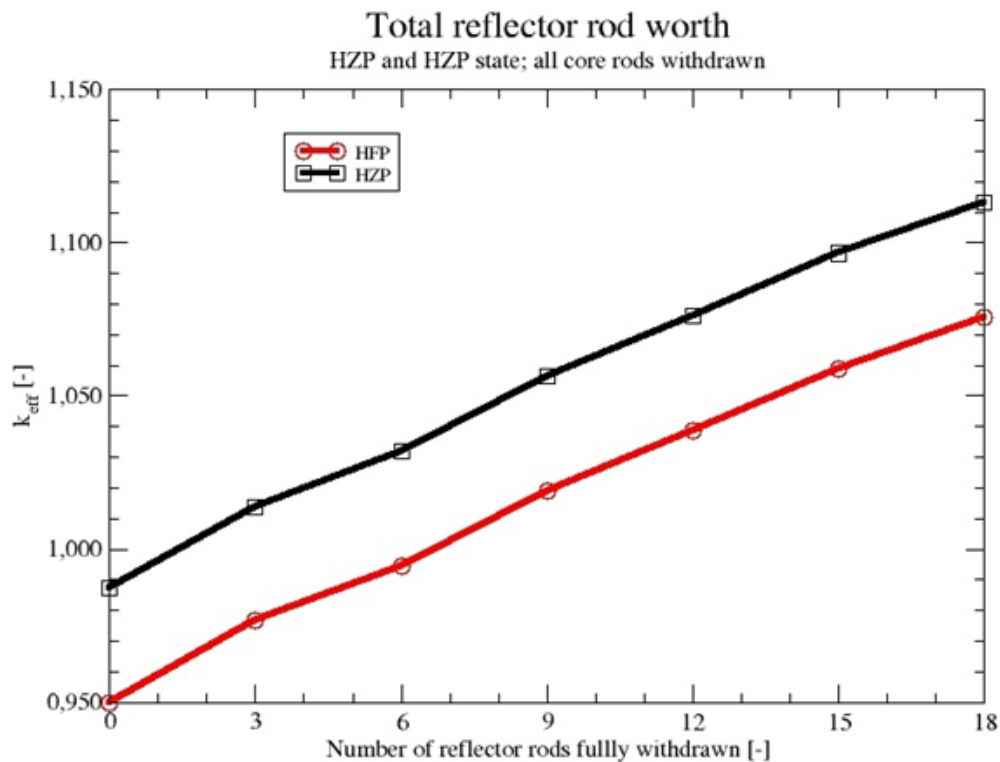


Fig.8. k_{eff} as function of the number of withdrawn control rods in the reflector for case 202 at BOL. All control rod in the core are out. The value for all rods out at HFP corresponds to the initial value in Fig. 6. Relative standard deviation in k_{eff} is 12 to 13 pcm.

Also, it is possible to remove one core rod and the closed set of 3 reflector rods in a **60 degrees sector** of the core, while maintaining subcriticality. This is necessary for the (re-) fuelling procedure.

Similar calculations are currently (January 2021) being performed for the “radially optimised” case 214. It is expected that this will yield similar results.

At elevated temperatures (Hot Zero Power - HZP; uniform temperature $T = 600K$) and Hot Full Power (HFP; temperature distribution from the steady-state SPECTRA thermal hydraulics calculation) the reactivity of the core is lower, and it is very well possible to keep the reactor subcritical with reflector rods only. This is desirable as the core rods are envisaged to be fully withdrawn during operation at (full) power. Fig. 8 shows, for case 202 with uniform initial burnable poison parameters, the k_{eff} at BOL, HZP/HFP, Xe-free, as function of the number of withdrawn control rods from the reflector. The withdrawal pattern of the reflector rods is such that more than 3 (or even more than 1) partially inserted rods are avoided, i.e. reflector rods are, as much as possible, either fully in or fully out. The control rods in the core have been fully withdrawn, as envisaged for full power operation. Note that the total worth of the reflector rods is approximately the same for HZP and HFP, viz. 12.4 %. This is large enough to compensate the full range of uncontrolled k_{eff} values indicated in Fig. 6, even in case of a Xe-free state at any time in the cycle. Similar calculations for case 214 are currently (January 2021) ongoing, and similar results are expected.

Table 3b. k_{eff} for characteristic control rod configurations at HZP and HFP, MOL, for 11 layer core, uniform 12 % initial enrichment and uniform burnable poison parameters (case 202). CR = Core Rods, RR = Reflector Rods. Standard deviation 0.012%

| Configuration | State | k-eff (no Xe) | k-eff (eq. Xe) | Remarks |
|---|-------|---------------|----------------|--|
| All CR in; all RR in | CZP | 0.87920 | 0.85508 | CZP state at MOL is subcritical with all rods in: OK |
| All rods in except CR4 and RR2 | CZP | 0.91520 | 0.88982 | CZP state at MOL can be kept subcritical with one stuck core rod and one stuck reflector rod: OK |
| CR1 out; RR1, RR2, RR3 out, other rods in | CZP | 0.93998 | 0.91387 | Approximately 60 degr. Sector free of rods at MOL, to accommodate (re-) load: OK |
| All core rods out; all reflector rods in except RR2 | HFP | 0.95256 | 0.92740 | HFP state at MOL can be kept subcritical with one stuck reflector rod: OK |
| All CR out; all RR in | HFP | 0.94233 | 0.91770 | HFP state at MOL can be kept subcritical by reflector rods only: OK |
| All rods out | HFP | 1.06624 | 1.03752 | HFP state at MOL; full power operation |
| All core rods out; all reflector rods in except RR2 | HZP | 0.97574 | 0.94836 | HZP state at MOL can be kept subcritical with one stuck reflector rod: OK |
| All CR in; all RR in | HZP | 0.81942 | 0.79819 | HZP state at MOL is subcritical with all rods in: OK |
| All CR out; all RR in | HZP | 0.96561 | 0.93868 | HZP state at MOL can be kept subcritical by reflector rods only: OK |
| All rods out | HZP | 1.08945 | 1.05751 | HZP state at MOL; start of full power operation |

Calculations on the influence of control rod insertion patterns on k_{eff} have also been performed for the Mid-Of-Life (MOL; 250 full power days) and (nearly) End-Of-Life (EOL; 525 full power days) states of the configuration of case 202. Results are shown in Tables 3b (MOL) and 3c (EOL). It can be concluded that, for both MOL and EOL, and for equilibrium xenon and zero xenon state, the effects of the respective control rod insertion patterns are very similar to those at BOL.

In the current design of the GEMINI+ reactor, also other control rod patterns are being considered, for which, however, no neutronics analyses have been performed (yet) [2]. Also, a reserve shutdown system, in the form of small absorber spheres (approx. 6 mm diameter; containing B_4C) is being considered. In the current configuration these spheres are supposed to use the same channels as the core control rods. This may require a re-design of the core control rods, e.g. cruciform shape instead of annular [2]. No neutronics analyses have been performed (yet) on either one of these configurations and it is currently assumed that the reactivity worth of either a

Table 3c. k_{eff} for characteristic control rod configurations at HZP and HFP, EOL, for 11 layer core, uniform 12 % initial enrichment and uniform burnable poison parameters (case 202). CR = Core Rods, RR = Reflector Rods.

| Configuration | State | k-eff (no Xe) | k-eff (eq. Xe) | Remarks |
|---|-------|---------------|----------------|--|
| All CR in; all RR in | CZP | 0.84782 | 0.81578 | CZP state at EOL is subcritical with all rods in: OK |
| All rods in except CR4 and RR3 | CZP | 0.88318 | 0.84979 | CZP state at EOL can be kept subcritical with one stuck core rod and one stuck reflector rod: OK |
| CR1 out; RR1, RR2, RR3 out, other rods in | CZP | 0.90680 | 0.87252 | Approximately 60 degr. Sector free of rods at EOL, to accommodate (re-) load: OK |
| All core rods out; all reflector rods in except RR3 | HFP | 0.91958 | 0.89552 | HFP state at EOL can be kept subcritical with one stuck reflector rod: OK |
| All CR out; all RR in | HFP | 0.90909 | 0.88540 | HFP state at EOL can be kept subcritical by reflector rods only: OK |
| All rods out | HFP | 1.03971 | 1.01130 | HFP state at EOL; full power operation |
| All core rods out; all reflector rods in except RR2 | HZP | 0.95553 | 0.92163 | HZP state at EOL can be kept subcritical with one stuck reflector rod: OK |
| All CR in; all RR in | HZP | 0.79776 | 0.77117 | HZP state at EOL is subcritical with all rods in: OK |
| All CR out; all RR in | HZP | 0.94512 | 0.91186 | HZP state at EOL can be kept subcritical by reflector rods only: OK |
| All rods out | HZP | 1.07177 | 1.03301 | HZP state at EOL; start of full power operation |

single channel filled with absorber spheres, or an inserted cruciform rod will have a reactivity value very similar to that of the current core control rod design. Obviously, this should be checked as part of the follow-up activities.

VI. POWER AND BURN-UP DISTRIBUTION

As mentioned in Section III, for the DLOFC transient calculations on the current 11-layered design [12] it is assumed that the radial distribution of the power is uniform, i.e. every column of fuel blocks has the same axial distribution of the power (per coated particle). This leads to an acceptable behaviour (peak fuel temperature < 1600 °C) in case of DLOFC. The calculations also showed that the DLOFC behaviour is less satisfactory when the power in the central fuel columns (C1, C2) is higher than in the peripheral fuel columns (C3, C4, C5). It is expected that the behaviour will even improve further when the power maximum is “pushed” further towards the peripheral fuel columns. As mentioned earlier (Section III), the second task of burnable poison is therefore to improve the radial power distribution. Preferably the (initial) enrichment of the fuel is still uniform (12 % for the current designs).

In Fig. 9 the axial distribution of power per coated particle (average over half block) is shown for all (31) fuel columns in the core for case 202 (uniform BP parameter distribution) at BOL/Xe-free ("A"), 250 days ("B") and 525 days ("C"). The highest power per coated particle (158 mW) occurs at BOL in column C1 (820 cm). The relative standard deviation of the power in the results shown is 0.22% for the peak values. Note that there is a large spread in peak values at the same elevation (820 cm), indicating a radial power distribution that is peaking in the centre column.

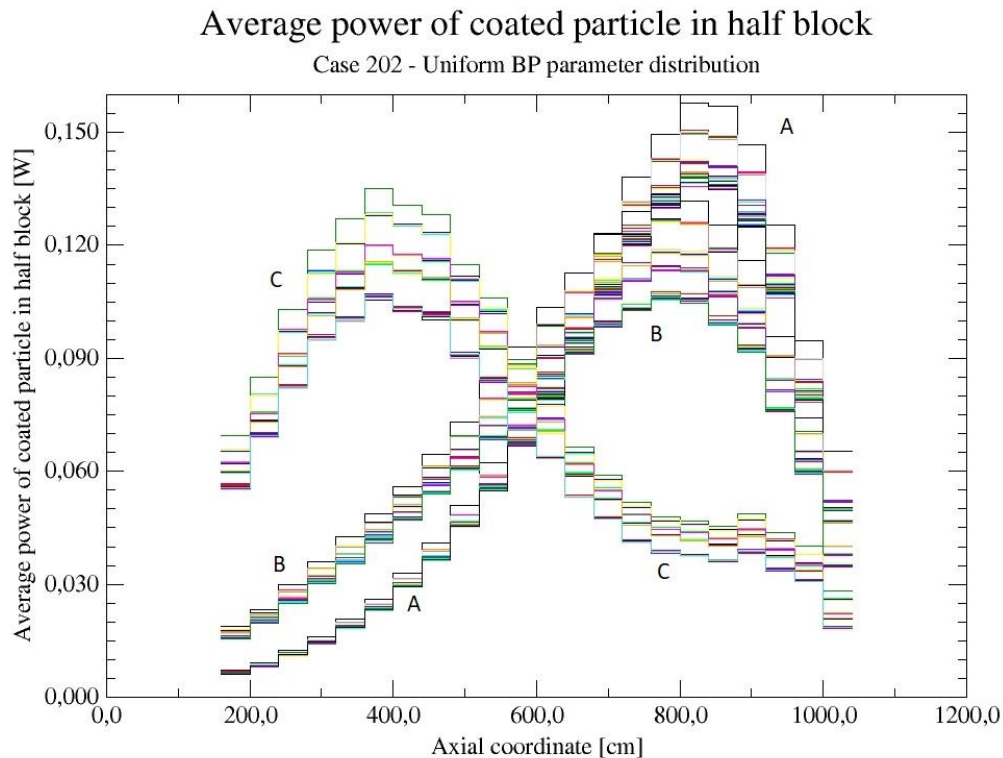


Fig. 9. Axial distribution of power per coated particle (average over half block) for all (31) fuel columns in the core for case 202 (uniform BP parameter distribution) at BOL/Xe-free ("A"), 250 days ("B") and 525 days ("C"). The highest power per coated particle (158 mW) occurs at BOL in column C1 (820 cm). The relative standard deviation of the power in the results shown is 0.22% for the peak values.

Introducing a radial profile in the BP parameters clearly improves this situation, as is shown in Fig. 10, which shows the axial distribution of power per coated particle (average over half block) for all (31) fuel columns in the core for case 214 (radially "optimised" BP parameter distribution; Table 2) at BOL/Xe-free ("A"), 250 days ("B") and 525 days ("C"). The highest power per coated particle (145 mW) occurs at BOL ("A") in a peripheral column of type C5 (at 820 cm). Note that the lowest power per coated particle at the same elevation is 138 mW, occurring in a central column of type C2. Clearly the spread in (peak) values at the same elevation has been reduced considerably, compared to case 202, indicating a much more "radially flat"

power profile: the difference between the highest and lowest peak value is less than 5 %. Also, the highest power does not occur in a central column, but in a peripheral column (C5-type, adjacent to the radial reflector; see Fig. 1),

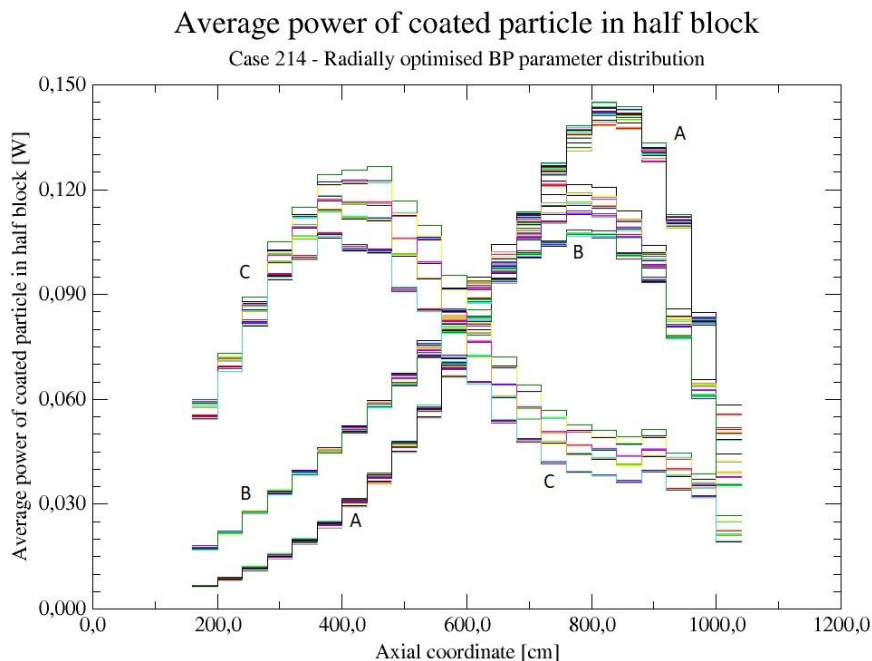


Fig. 10. Axial distribution of power per coated particle (average over half block) for all (31) fuel columns in the core for case 214 (radially “optimised” BP parameter distribution; Table 2) at BOL/Xe-free (“A”), 250 days (“B”) and 525 days (“C”). The highest power per coated particle (145 mW) occurs at BOL (“A”) in a peripheral column of type C5 (820 cm). Note that the lowest power per coated particle at the same elevation is 138 mW, occurring in a central column of type C2. The relative standard deviation of the power in the results shown is 0.22% for the peak values.

which is considered even more favourable. So, the restrictions on the power profile assumed in the transient (safety) calculations (i.e. “flat” radial profile) [2,12], can clearly be fulfilled by the use of burnable poison.

The final distribution of the burn up at EOL (550 full power operation days) is the topic of Figs. 11 and 12. In the SERPENT calculations the burn up has been determined on half block level. Figs. 11 and 12 show the frequency distribution of fuel in a given burn up interval, i.e. the number of blocks containing fuel at a final burn up in the interval indicated, for cases 202 and 214, respectively. Ideally, for a single batch loading scheme all fuel should end with the same final burn up. In the frequency distribution representation this means a single burnup range (at average burn up), containing all (341) blocks. This is clearly not yet achieved in cases 202 and 214, although it can be considered slightly better for case 214 (slightly lower maximum burn up, although still far above average). Further improvement can e.g. be expected from flattening the axial power profile.

A point of further discussion/investigation should be the power per coated particle (and per compact). Even for case 214 (“radially optimised” BP parameters) the maximum power per coated particle (averaged over half a

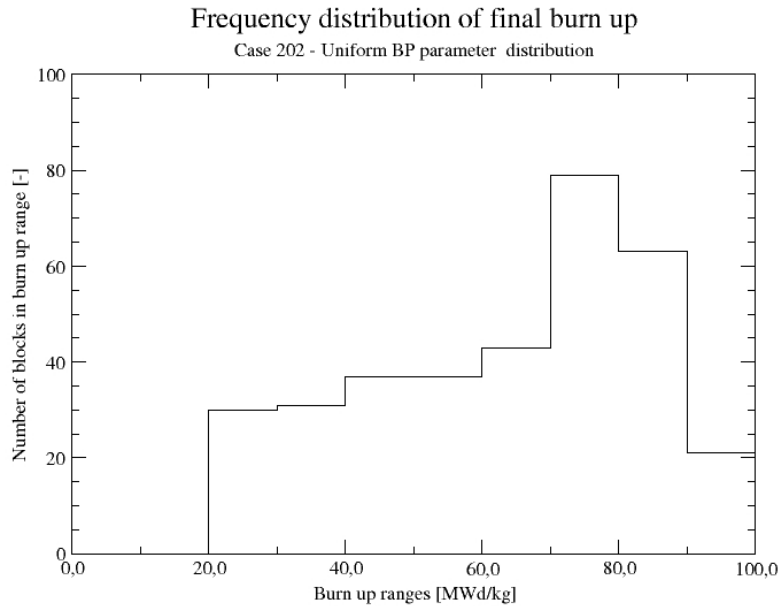


Fig. 11. Frequency distribution of the final burn up (per block) for case 202, i.e. the number of blocks containing fuel in the indicated burn up range. The maximum burn up is 98.5 MWd/kg. The average burn up is 63.8 MWd/kg.

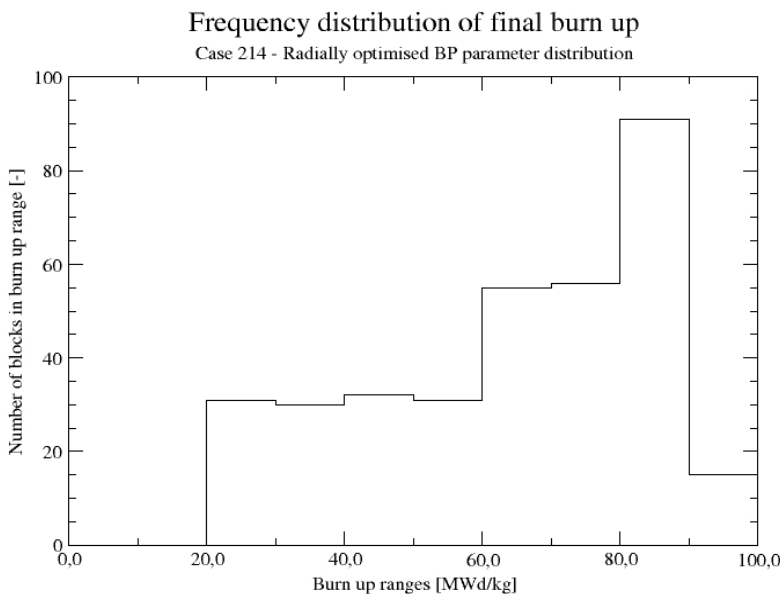


Fig. 12. Frequency distribution of the final burn up (per block) for case 202, i.e. the number of blocks containing fuel in the indicated burn up range. The maximum burn up is 94.6 MWd/kg. The average burn up is 63.8 MWd/kg.

block) is still 145 mW at BOL. This is higher than achieved/investigated in recent TRISO fuel irradiation tests [14]. The volume of a compact is 6.136 cm³. So, the power of a single compact filled with 2500 coated particles @ 145 mW would be 362.5 W, corresponding to a power density of 59.1 W/cm³. In the design of the HTR-PM [15], an average power of 0.6 kW per spherical fuel element ("pebble"; 250 MW thermal power and 420000 pebbles in core) is assumed during operation, with a maximum value of 1.8 kW. This corresponds

to an average value of 51 mW per coated particle, and a maximum value of 154 mW. This is even slightly higher than the maximum value found for the GEMINI+ HTGR, as shown in Fig. 10, while the average power per coated particle is of the same order of magnitude (approx. 37 % higher for the GEMINI+ HTGR than for the HTR-PM).

Nevertheless, further reduction of the maximum power per particle, if desired, could e.g. be achieved by increasing the number of coated particles per compact (however, see Section IX).

Another, perhaps more feasible, method of reducing the maximum power per coated particle (and per compact) would be again to flatten the axial power profile. In the current configuration, the average power per coated particle is 69.6 mW. The (axial) power peaking factor is therefore $145/69.6 = 2.08$ for case 214 at BOL. As can be seen in Figs. 9 and 10, in the early stages of the cycle ("A" and "B") the power peak occurs in the upper half of the core. Near the end of the cycle ("C") a similar peak occurs in the lower half of the core, reflecting that the fuel in upper half has been mostly depleted, due to the earlier high power in the upper half. A convenient way to show this effect is the axial offset F_{AO} :

$$F_{AO} = (P_{upper} - P_{lower}) / (P_{upper} + P_{lower})$$

In this equation P_{upper} is the power in the upper half of the core and P_{lower} is the power in the lower half. Fig. 13 shows the axial offset as function of operation time for cases 202 and 214. The curves nearly coincide, going from 0.58 at

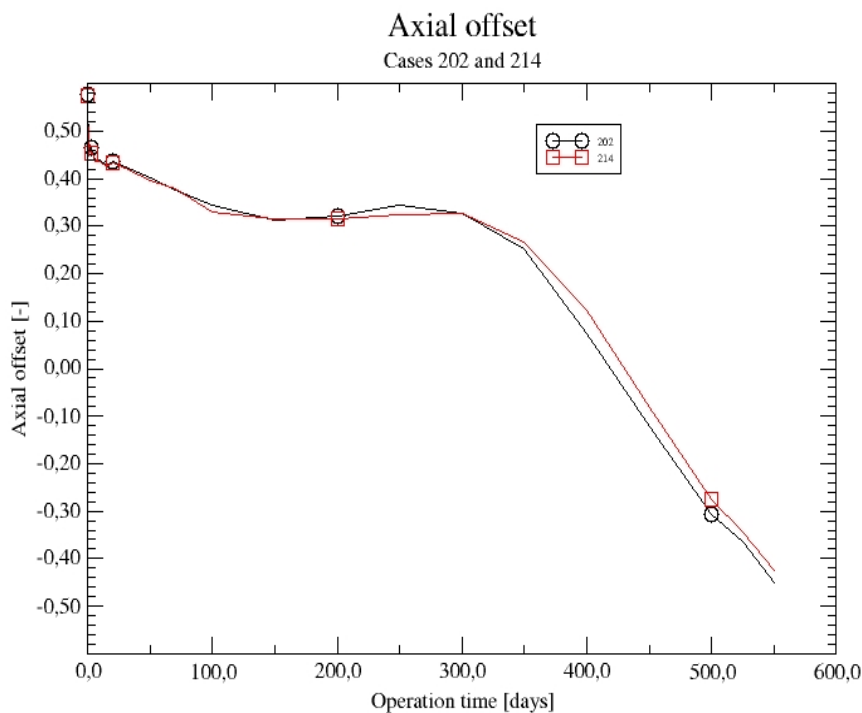


Fig. 13. Axial offset as function of operation time for cases 202 and 214.

BOL to -0.43 and -0.45 at EOL. The presence of a power- (flux-) dependent absorber (^{135}Xe) just after BOL already reduces the initial power peak (F_{AO} starts at 0.58 and decreases to approx. 0.45 at Xenon equilibrium, $t = 3$ days). This is also an indication that increasing the BP density in the upper half of the core could be effective, perhaps even without axially profiling the enrichment, in decreasing the initial power peak in the upper half at BOL, thereby also decreasing the power peak in the lower half towards EOL.

VII. TEMPERATURE COEFFICIENTS OF REACTIVITY

An important aspect for safe operation of any nuclear reactor are the temperature coefficients of reactivity α . In HTGRs usually the following distinction is made:

- Fuel (“ α_F ”): material in the kernel and the coating layers.
- Moderator (“ α_M ”): matrix material of the compacts and the graphite of the fuel blocks constituting the core.
- Reflector (“ α_R ”): graphite of top-, bottom- and radial reflectors.

The temperature coefficients of reactivity have been calculated as follows:

$$\alpha_x = [(1/k_{\text{eff,ref}}) - (1/k_{\text{eff,x}})] / \Delta T_x$$

In this equation $x = F$ (Fuel), M (Moderator), R (Reflector) or A (all materials), and $k_{\text{eff,ref}}$ is the multiplication factor for the reference state. This concerns the reference temperature distributions at CZP (all materials at 300 K), HZP (all materials at 600 K) and HFP (temperature distribution as calculated by SPECTRA at BOL and used in the HFP calculations presented so far). ΔT_x is the (spatially uniform) increase in temperature of the materials (F,M,R,A) of interest. In the calculations $\Delta T_x = 30$ K was used. To obtain sufficient accuracy in the calculated values, the calculations of $k_{\text{eff,ref}}$ and $k_{\text{eff,x}}$ were performed with 1000 cycles, 400000 neutrons per cycle and 100 inactive cycles. This resulted in a standard deviation of 5 pcm in the calculated values of k_{eff} and, consequently, an uncertainty of 0.3 pcm/K in the calculated values of α_x .

Table 4 shows the temperature coefficients of reactivity as calculated for the BOL, Xe-free state of case 202. For most states/configurations, the coefficients

Table 4. Temperature coefficients of reactivity (fuel, moderator, reflector) for case 202, BOL (Xe-free), in pcm/K. The uncertainty in the calculated values of the temperature coefficients is 0.3 pcm/K.

| Configuration/State | α_F (Fuel) | α_M (Moderator) | α_R (Reflector) | Sum | α_A |
|---------------------------------------|-------------------|------------------------|------------------------|--------|------------|
| CZP, all rods in | -10.0 | -38.1 | -162.0 | -210.1 | -48.7 |
| HZP, all rods in | -6.8 | -4.0 | -0.8 | -21.6 | -20.2 |
| HZP, core rods out, reflector rods in | -4.6 | -10.2 | 0.4 | -14.4 | -15.1 |
| HZP, all rods out | -4.1 | -8.6 | 1.2 | -11.5 | -11.3 |
| HFP, core rods out, reflector rods in | -5.3 | -9.7 | 0.3 | -14.7 | -14.4 |
| HFP, all rods out | -3.1 | -7.4 | 1.9 | -8.6 | -9.7 |

for all (F,M,R) materials are negative. However, for the HZP and HFP states, in which core rods and/or reflector rods have been withdrawn, the coefficients for the reflector are (slightly) positive. A positive coefficient of reactivity for the reflector temperature is a well-known phenomenon in HTGRs.

Comparing the sum of the (F,M,R) coefficients with the coefficient for temperature change in all materials shows that the reactivity effects are reasonably linear at HZP and HFP, but strongly non-linear at CZP.

The current coefficients have been calculated for a uniform increase of 30 K in temperature for the material (F,M,R,A) under consideration. To take into account the influence of localised changes in temperature on the reactivity in e.g. (transient) thermal hydraulic calculations, e.g. local **weight factors** can be used. In one-energy group approximation, and under the assumption that absorption is the dominant effect, it can be shown by first-order perturbation theory that the local neutron flux squared can be regarded as the proper weight function/weight factor for reactivity effects, caused by local variations of the effective local macroscopic absorption and fission cross sections [16]. So, in first order approximation (i.e. local variation in effective macroscopic cross sections is proportional to local variation in temperature) this is also the case for the reactivity effect of local temperature variations, i.e. the local weight factor.

The results shown so far concern case 202 (uniform initial BP parameter distribution) at BOL. Calculations of temperature coefficients of reactivity are currently (January 2021) ongoing for case 202 beyond BOL (i.e. MOL and EOL) and also for all corresponding states of case 214. Table 5 shows some results for case 202 at MOL (250 full power days) and EOL (525 full power days), at

Table 5. Temperature coefficients of reactivity (fuel, moderator, reflector) for case 202, MOL (250 full power days) and EOL (525 full power days), in pcm/K. The uncertainty in the calculated values of the temperature coefficients is 0.3 pcm/K.

| MOL | | | |
|--------------|------------------------|---------------|--------------|
| State | Coefficient | Eq. Xe | No Xe |
| CZP | α_A | -42.1 | -40.9 |
| CZP | α_F (Fuel) | -11.4 | -11.0 |
| CZP | α_M (Moderator) | -30.4 | -29.6 |
| CZP | α_R (Reflector) | -86.7 | -83.3 |
| CZP | Sum | -128.5 | -123.9 |
| HZP | α_F (Fuel) | -7.5 | -6.7 |
| EOL | | | |
| State | Coefficient | Eq. Xe | No Xe |
| CZP | α_A | -46.9 | -45.6 |
| CZP | α_F (Fuel) | -10.2 | -11.2 |
| CZP | α_M (Moderator) | -36.3 | -34.6 |
| CZP | α_R (Reflector) | -113.9 | -114.6 |
| CZP | Sum | -160.4 | -160.4 |
| HZP | α_F (Fuel) | -6.3 | -6.7 |

CZP and HZP, all rods in. Comparing the results at MOL and EOL (Table 5) with those at BOL (Table 4), it can be concluded that the reactivity coefficients seem to retain the same characteristics (both at equilibrium and zero xenon) throughout the entire cycle.

VIII. AXIAL XE-OSCILLATIONS?

In the current design of the GEMINI+ HTGR the core height has been increased to 8.8 m. This has raised the concern of the possibility of occurrence of axial oscillations (axial instability) of the power, related to the changing densities of ^{135}Xe in the upper and lower half of the core. As a relatively simple first check, the following test was performed for case 202:

- At BOL, HFP, all core rods are out, reflector rods are 50% inserted (all reflector rod tips at 600 cm elevation), followed by full power operation for 3 days until Xe-equilibrium. This was calculated with the normal time steps, also used in the full burn up calculations. At $t = 3$ days, the reactor state is written to a restart file.
- At $t = 3$ days the calculation is continued from the restart file, with the reflector rods fully withdrawn. This calculation was done twice, with different time steps (32 time steps of 0.1 day and 2 time steps of 0.1 day, followed by 15 time steps of 0.2 days, respectively) to detect possible dependence upon the choice of the time steps.

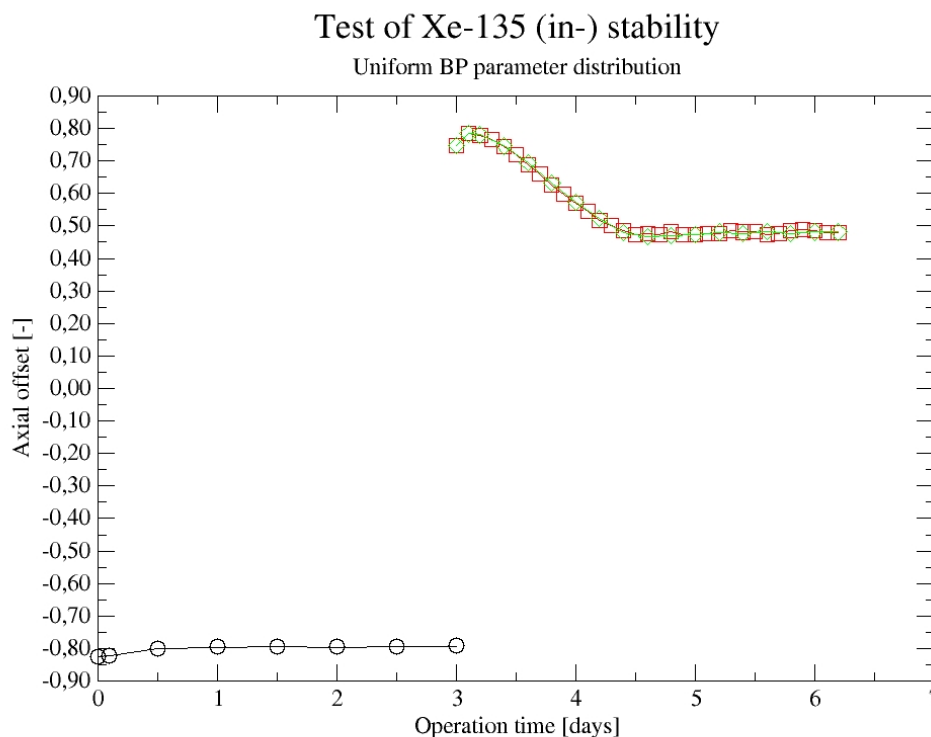


Fig. 14. Test of axial ^{135}Xe -related instability.

During the entire test, the same HFP temperature profile was used, excluding thermal feedback effects.

Results of this test are shown in Fig. 14. In this figure the axial offset F_{AO} is shown as function of time for the first (“black circles”) and second phase (“red squares” and “green diamonds”) of the test. In the first phase, all reflector rods are 50 % inserted. As the total reactor power is being kept constant at 180 MWth, the vast majority of the power is being generated in the lower half of the core, resulting in a strongly negative axial offset: -0.83 at BOL, increasing to -0.80 at Xe-equilibrium. A relatively high concentration of ^{135}Xe and ^{135}I has been built up in the lower half, where most of the power is being generated. At $t = 3$ days, the reflector rods are fully withdrawn. This immediately pushes the power peak to the upper half of the core, resulting in a strongly positive axial offset of 0.74. Decaying ^{135}I into ^{135}Xe in the lower half suppresses the power in the lower half further for a while, causing the axial offset to increase further to 0.78. Because of the now high power in the upper half, both ^{135}I and ^{135}Xe concentrations are increasing in the upper half, while still decreasing in the lower half, until equilibrium is reached again at $t = 4.6$ days, corresponding to the “usual” axial offset of the reactor at HFP near BOL, as shown in Fig. 13. Apart from the little “overshoot”, immediately after withdrawal of the reflector rods, no “oscillatory” behaviour seems to occur.

It should be noted, however, that highly positive or negative values of the axial offset mean that almost the full reactor power is generated in only half the core, resulting in even higher local power densities in coated particles and compacts. This should be avoided anyway. Therefore, it is advisable to avoid as much as possible partially inserted (reflector) rods during full power operation: rods should, as much as possible, be either fully in or fully out.

In the test presented here, a constant HFP temperature profile has been used, thereby excluding thermal feedback effects. It is desirable to repeat the test with full thermal feedback, also at other points in time in the cycle.

IX. STEAM INGRESS

A final topic is the ability to render the reactor subcritical in case of steam ingress (HZP/HFP state only). Fig. 15 shows the influence of the steam density in the coolant on the k_{eff} , for 12 % enrichment and uniform BP parameters as in case 202. In case of 2500 coated particles per compact, the reactor can be kept subcritical with the core rods only with a maximum steam density of 0.09 g/cm³ steam in the coolant. When both core and reflector rods can be used this is 0.15 g/cm³. Higher numbers (3000 and 3760) of coated particles per compact result in a lower C/U-ratio (moderator-to-fuel ratio) in the core and a (slightly) higher reactivity increase due to steam ingress. This will not necessarily be detrimental, as some other parameters (e.g. BP parameters, fuel enrichment) may be adapted to lower the uncontrolled (all rods out) BOL k_{eff} .

Also note that, as can be seen in Fig. 15, the reactivity worths of the control rods decrease with increasing steam density in the core. So, in any case,

measures will be necessary to limit the possible amount of steam that can enter the primary circuit.

Similar to the calculation of the temperature reactivity coefficients, the analyses of steam ingress will also need to be done for points in time beyond BOL, also for the further (axially) optimised configurations of the BP parameter distribution.

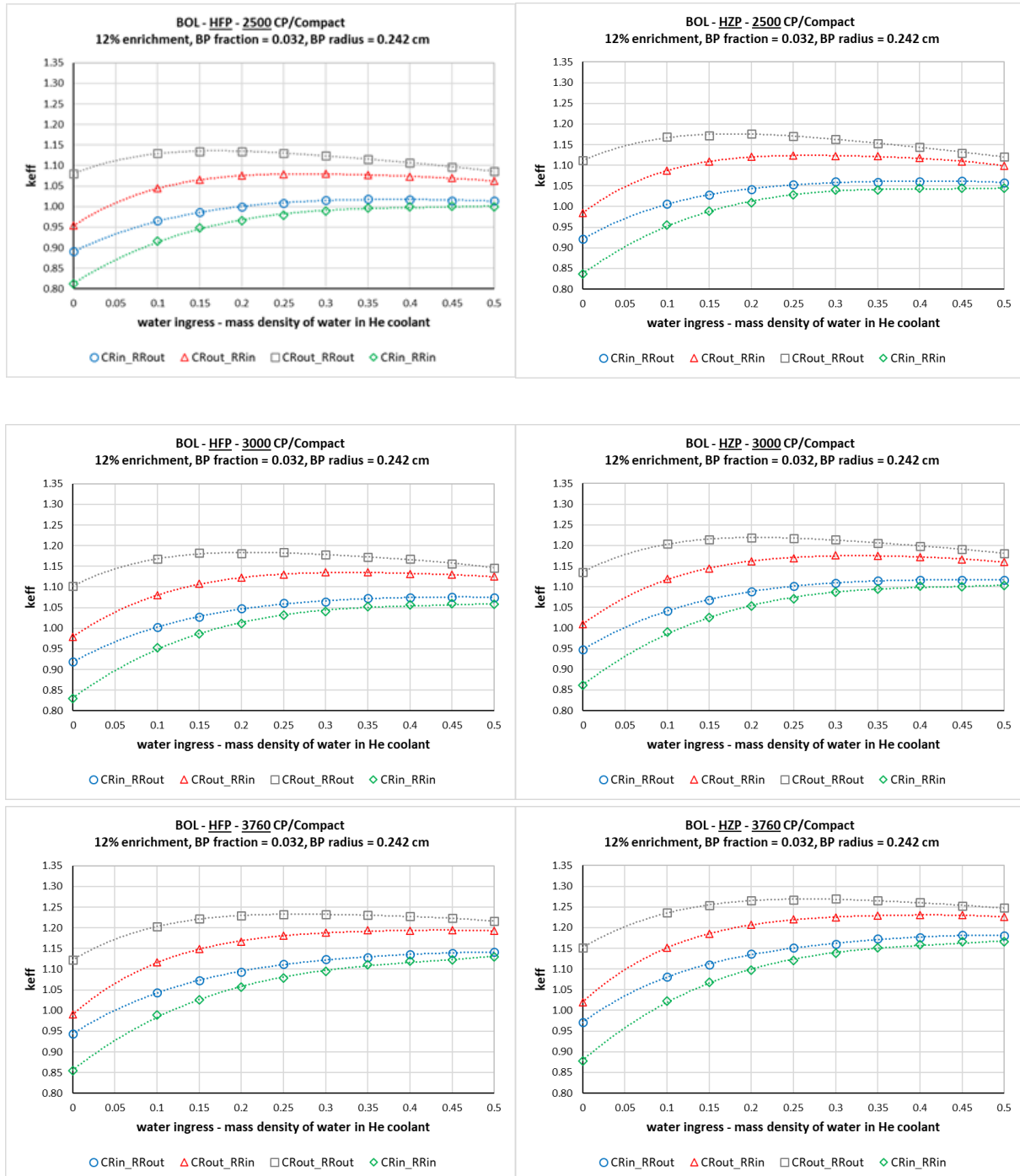


Fig. 15. Steam ingress at BOL/HFP and HZP, for 2500, 3000 and 3760 coated particles per compact, 12 % enrichment and uniform initial BP parameter distribution as in case 202.

X. FLUX INSTRUMENTATION AND STARTUP SOURCE

As is described in the final GEMINI+ Safety Options Report [17], The instrumentation for measuring the (thermal) neutron field is partly located in 6 regularly spaced channels in the permanent reflector. For the purpose of the present analysis it is assumed that these channels are located in the 6 slightly wider parts of the permanent reflector, each located “behind” the central 0 rod of each set of 3 reflector rods (see Fig. 1). This concerns the [17]:

- 18 in-vessel fission chambers located in the permanent reflector at 3 levels of the core (top, centre and bottom) will control the **flux during operation at full and partial power** (thermal flux range: $10^3 - 10^{13} \text{ cm}^{-2}\text{s}^{-1}$).
- in-vessel proportional counters of the same type as those used for start-up and shutdown (see below) will be used for controlling the **flux during refuelling**, but as the flux is very low in such conditions, these counters will be located inside the vessel at the level of the core centre. They will be introduced in 3 regularly spaced of the 6 channels used for the fission chambers. During power operation, these detectors will be removed beyond the core region.

Another set of 6 regularly spaced instrumentation channels is located in the reactor cavity concrete. The flux instrumentation in these channels consist of [17]:

- 6 ex-vessel proportional counters located at the core centre level will control the **flux during start-up and shutdown operation** (thermal flux range $5 \times 10^{-2} - 5 \times 10^4 \text{ cm}^{-2}\text{s}^{-1}$).

As this part of the system has not yet been included in the SERPENT neutronics model, these detectors have not been included in the analysis presented here.

Table 6 shows the results (k_{eff} and thermal flux at detector positions for a (hypothetical) 180 MW thermal power of the reactor. The configuration for these calculations is “case 202” (see earlier sections). The (fission) neutron source at 180 MW is $1.3437 \times 10^{19} \text{ s}^{-1}$. Figs. 16 shows the vertical distribution of

Table 6. k_{eff} and thermal neutron flux in the instrumentation channels in the permanent reflector.

| Case description (base case: run 202) | K-eff [-] | Thermal flux (top) [$\text{cm}^{-2}\text{s}^{-1}$] | Thermal flux (midplane) [$\text{cm}^{-2}\text{s}^{-1}$] | Thermal flux (bottom) [$\text{cm}^{-2}\text{s}^{-1}$] | Thermal flux (max) [$\text{cm}^{-2}\text{s}^{-1}$] |
|---|--------------|--|---|---|--|
| CZP; all rods in (Run 179) | 0.91284(12) | 3.600E+11 | 3.100E+12 | 1.170E+12 | 3.200E+12 |
| CZP; rods in 60 degr. sector out (reload); high channel (Run 182) | 0.97710(13) | 3.630E+12 | 2.870E+13 | 8.500E+12 | 2.870E+13 |
| CZP; rods in 60 degr. sector out; low channel (Run 182) | 0.97710(13) | 1.900E+11 | 1.730E+12 | 6.400E+11 | 1.730E+12 |
| HFP; CR out; RR in (Run 185) | 0.95005(12) | 2.560E+12 | 3.600E+12 | 3.000E+11 | 6.200E+12 |
| HFP; all rods out (Run 192) | 1.07566(12) | 1.000E+13 | 1.650E+13 | 1.680E+12 | 2.500E+13 |

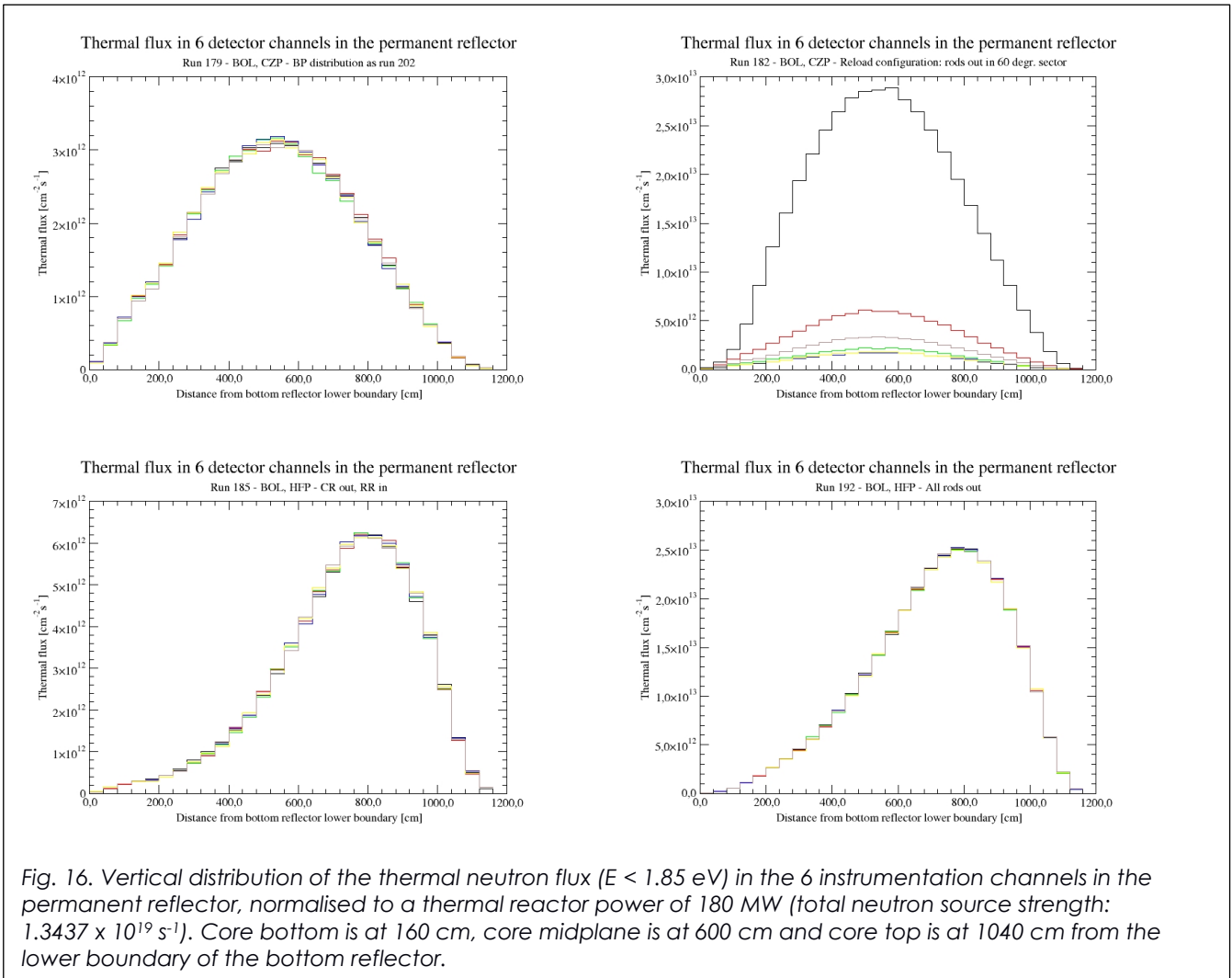


Fig. 16. Vertical distribution of the thermal neutron flux ($E < 1.85$ eV) in the 6 instrumentation channels in the permanent reflector, normalised to a thermal reactor power of 180 MW (total neutron source strength: $1.3437 \times 10^{19} \text{ s}^{-1}$). Core bottom is at 160 cm, core midplane is at 600 cm and core top is at 1040 cm from the lower boundary of the bottom reflector.

the thermal neutron flux (energy $E < 1.85$ eV) in the instrumentation channels in the permanent reflector for this situation. Note that in the CZP states (runs 129 and 182) the peak of the thermal flux distribution is at or near the core midplane, whereas in the HFP situation the maximum of the flux is at approx. 800 cm from the lower boundary of the bottom reflector. This corresponds to the power peak in the upper half of the core (see Fig. 9). Note that for HFP, all rods out (run 192), the thermal neutron flux at core midplane is $1.56 \times 10^{13} \text{ cm}^{-2}\text{s}^{-1}$ and the maximum thermal flux (at 800 cm elevation) is $2.5 \times 10^{13} \text{ cm}^{-2}\text{s}^{-1}$. This is slightly higher than the upper boundary of the thermal flux range of the currently envisaged fission chamber.

On the basis of the calculations at CZP it is possible to estimate the “external” neutron source strength, required to obtain a measurable neutron signal in the proportional counters placed in any instrumentation channel in the permanent reflector at core midplane during refuelling operation, obviously in subcritical condition. The minimum required thermal flux for detection by the envisaged proportional counter is $5 \times 10^{-2} \text{ cm}^{-2}\text{s}^{-1}$. Excluding source multiplication ($M = (1 - k_{eff})^{-1}$), the position opposite to the extracted control rods in the 60 degrees sector (Fig. 16, case 182, lowest curve at 600 cm) requires the highest “external” source strength to obtain a signal in the proportional counter: **$3.91 \times 10^5 \text{ s}^{-1}$** . If a detector signal is also required in the

positions at core bottom and core top, the required source strength becomes $3.56 \times 10^6 \text{ s}^{-1}$. This estimation does not take into account the specific location of the “external” source. This should be done by a so-called fixed source calculation, to be part of further, detailed design analyses of the GEMINI+ reactor system. These future analyses should also include the instrumentation channels in the reactor cavity concrete.

XI. CONCLUSIONS

Extensive neutronics calculations have been performed on the current (June 2020) design of the 180 MWth GEMINI+ HTGR. Neutronics features seem quite promising, but further improvements and therefore further investigations would be desirable, especially concerning:

- Temperature coefficients of reactivity, control rod worths, etc. beyond BOL at operational HZP and HFP states, also for further optimised configurations of the BP parameter distribution.
- Thermal hydraulic feedback, reflecting the considerable change axial power profile during the operation cycle. In the current calculations, the temperature distribution has been kept constant throughout the operation cycle, as was initially envisaged. Adapting this to the actual power distribution at each point in time would be desirable.
- Further reduction of the axial power peaking, thereby reducing the maximum power per compact and per coated particle and also improving the fuel utilisation. Possible methods are axial profiling of BP parameters, axial profiling of enrichment and/or a multi-batch loading scheme.
- Increasing the number of coated particles per compact, possibly in combination with changing the enrichment and/or the BP parameter distribution.

Acknowledgement

This work is part of the GEMINI+ project, funded from the European Union's Horizon 2020 research and innovation programme under grant agreement No. 755478.

The high precision monte carlo calculations were carried out on the HPC cluster of the Swierk Computing Centre (CIS), National Centre for Nuclear Research (NCBJ), Poland.

References

- [1] “GEMINI+ - Research and development in support of the GEMINI Initiative“, Euratom Horizon 2020 project 755478, 1 September 2017 - 31 August 2020.
- [2] B. Lindley, M. Davies (Jacobs), D. Hittner (LGI), M.M. Stempniewicz, E.A.R. de Geus (NRG), J. Kuijper (NUCLIC), G. Brinkmann, D. Vanvor (BriVaTech),

- "Final Description and Justification of the GEMINI+ System", GEMINI+ Deliverable D2.5, 30 June 2020.
- [3] "GT-MHR Reactor System Design Description" – Int. GT-MHR 100002 – RE – 11.6, Rev.1, November 1997.
- [4] "Preliminary Safety Information Document for the Standard MHTGR" – DOE/HTGR – 086 – 024 – Vol. 1 (1986)SC-HTGR, 1986.
- [5] L. Lommers, F. Shahrokhi, J. Mayer III, F. Southworth, "AREVA Modular Steam Cycle – High Temperature Gas-Cooled Reactor Development Progress", Proc. HTR 2014, Weihai, China, 27-31 October 2014.
- [6] W. von Lensa, "NBG-17 graphite composition", private communication, 14 June 2018.
- [7] Leppänen, J., et al. (2015) "The SERPENT Monte Carlo code: Status, development and applications in 2013", Ann. Nucl. Energy, 82 (2015) 142-150.
- [8] "SPECTRA - Sophisticated Plant Evaluation Code for Thermal-Hydraulic Response Assessment, Version 3.61, January 2020, Volume 1 – Program Description, Volume 2 – User's Guide, Volume 3 – Verification and Validation", NRG report K6223/20.166353 MSt-200130, Arnhem, January 2020, <https://www.nrg.eu/fileadmin/nrg/Documenten/Spectra-Vol1.pdf>
- [9] M.M. Stempniewicz, "Thermal-Hydraulic Model of the GEMINI+ HTR Plant - Safety Analysis, WP1.6", NRG report 24203/19.153415, 30 May 2019.
- [10] M.M. Stempniewicz, "TH Analyses of GEMINI+ HTR Plant (8.0 m) Results of PLOFC and DLOFC Scenarios", NRG report 24203/19.153912, 30 June 2019.
- [11] M.M. Stempniewicz, "GEMINI+ HTR Plant Model - Conversion from 8.000 m core to 8.800 m core", NRG report 24203/19.154307 Rev. 0, 12 August 2019.
- [12] M.M. Stempniewicz, "TH Analyses of GEMINI+ HTR Plant (8.8 m) - Results of PLOFC and DLOFC Scenarios", NRG report 24203/19.154308, 20 July 2019.
- [13] NCBJ to NUCLIC, Internal communication of the GEMINI+ project, 2019/2020.
- [14] M. Feltus, "TRISO FUELS", Webinar, Gen IV International Forum, 18 December 2019, https://www.gen-4.org/gif/jcms/c_114200/gen-iv-webinar-series-36-madeline-feltus-webinar-presentation-18-december-2019.
- [15] "Status report 96 - High Temperature Gas Cooled Reactor - Pebble-Bed Module (HTR-PM)", Advanced Reactor Information System (ARIS), IAEA, <https://www.iaea.org/resources/databases/advanced-reactors-information-system-aris>.
- [16] H. van Dam, T.H.J.H. van der Hagen, J.E. Hoogenboom, "Nuclear Reactor Physics", Lecture notes AP3341, Delft University of Technology, The Netherlands, April 2005.
- [17] G. Brinkmann, D. Vanvor, A. Jung, "Final GEMINI+ Safety Options Report", GEMINI+ Deliverable D2.7, 20 April 2020.

Part B - Initial SERPENT neutronics calculations on basic HTGR configuration A (no burnable poison) - GEMINI+, WP2, Task 4.2

Part B contains the results of the neutronics calculations on the basic, 10-layer design of the GEMINI+ HTGR, without burnable poison, as presented earlier (September 2019) for internal purposes in NUCLIC note N19060 version 02 [1].

[1] J.C. Kuijper, D. Muszynski, "Initial SERPENT neutronics calculations on basic HTGR configuration A (no burnable poison) - GEMINI+, WP2, Task 4.2", NUCLIC note N19060 version 02, 4 September 2019.

Introduction - Objectives

In Work Package 2, Task 2.4 of the GEMINI+ project [1] neutronics calculations have to be performed on one or more designs of a small, 180 MWth, prismatic HTGR. The objectives of the task are the following:

“...to calculate core and reflector (prompt and decay) power distribution (initial and/or equilibrium cycle) and associated temperature distribution in the reactor pressure vessel and its internals. The calculations will be performed for the different options considered in WP2 and WP3. These include e.g. the study of innovative design changes, e.g. the use of alternative reflector materials to obtain a smaller reactor diameter. A reference configuration will be selected. If needed, the fast fluence on the reactor vessel and critical structures will also be calculated. Converged steady-state distributions of power and temperatures will be obtained by a small number of iterations between a 3-D core neutronics (power) model (by NUCLIC) and a 3-D core thermal hydraulics model (by NRG), consistent with the T/H models employed in the transient analyses in WP1, task 1.6.

Steady-state power and temperature distributions for the reference configuration and, if needed for the decision, also for selected different options, will be used as initial conditions for accident calculations in task 1.6 of WP1. Also, reactivity feedback coefficients will be generated for those accidents transient cases for which re-criticality cannot be excluded.”

This note presents the (initial) neutronics studies and calculations, directly based on the initial configurations, as given in [2]. See note N18062 [3] for the planning of the work. The follow-up work (see note N19059 [4]) will include the introduction of burnable poison to improve the reactor characteristics, e.g. the BOL (“Beginning of Life”) to EOL (“End-of-Life”) reactivity swing and the power distribution.

Initial neutronics focus

The initial SERPENT [5] neutronics calculations on prismatic HTGR designs in the GEMINI+ project focused on the following topics:

1. Fast (> 1 MeV and/or > 0.1 MeV) and total flux/fluence of core barrel and pressure vessel (average and local peak values).
2. Burn up and core lifetime (for a given initial fuel loading). Reactivity change over the lifetime of the core.
3. Decay heat fraction and effective delayed neutron fractions (per time-group).
4. Detailed (3-D) power distribution (including -peak- power).
5. Influence of temperature (distribution) on reactivity.
6. Influence of poisons (Xe-235 and Sm-149) on reactivity.
7. Influence of control rods on reactivity.

8. Iterative calculations with both SERPENT and the thermal hydraulics code SPECTRA [6], using updated distributions for temperature and power,

Table 1. Main configuration characteristics of **Configuration A** (SERPENT model) (see [2] for further details).

| Parameter | Value | Unit |
|---|---------------------|------|
| Reactor/core configuration | - | - |
| # Radial rings of fuel blocks (ring around center column is first ring) | 3 | - |
| # Fuel block columns | 25 | - |
| # Control block columns | 6 | - |
| # Axial fuel/control block layers | 10 | - |
| Distance between side faces of adjacent blocks | 0.2 | cm |
| Core height | 800 | cm |
| # Replaceable reflector rings | 2 | - |
| # Replaceable reflector columns | 54 | - |
| Bottom reflector (with coolant holes) | - | - |
| Reflector material | NBG-17 graphite [9] | |
| Reflector thickness | 160 | cm |
| Top reflector (with coolant and control rod holes) | - | - |
| Reflector material | NBG-17 graphite [9] | - |
| Reflector thickness | 120 | cm |
| Core barrel | - | - |
| Core barrel inner radius | 199.1 | cm |
| Core barrel effective outer radius | 201.1 | cm |
| Core barrel material | steel 800H [2] | - |
| Core barrel height (in SERPENT model) | 1080 | cm |
| Reactor Pressure Vessel | - | - |
| RPV inner radius | 234.1 | cm |
| RPV outer radius | 244.05 | cm |
| RPV material | steel SA508 [2] | - |
| RPV height (in SERPENT model) | 1080 | cm |
| Fuel block configuration (without BP) | - | - |
| Block height | 80 | cm |
| Hexagon flat-to-flat distance | 36 | cm |
| Block material | NBG-17 graphite [9] | - |
| Triangular pitch | 1.9 | cm |
| # channels with fuel compacts | 216 | - |
| Compact channel diameter | 1.27 | cm |
| # small coolant channels | 6 | - |
| Small coolant channel diameter | 1.27 | cm |
| # large coolant channels | 102 | - |
| Large coolant channel diameter | 1.6 | cm |
| Control block configuration | - | - |
| Block height | 80 | cm |
| Hexagon flat-to-flat distance | 36 | cm |
| Block material | NBG-17 graphite [9] | - |
| Triangular pitch | 1.9 | cm |
| # channels with fuel compacts | 178 | - |
| Compact channel diameter | 1.27 | cm |
| # small coolant channels | 5 | - |
| Small coolant channel diameter | 1.27 | cm |
| # large coolant channels | 102 | - |
| Large coolant channel diameter | 1.6 | cm |
| Control rod channel diameter | 13 | cm |

respectively, to obtain a converged power- and temperature field, so far at BOL state only.

Table 1 (cont.). Main (initial) characteristics of **Configuration A** (SERPENT model) (see [2] for further details).

| Parameter | Value | Unit |
|-----------------------------------|------------------|-------------------|
| Control rod configuration (model) | - | - |
| # core rods | 6 | - |
| # reflector rods | 18 | - |
| Rod geometry | Annular | - |
| Rod length | 800 | cm |
| Inner radius | 3.75 | cm |
| Outer radius | 5.25 | cm |
| Absorber material | B ₄ C | - |
| Absorber material density | 2.52 | g/cm ³ |
| Fuel compact configuration | - | - |
| Matrix material | C | - |
| Matrix material density | | g/cm ³ |
| # coated particles per compact | 2500 | - |
| Coated particle configuration | - | - |
| Kernel diameter | 500 | micron |
| Kernel material | UO ₂ | - |
| Kernel density | 10.4 | g/cm ³ |
| Buffer layer thickness | 95 | micron |
| Buffer layer material | C | - |
| Buffer layer density | 1.05 | g/cm ³ |
| Inner PyC layer thickness | 40 | micron |
| Inner PyC material | C | - |
| Inner PyC density | 1.90 | g/cm ³ |
| SiC layer thickness | 35 | micron |
| SiC material | SiC | - |
| SiC density | 3.18 | g/cm ³ |
| Outer PyC layer thickness | 40 | micron |
| Outer PyC material | C | - |
| Outer PyC density | 1.90 | g/cm ³ |

NUCLIC used SERPENT version 2.1.29 in conjunction with JEFF 3.1.1 nuclear data for the calculations. This mainly comprised test runs for (further) development of the models. Calculations with improved statistics were performed on the computer cluster of NCBJ by SERPENT version 2.1.30 with JEFF 3.1.1 nuclear data. For a detailed description of SERPENT (version 2) input options, see [6].

Main features of the configuration(s)

The initially proposed reactor (core) configurations have been described in [2]. From these, two configurations were initially selected for the thermal

hydraulics studies by NRG Arnhem, NL, using the SPECTRA code [7,8]. These configurations are shown in Fig. 1.

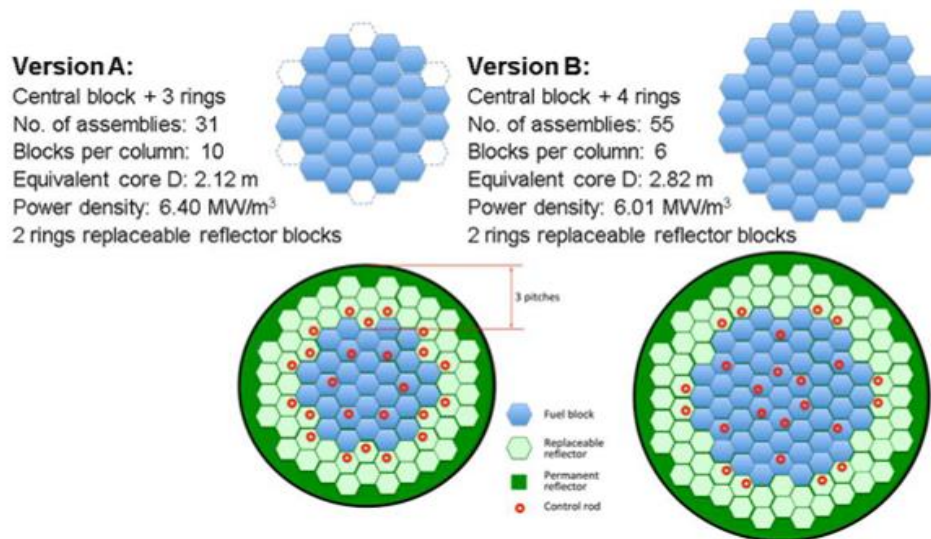


Fig. 1. Configurations A and B [2].

It was decided (see [4]) to focus the neutronics analysis on Configuration (“Version”) A, as this was considered to be the more favourable configuration from the point of view of transport of the reactor vessel (smaller vessel diameter than for Configuration B), while it is expected that the neutronic and thermal hydraulic properties will still be acceptable. The latter is obviously to be confirmed by the foreseen computational analyses.

Main characteristics of the basic Configuration A model are listed in Table 1. Some aspects of the SERPENT geometry are shown in Figs. 2 - 4. Note that the model includes 24 control rods (6 in the core, 18 in the reflector) that can be axially positioned individually.

Fuel management/loading

The fuel management/loading has been kept as simple as possible. A single batch loading scheme, with fresh fuel in the entire core at BOL, was assumed for these initial calculations. Core life should be 18 to 24 months. The fuel model is a 75 cm stack of 15 compacts containing 37500 UO₂ coated particles per stack (i.e. **2500 per compact**, which is lower than was proposed in [2]). All coated particles have been modelled and positioned explicitly. The initial core design does not include burnable poison. However, it is envisaged that it will be necessary to include this in order to reduce the BOL (Beginning Of Life)-to-EOL (End Of-Life, after 18 to 24 months of operation) reactivity swing, as well as to improve the spatial power distribution.

Temperature distribution

Initial test calculations (as well as calculations at CZP - “Cold Zero Power” - uniform room temperature; 300K) were performed using a uniform temperature distribution for each of the materials. Later, the SERPENT “multi-

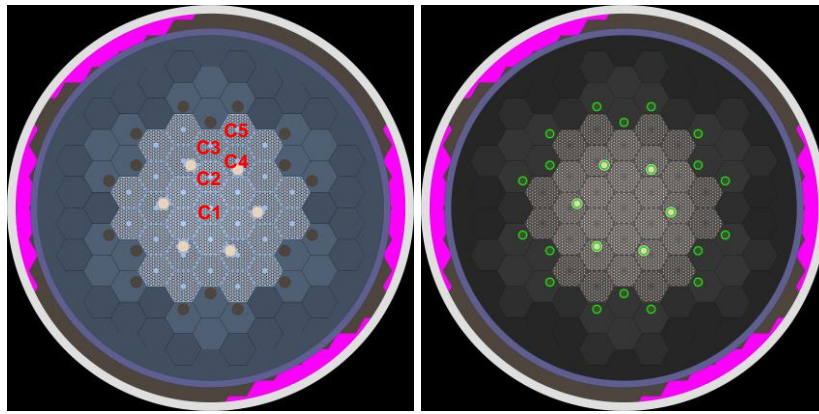


Fig. 2. Horizontal cross section of SERPENT model of configuration A, without (left) and with (right) annular control rods. The different shades of grey indicate differences in temperature. The purple sections indicate areas not covered by the "multi-physics" temperature input for core and reflector (as it is currently used; no influence on the results). As these only comprise the outer sections, the influence on the neutronics is negligible. "C1" - "C5" indicate 5 columns of fuel (or control) blocks, that are representative for the different columns in the core.

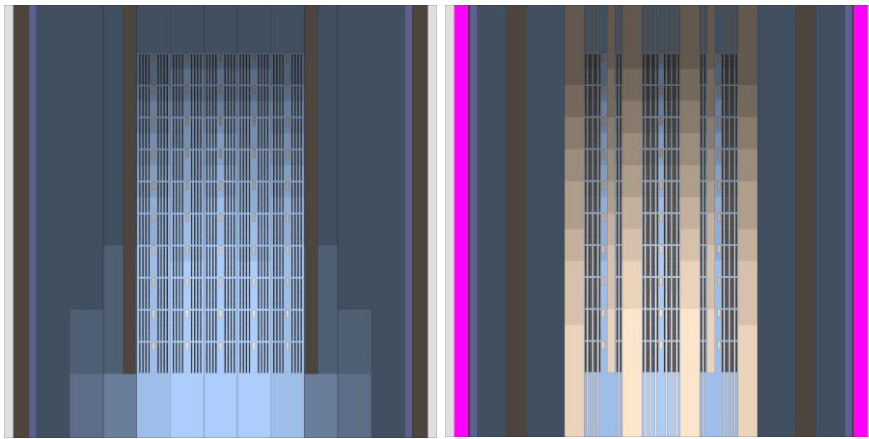


Fig. 3. Vertical cross sections of the SERPENT model of configuration A, without control rods. The different shades indicate differences in temperature.

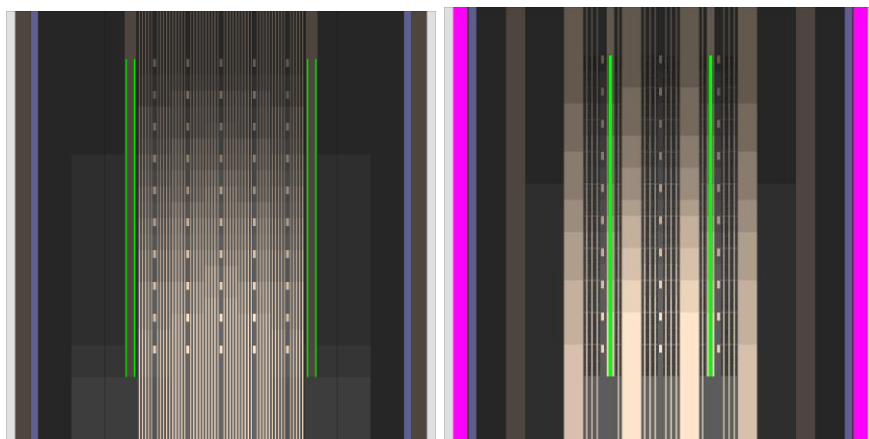


Fig. 4. Vertical cross sections of the SERPENT model, with annular control rods fully inserted. The different shades indicate differences in temperature. In the picture on the right the cut just "touches" two control rods.

physics" interface [6] was used to include 3-D temperature distributions, originating from calculations by the SPECTRA code [7,8]. SERPENT uses "on-

the-fly" cross section processing to adjust to local material temperatures [5,6]. Therefore, it is not necessary to use different materials to represent the same material at locations with different temperatures. It should be noted that most of the initial calculations at HFP ("Hot Full Power") have been performed with the initial temperature distribution originating from the initial SPECTRA calculation [7], i.e. without iterations to obtain a converged combined power and temperature distribution. So far, the full core burn up calculation have been performed assuming the initial temperature distribution for the entire life of the core (BOL to EOL). The validity of this approximation may be limited if the power distribution is changing considerably during burn up.

Core burn-up modelling

The implementation of core burn-up calculations initially assumes a subdivision of the core into 10 layers (1 per fuel block layer), making use of SERPENT's universe-based automatic subdivision of burnable (depleting) materials ("div" keyword [5,6]). In later calculations this has been further refined to 1 depletion zone per block for the fuel (so 310 depletion zones for the entire model). In order to accommodate the analysis of burnable poison behaviour, further refinement is expected to be necessary.

BOL-to-EOL core burn up is calculated with all control rods out. This may be changed in the follow-up activities: assuming that a burnable poison configuration can be found that can keep the BOL-to-EOL reactivity variation sufficiently limited, the calculation could also be performed with partially inserted reflector rods (fixed position), hereby more closely approximating an exactly critical reactor during burn up.

SERPENT input parameter settings

The SERPENT job decks used for the calculations presented in this note have been put on the GEMINI+ electronic content collaboration portal [10] (cases 1-39). The results presented in this note have all been obtained with relatively good statistics (neutron population parameters "set pop 100000 1000 20", i.e. 100000 neutrons per cycle, 1000 cycles, 20 idle cycles at the start) on the NCBJ computer cluster. This is in contrast with the runs with not so good statistics used for the development and testing of the job decks ("set pop 5000 100 20").

Results & discussion

Tables 2 and 3a - 3c give an overview of the initial neutronics calculations, together with the most important direct results. "Temperature profile 05" is the initial temperature profile from the SPECTRA thermal hydraulics calculations, assuming a cosine-shaped power profile [7]. Temperature profiles 6, 7, and 8 (cases 32 - 34) are the results from further neutronic and thermal hydraulic iterations at BOL. The cases 35 - 39 are depletion calculations, for which further information (at 3 and 550 full power days) is given in Tables 3b and 3c.

In the subsections below, some derived results (e.g. difference in k_{eff} between two cases, but also axial power distributions) will be addressed and discussed.

Influence of Xe-135 and Sm-149 on k_{eff} /reactivity

In Table 4 the influence is shown of Xe-135 and Sm-149 (equilibrium density, reached for Xe-135 after approx. 3 full power days, and for Sm-149 after about 15 full power days) on both k_{eff} and reactivity. Note that the reactivity ($\Delta\rho$) effects of Xe-135 and Sm-149 are virtually linear.

Table 4. Influence of Xe-135 and Sm-149 on k_{eff} /reactivity. Configuration A. 14.3% enrichment. No BP. Reactivity effect of Xe-135 and Sm-149 at BOL, HFP. Xe-eq. is reached after approx 2.5 days. Sm-eq. is reached after approx. 2 weeks.

| Case description | Case ID | Δk_{eff} [%] ^{*)} | $\Delta\rho$ [pcm] ^{*)} |
|-----------------------|------------------|------------------------------------|----------------------------------|
| Xe-135 eq., no Sm-149 | 15_20190327_0929 | -3.61 | -1880 |
| Sm-149 eq., no Xe-135 | 14_20190327_0430 | -0.85 | -433 |
| Xe-135 and Sm-149 eq. | 13_20190326_2327 | -4.42 | -2312 |

^{*)}Reference state is HFP, no Xe-135, no Sm-149 (case ID 04_20190325_0730). Xe- and Sm-reactivity effects are linear (1880 + 433 = 2313 \approx 2312 pcm).

Control rod worth at different values of the enrichment

Table 5 (a-d) shows the control rod worths at Hot Full power (HFP) and Cold Zero Power (CZP - "room temperature"), BOL. Not that for this particular configuration (configuration A: uniform -# coated particles per compact, enrichment- fuel blocks and uniform control blocks in the core at BOL; no burnable poison, the 6 in-core rods have a higher worth than the 18 reflector rods. The control rod worth increases with decreasing enrichment but decreases when the temperature is lowered (HFP to CZP state). It is preferred that the reactor can be shut down (and kept in subcritical state) by the reflector rods only (and without the most reactive rod inserted - "stuck rod condition"). This is not possible in the current configuration A, as the currently expected total variation in reactivity (k_{eff}) is too large (i.e. > 16.0%; influence of Xe-135 en Sm-149, BOL-to-EOL depletion, temperature effects; see respective subsections).

Reactivity effect of cooling down from HFP to CZP state

Table 6 shows the influence of cooling down the reactor (from HFP to CZP state) on k_{eff} for different values of the enrichment. Not that the positive reactivity effect associated with cooling down becomes larger for decreasing enrichment.

Evolution of k_{eff} from BOL to EOL

Cases 29_20190329_1504 to 39_20190522_1540 (see Tables 3a-3c) concern the depletion of the fuel during operation from 0 to 550 full power days. The average burn up of the fuel at 500 full power days is approx. 68.3 MWd/kg. In Fig. 5 the evolution of k_{eff} (from BOL to EOL = 550 full power days) is shown for cases 35_20190522_0045 to 39_20190522_1540. Comparing cases 35 and 36, it can be concluded that the number of depletions zones does not seem to have a large influence on the evolution of k_{eff} , as the curves virtually overlap.

However, the evolution of the power distribution (see next section) will certainly be different.

All curves show an initial sharp drop in k_{eff} , associated to ^{135}Xe reaching its equilibrium density (also see Tables 3a – c). Obviously, a further decrease in k_{eff} occurs while progressing until EOL (550 full power days). In Table 7 an overview is given of these changes in k_{eff} and associated changes in reactivity $\Delta\rho$. Note that the equilibrium Xe-effect amounts to approx. -5%, relatively independent from the initial value of the enrichment. The reactivity effect (expressed in pcm) of reaching Xe-equilibrium varies from -2671 pcm (14.3% effective enrichment) to -3548 pcm (6% enrichment). The BOL to EOL reactivity swing varies from -20243 pcm (14.3% effective enrichment) to -59343 pcm (6% enrichment). Note that, from the cases shown, only those with 14% enrichment (14.3 effective) and 12% enrichment can reach 550 full power days. For the other cases, the -uncontrolled- k_{eff} drops below 1 well before the target of 550 full power days has been reached.

Power distribution from BOL to EOL

Even if the (initial) distribution of fuel density (and enrichment) is uniform, the power distribution is not expected to be uniform, both for an assumed flat temperature distribution over the core (e.g. cases 01_20190314_0959 and all “room temperature” (CZP) cases; Tables 2 and 3a – c). In general, generating power in the core will cause a non-uniform temperature distribution (also see next section), and also in that case the power distribution is not expected to be uniform. Such a non-uniform power distribution will cause fuel to deplete in a non-uniform fashion. This will decrease the power in those areas where the power was high, leading to a flattening of the power profile. This is demonstrated in Fig. 6, which shows, for case 35_20190522_0045 the vertical power distribution over the columns of fuel- and control blocks C1 - C5, at BOL, 250 full power days and 550 full power days. It can be seen clearly that the vertical power profile for all columns becomes flatter (i.e. lower peak factor), while going from BOL to EOL. This observation is also of importance as the current calculations are being performed assuming a constant temperature distribution, which is connected to the initial power distribution. A changing power distribution would probably necessitate re-calculation of the temperature distribution at multiple points in time between BOL and EOL. This has to be addressed in the follow-up activities. Delayed neutron fraction SERPENT calculates effective delayed neutron fractions (total and per time group; the latest neutron cross section libraries assume 8 delayed neutron groups [5,6]). Fig. 7 shows the history of the total effective delayed neutron fraction for cases 35_20190522_0045 (14.3% effective enrichment; 10 depletion zones), 36_20190522_0114 (14.3% effective enrichment; 310 depletion zones), 37_20190522_1534 (12% enrichment), 38_20190522_1535 (9% enrichment) and 39_20190522_1540 (6% enrichment). At BOL, the effective delayed neutron fraction β_{eff} is approx. 0.68% for enrichments of 6 - 14.3%. However, towards EOL, β_{eff} is decreasing. This effect is stronger as the enrichment is lower, which can be expected as a larger fraction of the power

and the fission neutrons will be generated by ^{239}Pu (delayed neutron fraction 0.21%) at lower initial enrichments.

Decay heat

SERPENT also calculates the total decay power as well as the specific contributions from actinides and fission products. Figs. 8a - 8c show the total decay power, actinide contribution and fission product contribution, respectively, as function of operation time for cases 35_201909522_0045 (14.3% effective enrichment; 10 depletion zones), 36_20190522_0114 (14.3% effective enrichment; 310 depletion zones), 37_20190522_1534 (12% enrichment), 38_20190522_1535 (9% enrichment) and 39_20190522_1540 (6% enrichment). Note that the total reactor power is 180 MWth. For all cases, the contribution from actinides is about two orders of magnitude lower than that from the fission products. For low enrichments, the actinide contribution grows faster than for high enrichments. In order to obtain the same reactor power, the (thermal) flux needs to be higher for lower enrichments, which causes Np, Pu, and higher actinides to build up faster.

Iteration of power and temperature distribution at BOL

As stated above (section "Power distribution from BOL to EOL"), in HFP cases the temperature distribution will not be uniform: generally, the (fuel kernel-, coatings-, graphite and coolant-) temperature will increase in the downward direction along the flow path of the coolant through the core. For a given power distribution, an associated temperature distribution will emerge, which on its turn influences the power distribution through temperature-induced changes in the local effective neutron cross sections. For the steady-state condition a combined, converged power and temperature field will emerge. For the BOL situation this can be simulated by iterating between neutronics (SERPENT), to calculate the power distribution, and (steady state) thermal hydraulics (SPECTRA [7,8]), to calculate the temperature distribution. Figs. 9a - 9e show the consecutive iterations of the vertical power distributions in columns C1 - C5 (see Fig. 2 for their locations in the core) at BOL: cases 2, 32, 33 and 34 (see Table 2). In case 2 the power profile is calculated, assuming an initial temperature (which was calculated by the SPECTRA code, assuming a cosine-shaped power distribution). Cases 32, 33 and 34 use temperature profiles, calculated by SPECTRA on the basis of the previous power profile. The combined power and temperature distribution can be considered converged after 4 iterations.

Fast flux ($E > 1$ MeV) distribution in the pressure vessel

An important piece of information is the fast flux ($E > 1$ MeV) in the pressure vessel, as it will be influencing the operation lifetime of the vessel. The SERPENT code can extract the information by defining a "detector" [5,6] in the vessel. In this case two such detectors have been used: one to calculate the average fast ($E > 1$ MeV) flux in the vessel and one to calculate the average fast flux in 9 annular segments of 120 cm height each. Both detectors cover the entire height of bottom reflector, core and top reflector, i.e. 1080 cm in total.

It should be noted that the methodology for k_{eff} -calculation in SERPENT (and monte carlo neutronics codes in general) requires that the fission source be being corrected at every iteration by means of dividing by the current estimate of k_{eff} , in order to keep the total neutron population more or less constant. For states that are approximately critical (so $k_{\text{eff}} \approx 1$) the calculated fission source strength (and the related fast flux) will be close to reality. However, for states deviating significantly from $k_{\text{eff}} = 1$, the fast flux should be multiplied by k_{eff} to obtain a more realistic value, i.e. a value that could be expected if the reactor would have been kept in an exactly critical state by means of a homogenously distributed thermal absorber. This would then be compensating for the reduction of the fast (fission) neutron source by a factor k_{eff} .

Fig. 10 shows the vertical distribution of the fast flux (not corrected for k_{eff}) in the vessel (radially and azimuthally integrated) at different moment in the cycle (BOL, Xe-equilibrium and EOL), for cases 36_20190522_0114 (14.3% effective enrichment), 37_20190522_1534 (12% enrichment), 38_20190522_1535 (9% enrichment) and 39_20190522_1540 (6% enrichment). It should be noted that the results of the latter two may be of lesser importance, as the reactor will not be able to reach the required 550 full power days (see section "Evaluation of k_{eff} from BOL to EOL"). The peak value is approx. $1.7 \times 10^8 \text{ cm}^{-2}\text{s}^{-1}$. However, this value occurs for case 39, with 6% enrichment, at EOL. This state cannot actually be reached, as the reactor will have become subcritical well before EOL is reached. It should also be noted that the uncertainty (standard deviation) is at least 10% for the high values of the fast flux, but larger for the lower values.

Tables 8a-8c show the k_{eff} -corrected values of the average and peak values of the fast ($E > 1 \text{ MeV}$) flux in the pressure vessel for cases 36_20190522_0114 (14.3% effective enrichment) to 39_20190522_1540 (6% enrichment). For comparison, the uncorrected peak values for the same cases can be found in Table 2. Fig. 11 shows the k_{eff} -corrected version of Fig. 10.

Note that the values of the average fast flux are virtually independent of the enrichment (contrary to what was found without k_{eff} -correction; see Fig. 10). This also seem to hold for the peak values, although the standard deviation is currently still too large (approx. 10 - 15%) to draw a firm conclusion about this. The burnup level definitely influences both average and peak fast flux in the pressure vessel. At BOL (0 full power days) and Xe-equilibrium (3 full power days) the average value of the fast flux is $8 \times 10^7 \text{ cm}^{-2}\text{s}^{-1}$. At EOL the values has increased to $8.5 \times 10^7 \text{ cm}^{-2}\text{s}^{-1}$. This can be attributed to the fact that the fuel in the centre of the core is depleting faster, due to the initial higher power in that location. This causes the main source of fast neutrons to move outward, i.e. closer to the vessel.

The (k_{eff} -corrected) peak value of the fast flux in the pressure vessel (averaged over the 4 values of enrichment considered) is decreasing with operation time: 1.60×10^8 , 1.57×10^8 and $1.28 \times 10^8 \text{ cm}^{-2}\text{s}^{-1}$, at BOL (0 full power days), Xe-equilibrium (3 full power days) and EOL (550 full power days),

respectively. The maximum peak values found is $1.72 \times 10^8 \text{ cm}^{-2}\text{s}^{-1}$, for 12% enrichment at BOL (case 37, see Table 8a).

The peak factor of the fast flux in the vessel (= peak value/average value) also decreases from 2 at BOL/Xe-equilibrium to 1.5 at EOL (compare values from Table 8c with those from Tables 8a/b). This can be attributed to the vertical power profile (and associated fast neutron source) becoming flatter during operation from BOL to EOL. The fast flux distribution in the cavity outside the vessel (see “Fast flux in reactor cavity”) is expected to change accordingly as well.

Maximum fast fluence ($E > 1 \text{ MeV}$) in pressure vessel

The fast flux in the pressure vessel will give rise to a fast fluence by integration over the entire life of the reactor, i.e. 60 full power years ($\approx 1.89 \times 10^9 \text{ s}$). A very conservative assumption would be the peak flux ($1.72 \times 10^8 \text{ cm}^{-2}\text{s}^{-1}$) occurring all the time at the same position. This would give a fluence of $3.26 \times 10^{17} \text{ cm}^{-2}$ at that location. This is still at least about one order of magnitude lower than the limit values currently known [11, 12].

Fast flux in reactor cavity

The fast flux distribution in the pressure vessel also gives an indication of the fast flux in the **reactor cavity (just) outside the vessel**. In particular the 2nd segment (between 120 and 240 cm from the bottom of the bottom reflector) may be of importance, as this would be close to the **vessel support structure**. Depending upon the specific case (enrichment) and point of time into the cycle (BOL, Xe-eq. or EOL), the fast flux in this segment varies between $7.24 \times 10^7 \text{ cm}^{-2}\text{s}^{-1}$ ($\pm 14\%$; 12% enrichment; Xe-eq.) and $1.20 \times 10^8 \text{ cm}^{-2}\text{s}^{-1}$ ($\pm 12\%$; 6% enrichment; EOL).

Conclusions & recommendations

Results have been presented from the initial SERPENT calculations on GEMINI+ HTGR configuration A with uniform initial fuel density and enrichment for all coated fuel particles, identical initial loading of all fuel blocks and all control blocks, and without burnable poison. Clearly, SERPENT is capable to perform detailed neutronics (and depletion) calculations, taking into account geometrical details as well as detailed temperature distributions by means of the multi-physics input option.

However, the initial configuration A exhibits some deficiencies:

- The BOL to EOL reactivity swing is too large (for 12% enrichment: from $k_{\text{eff}} = 1.3712$ at BOL to 1.022 at EOL - 550 full power days, i.e. $\Delta k_{\text{eff}} = -0.3488$ or $\Delta \rho = -24900 \text{ pcm}$ - including Xe-135 and Sm-149 build-up). The desired value of $\Delta \rho$ would be less than 5000 pcm (including Xe-135 and Sm-149 build-up). This would enable maintaining the reactor in shutdown state for an indefinite amount of time, even at CZP, by the reflector rods only.
- Power distribution (at BOL) is not sufficiently flat, with the highest power occurring in the central column of fuel blocks. This is expected to give

unfavourable results (too high fuel temperature) in case of a DLOFC transient.

Follow-up activities will focus on reducing/eliminating these deficiencies, by introducing burnable poison, and optimised distributions of enrichment and fuel (coated particle densities in the compacts). Further issues that have to be taken into account are water/steam ingress into the core, more detailed analysis of the influence of temperature variations on reactivity (for the calculation of temperature coefficients of reactivity and associated weighting factors, to be used in transient thermal hydraulics calculation with point kinetics), and the possibility of the occurrence of a control rod getting stuck in the top reflector ("stuck rod condition" - most reactive control rod). The plan for these follow-up activities is given in [3]. For the time being the basic configuration A will be maintained (i.e. number and position of fuel-, control- and reflector blocks). Should it turn out to be impossible to ensure operation within specifications, further modifications of the configuration are not excluded.

References

- [1] "GEMINI+ - Research and development in support of the GEMINI initiative", Euratom Horizon 2020 project 755478, 1 September 2017 - 31 August 2020.
- [2] D. Hittner, "GEMINI+, Task 2.2: Data on block type HTGR core configuration", LGI report RAD0004, Rev. 2, 29. November 2017.
- [3] J.C. Kuijper, "Task 2.4 Work Plan for further SERPENT neutronics analyses to arrive at a moderately optimised prismatic HTGR core design based on configuration A", NUCLIC Note N19059, 1. May 2019.
- [4] J.C. Kuijper, "Initial SERPENT neutronics calculations in GEMINI+, WP2, Task 4.2. Division of work between NUCLIC and TU Dresden", NUCLIC Note N18062, 18. January 2019.
- [5] Leppänen, J., et al. (2015) "The SERPENT Monte Carlo code: Status, development and applications in 2013", Ann. Nucl. Energy, 82 (2015) 142-150.
- [6] "SERPENT Wiki, Input syntax manual", http://SERPENT.vtt.fi/mediawiki/index.php/Input_syntax_manual, 25. July 2019.
- [7] M.M. Stempniewicz and E.A.R. de Geus, "Model of the GEMINI+ Reactor Configuration A - Design-Support Analyses, WP2.4", NRG report 24203/18.148942, 20 July 2018.
- [8] M.M. Stempniewicz, "Model of the GEMINI+ Reactor Configuration B - Design-Support Analyses, WP2.4", NRG note NRG-24203/18.149166 Rev. 0, 20 July 2018.
- [9] W. von Lensa, "NBG-17 graphite composition", private communication, 14. June 2018.
- [10] "ECCP GEMINI Plus - Electronic Content Collaboration Platform", <https://app.lgi-consulting.org/ecm/geminiplus-ecm>, section 3, "Technical Work Packages", WP2 "Configuration for an industrial high temperature

nuclear cogeneration system”, Task 2.4, “Core configuration”,
“Neutronics”, 25. July 2019.

[11] N. Tricot and U. Jendrich, “Neutron fluence at the reactor pressure vessel wall - A comparison of French and German procedures and strategies in PWRs”, Report IRSN No. 546, January 2003.

[12] H. Tuomisto, Fortum, Email 12 June 2019, 18:06.

[13] M.M. Stempniewicz, NRG, Email 11 July 2019, 15:45.

Table 2. Overview of SERPENT calculations by NUCLIC and NCBJ (results at BOL). No burnable poison. Uniform fuel and control blocks in the core. Cases 32 - 34 are consecutive iterations of SERPENT and SPECTRA to obtain a converged power and temperature profile at BOL. Cases 29 - 31 and 35 - 39 are depletion calculations up to 550 full power operation days, for which only data at BOL have been given in this table. See Table 3 (b and c) for data at other points in time. Raw calculation results have been uploaded to the GEMINI+ ECCP [10]. Case IDs consist of a unique sequence number and an also unique date/time ("yyyymmdd_HHMM") indicator. A dash ("-") indicates that the parameter has not been calculated or extracted. "N/A" indicates that the parameter value has been calculated but is meaningless for the specific case. Note that the actual effective enrichment is 14.3% where "14%" has been indicated. This is due to a typo in the SERPENT input deck, which has been left untouched for consistency reasons. This also holds for Tables 3a - c. The values for the vessel peak fast fluence have **not** been corrected for k_{eff} .

| Case ID [##_yyyymmdd_HHMM] | Description | k-eff (BOL) | Rel. Stand. Dev. | Power peaking factor Fq (w.r.t. average power per half block) | Rel. Stand. Dev. | Vessel fast flux (> 1 MeV) peak [cm ⁻² s ⁻¹] | Rel. Stand. Dev. |
|-------------------------------|--|-------------|------------------|---|------------------|--|------------------|
| 01_20190314_0959 | Flat temperature distribution; Hot; test/use of multi-physics interface; OTF thermal scatter data interpolation. | 1.38345 | 1.20E-05 | 1.52 | - | 1.051E+08 | - |
| 02_20190321_1440 | HFP temperature distribution from SPECTRA; multi-physics interface; OTF thermal scatter data interpolation. | 1.40575 | 6.10E-05 | 1.74 | - | 1.259E+08 | - |
| 03_20190325_0534 | Annular B4C control rods (ANTARES-type) implemented; reference - all rods out; room temperature ("cold" fuel, | 1.46188 | 5.70E-05 | 1.62 | - | N/A | - |

| | | | | | | | |
|------------------|--|---------|----------|------|---|-----------|---|
| | moderator and reflector) | | | | | | |
| 04_20190325_0730 | Annular B4C control rods (ANTARES-type) implemented; reference - all rods out; HFP temperature distribution from SPECTRA | 1.40418 | 6.20E-05 | 1.70 | - | 1.328E+08 | - |
| 05_20190325_1007 | Annular B4C control rods (ANTARES-type) implemented; cold shutdown; all rods in; room temperature | 0.96269 | 1.10E-04 | N/A | - | N/A | - |
| 06_20190325_2316 | Annular B4C control rods (ANTARES-type) implemented; core rods in; room temperature | 1.18132 | 8.10E-05 | 1.72 | - | N/A | - |
| 07_20190325_1553 | Annular B4C control rods (ANTARES-type) implemented; reflector rods in; room temperature | 1.30159 | 7.50E-05 | 2.48 | - | N/A | - |
| 08_20190325_1945 | Massive B4C control rods implemented; all rods in; room temperature | 0.94444 | 1.10E-04 | N/A | - | N/A | - |
| 09_20190325_1135 | Annular B4C control rods (ANTARES-type) implemented; all rods in; HFP temperature | 0.89056 | 1.10E-04 | N/A | - | N/A | - |

| | | | | | | | |
|------------------|---|---------|----------|------|---|-----------|---|
| | distribution from SPECTRA | | | | | | |
| 10_20190325_1321 | Annular B4C control rods (ANTARES-type) implemented; core rods in; HFP temperature distribution from SPECTRA | 1.12210 | 8.60E-05 | 2.05 | - | N/A | - |
| 11_20190325_1736 | Annular B4C control rods (ANTARES-type) implemented; reflector rods in; HFP temperature distribution from SPECTRA | 1.22629 | 8.00E-05 | 3.06 | - | N/A | - |
| 12_20190325_2109 | Massive B4C control rods implemented; all rods in; HFP temperature distribution from SPECTRA | 0.87371 | 1.20E-04 | N/A | - | N/A | - |
| 13_20190326_2327 | HFP temperature distribution from SPECTRA; Xe-and Sm-equilibrium at BOL; all rods out | 1.36002 | 2.60E-05 | 1.71 | - | 1.129E+08 | - |
| 14_20190327_0430 | HFP temperature distribution from SPECTRA; Sm-equilibrium at BOL only; no Xe; all rods out | 1.39570 | 2.70E-05 | 1.71 | - | 1.217E+08 | - |
| 15_20190327_0929 | HFP temperature distribution from SPECTRA; Xe-equilibrium at BOL | 1.36807 | 2.70E-05 | 1.71 | - | 1.297E+08 | - |

| | | | | | | | |
|------------------|--|---------|----------|------|---|-----------|---|
| | only; no Sm; all rods out | | | | | | |
| 16_20190327_1431 | HFP temperature distribution from SPECTRA; reference; no Sm; no Xe; all rods out | 1.40415 | 2.70E-05 | 1.71 | - | 1.136E+08 | - |
| 17_20190327_2302 | Enrichment 6%; room temperature | 1.30556 | 1.90E-04 | 1.75 | - | 1.342E+08 | - |
| 18_20190327_2313 | Enrichment 6%; room temperature; all rods in | 0.77553 | 3.50E-04 | N/A | - | N/A | - |
| 19_20190328_0833 | Enrichment 6%; HFP; all rods in | 0.67770 | 4.50E-04 | N/A | - | N/A | - |
| 20_20190328_1335 | Enrichment 6%; HFP | 1.22781 | 2.20E-05 | 1.90 | - | 1.327E+08 | - |
| 21_20190328_0027 | Enrichment 9%; room temperature | 1.39043 | 1.90E-05 | 1.68 | - | 1.121E+08 | - |
| 22_20190327_2252 | Enrichment 9%; room temperature; all rods in | 0.87094 | 3.70E-05 | N/A | - | N/A | - |
| 23_20190328_1259 | Enrichment 9%; HFP; all rods in | 0.78442 | 3.90E-05 | N/A | - | N/A | - |
| 24_20190328_1533 | Enrichment 9%; HFP | 1.32242 | 2.10E-05 | 1.81 | - | 1.189E+08 | - |
| 25_20190327_2221 | Enrichment 12%; room temperature | 1.43775 | 1.90E-05 | 1.64 | - | 1.072E+08 | - |
| 26_20190327_2232 | Enrichment 12%; room temperature; all rods in | 0.93023 | 3.50E-05 | N/A | - | N/A | - |
| 27_20190328_0005 | Enrichment 12%; HFP; all rods in | 0.85264 | 3.70E-05 | N/A | - | N/A | - |
| 28_20190328_0016 | Enrichment 12%; HFP | 1.37630 | 2.00E-05 | 1.75 | - | 1.158E+08 | - |
| 29_20190329_1504 | Enrichment 14%; HFP; all rods out; burnup to 550 days; | 1.40428 | 8.70E-05 | 1.70 | - | 1.121E+08 | - |

| | | | | | | | |
|------------------|--|---------|----------|------|----------|-----------|----------|
| | temperature profile 05 | | | | | | |
| 30_20190329_1618 | Enrichment 14%; HFP; all rods out; burnup to 550 days; temperature profile 05 | 1.40418 | 8.70E-05 | 1.71 | - | 1.223E+08 | - |
| 31_20190330_0824 | Enrichment 14%; HFP; all rods out; burnup to 550 days; temperature profile 05 | 1.40422 | 6.10E-05 | 1.70 | - | 1.280E+08 | - |
| 32_20190415_1857 | Enrichment 14%; HFP; temperature profile 06 | 1.39708 | 6.20E-05 | 1.59 | - | 1.060E+08 | - |
| 33_20190507_1340 | Enrichment 14%; HFP; temperature profile 07 | 1.39968 | 6.10E-05 | 1.64 | - | 1.350E+08 | - |
| 34_20190516_1206 | Enrichment 14%; HFP; temperature profile 08 | 1.39901 | 8.50E-05 | 1.69 | 2.20E-03 | 1.170E+08 | 1.10E-01 |
| 35_20190522_0045 | Configuration A; 10 burnup zones; Enrichment 14%; HFP; all rods out; burnup to 550 days; temperature profile 08 | 1.39930 | 8.70E-05 | 1.70 | 2.20E-03 | 1.206E+08 | 5.00E-02 |
| 36_20190522_0114 | Configuration A1; 310 burnup zones (1 per fuel/control block); Enrichment 14%; HFP; all rods out; burnup to 550 days; temperature profile 08 | 1.39931 | 8.50E-05 | 1.70 | 2.20E-03 | 9.810E+07 | 1.10E-01 |

| | | | | | | | |
|------------------|---|---------|----------|------|----------|------------|----------|
| 37_20190522_1534 | Configuration A1; 310 burnup zones (1 per fuel/control block); Enrichment 12%; HFP; all rods out; burnup to 550 days; temperature profile 08 | 1.37115 | 8.60E-05 | 1.72 | 2.10E-03 | 1.256E+08 | 1.00E-01 |
| 38_20190522_1535 | Configuration A; 310 burnup zones (1 per fuel/control block; Enrichment 9%; HFP; all rods out; burnup to 550 days; temperature profile 08 | 1.31683 | 8.70E-05 | 1.78 | 2.00E-03 | 1.265E+08 | 1.04E-01 |
| 39_20190522_1540 | Configuration A; 310 burnup zones (1 per fuel/control block; Enrichment 6%; HFP; all rods out; burnup to 550 days; temperature profile 08 | 1.22118 | 8.54E-05 | 1.85 | 1.94E-03 | 1.3529E+08 | 9.70E-02 |

Table 3a. Overview of SERPENT depletion calculations by NUCLIC and NCBJ (results at BOL). No burnable poison. Uniform fuel and control blocks in the core. See caption of Table 2 for further information.

| Case ID [##_yyyymmdd_HHMM] | Description | k-eff (BOL) | Rel. Stand. Dev. | Power peaking factor Fq (w.r.t. average power per half block) | Rel. Stand. Dev. | Power peaking factor FdH (w.r.t. average power per column) | Rel. Stand. Dev. |
|-------------------------------|--|-------------|------------------|---|------------------|--|------------------|
| 29_20190329_1504 | Enrichment 14%; HFP; all rods out; burnup to 550 days | 1.4043E+00 | 8.7000E-05 | 1.7027E+00 | - | - | - |
| 30_20190329_1618 | Enrichment 14%; HFP; all rods out; burnup to 550 days | 1.4042E+00 | 8.7000E-05 | 1.7082E+00 | - | - | - |
| 31_20190330_0824 | Enrichment 14%; HFP; all rods out; burnup to 550 days | 1.4042E+00 | 6.1000E-05 | 1.7000E+00 | - | - | - |
| 35_20190522_0045 | Configuration A; 10 burnup zones; Enrichment 14%; HFP; all rods out; burnup to 550 days; temperature profile 08 | 1.3993E+00 | 8.7000E-05 | 1.7000E+00 | 2.2000E-03 | 1.1900E+00 | 6.0000E-04 |
| 36_20190522_0114 | Configuration A1; 310 burnup zones (1 per fuel/control block); Enrichment 14%; HFP; all rods out; burnup to 550 days; temperature profile 08 | 1.3993E+00 | 8.5000E-05 | 1.7000E+00 | 2.2000E-03 | 1.1860E+00 | 6.0000E-04 |
| 37_20190522_1534 | Configuration A1; 310 burnup zones (1 per fuel/control block); Enrichment 12%; HFP; all rods out; burnup to 550 | 1.3712E+00 | 8.6000E-05 | 1.7200E+00 | 2.1000E-03 | 1.2000E+00 | 6.0000E-04 |

| | | | | | | | |
|------------------|---|------------|------------|------------|------------|------------|------------|
| | days; temperature profile 08 | | | | | | |
| 38_20190522_1535 | Configuration A; 310 burnup zones (1 per fuel/control block; Enrichment 9%; HFP; all rods out; burnup to 550 days; temperature profile 08 | 1.3168E+00 | 8.7000E-05 | 1.7800E+00 | 2.0000E-03 | 1.2260E+00 | 5.7000E-04 |
| 39_20190522_1540 | Configuration A; 310 burnup zones (1 per fuel/control block; Enrichment 6%; HFP; all rods out; burnup to 550 days; temperature profile 08 | 1.2212E+00 | 8.5400E-05 | 1.8470E+00 | 1.9400E-03 | 1.2600E+00 | 5.4000E-04 |

Table 3b. Overview of SERPENT depletion calculations by NUCLIC and NCBJ (results at xenon equilibrium; 3 full power days). No burnable poison. Uniform fuel and control blocks in the core. See caption of Table 2 for further information.

| Case ID [##_yyyymmdd_HHMM] | Description | k-eff (3 full power days) | Rel. Stand. Dev. | Power peaking factor Fq (w.r.t. average power per half block) | Rel. Stand. Dev. | Power peaking factor FdH (w.r.t. average power per column) | Rel. Stand. Dev. |
|-------------------------------|---|------------------------------|---------------------|--|---------------------|---|---------------------|
| 29_20190329_1504 | Enrichment 14%; HFP; all rods out; burnup to 550 days | - | - | - | - | - | - |
| 30_20190329_1618 | Enrichment 14%; HFP; all rods out; burnup to 550 days | - | - | - | - | - | - |
| 31_20190330_0824 | Enrichment 14%; HFP; all rods out; burnup to 550 days | - | - | - | - | - | - |
| 35_20190522_0045 | Configuration A; 10 burnup zones; Enrichment 14%; HFP; all rods out; burnup to 550 days; temperature profile 08 | 1.3489E+00 | 8.2000E-05 | 1.5800E+00 | 2.2000E-03 | 1.1900E+00 | 6.0000E-04 |
| 36_20190522_0114 | Configuration A1; 310 burnup zones (1 per fuel/control block); Enrichment 14%; HFP; all rods out; burnup to 550 days; temperature profile 08 | 1.3483E+00 | 8.2000E-05 | 1.5580E+00 | 2.2000E-03 | 1.1800E+00 | 6.0000E-04 |
| 37_20190522_1534 | Configuration A1; 310 burnup zones (1 per fuel/control block); Enrichment 12%; HFP; all rods out; burnup to 550 | 1.3188E+00 | 8.3000E-05 | 1.5600E+00 | 2.2000E-02 | 1.2000E+00 | 6.0000E-04 |

| | | | | | | | |
|------------------|---|------------|------------|------------|------------|------------|------------|
| | days; temperature profile 08 | | | | | | |
| 38_20190522_1535 | Configuration A; 310 burnup zones (1 per fuel/control block; Enrichment 9%; HFP; all rods out; burnup to 550 days; temperature profile 08 | 1.2640E+00 | 8.3000E-05 | 1.6700E+00 | 2.0000E-03 | 1.2200E+00 | 5.7000E-04 |
| 39_20190522_1540 | Configuration A; 310 burnup zones (1 per fuel/control block; Enrichment 6%; HFP; all rods out; burnup to 550 days; temperature profile 08 | 1.1705E+00 | 8.1932E-05 | 1.7421E+00 | 2.0300E-03 | 1.2532E+00 | 5.4000E-04 |

Table 3c. Overview of SERPENT depletion calculations by NUCLIC and NCBJ (results at EOL; 550 full power days). No burnable poison. Uniform fuel and control blocks in the core. See caption of Table 2 for further information.

| Case ID [##_yyyymmdd_HHMM] | Description | k-eff (EOL) | Rel. Stand. Dev. | Power peaking factor Fq (w.r.t. average power per half block) | Rel. Stand. Dev. | Power peaking factor FdH (w.r.t. average power per column) | Rel. Stand. Dev. |
|-------------------------------|--|-------------|------------------|---|------------------|--|------------------|
| 29_20190329_1504 | Enrichment 14%; HFP; all rods out; burnup to 550 days | - | - | - | - | - | - |
| 30_20190329_1618 | Enrichment 14%; HFP; all rods out; burnup to 550 days | - | - | - | - | - | - |
| 31_20190330_0824 | Enrichment 14%; HFP; all rods out; burnup to 550 days | - | - | - | - | - | - |
| 35_20190522_0045 | Configuration A; 10 burnup zones; Enrichment 14%; HFP; all rods out; burnup to 550 days; temperature profile 08 | 1.0904E+00 | 7.6000E-05 | 1.2600E+00 | 2.7000E-03 | 1.1800E+00 | 6.1000E-04 |
| 36_20190522_0114 | Configuration A1; 310 burnup zones (1 per fuel/control block); Enrichment 14%; HFP; all rods out; burnup to 550 days; temperature profile 08 | 1.0868E+00 | 7.6000E-05 | 1.2200E+00 | 2.7000E-03 | 1.1400E+00 | 6.0000E-04 |
| 37_20190522_1534 | Configuration A1; 310 burnup zones (1 per fuel/control block); Enrichment 12%; HFP; all rods out; burnup to 550 | 1.0222E+00 | 7.5000E-05 | 1.2400E+00 | 2.7000E-03 | 1.1500E+00 | 6.1000E-04 |

| | | | | | | | |
|------------------|---|------------|------------|------------|------------|------------|------------|
| | days; temperature profile 08 | | | | | | |
| 38_20190522_1535 | Configuration A; 310 burnup zones (1 per fuel/control block; Enrichment 9%; HFP; all rods out; burnup to 550 days; temperature profile 08 | 8.9776E-01 | 6.9000E-05 | 1.3100E+00 | 2.5900E-03 | 1.1840E+00 | 5.9000E-04 |
| 39_20190522_1540 | Configuration A; 310 burnup zones (1 per fuel/control block; Enrichment 6%; HFP; all rods out; burnup to 550 days; temperature profile 08 | 7.0806E-01 | 6.0893E-05 | 1.3377E+00 | 2.5500E-03 | 1.2586E+00 | 5.6000E-04 |

Table 8a. k_{eff} -corrected values of the fast ($E > 1 \text{ MeV}$) flux in the pressure vessel at BOL.

| Case ID [##_yyymmdd_HHMM] | Description | $k\text{-eff (BOL)}$ | k_{eff} -corrected Vessel fast flux ($> 1 \text{ MeV}$) average [$\text{cm}^{-2}\text{s}^{-1}$] | Rel. Stand. Dev. | k_{eff} -corrected Vessel fast flux ($> 1 \text{ MeV}$) peak [$\text{cm}^{-2}\text{s}^{-1}$] | Rel. Stand. Dev. |
|------------------------------|---|----------------------|--|------------------|---|------------------|
| 36_20190522_0114 | Configuration A1; 310 burnup zones (1 per fuel/control block); Enrichment 14%; HFP; all rods out; burnup to 550 days; temperature profile 08 | 1.3993E+00 | 7.5283E+07 | 5.0000E-02 | 1.3727E+08 | 1.1000E-01 |
| 37_20190522_1534 | Configuration A1; 310 burnup zones (1 per fuel/control block); Enrichment 12%; HFP; all rods out; burnup to 550 days; temperature profile 08 | 1.3712E+00 | 8.5971E+07 | 5.0000E-02 | 1.7222E+08 | 1.0000E-01 |
| 38_20190522_1535 | Configuration A; 310 burnup zones (1 per fuel/control block); Enrichment 9%; HFP; all rods out; burnup to 550 days; temperature profile 08 | 1.3168E+00 | 8.4659E+07 | 4.8000E-02 | 1.6658E+08 | 1.0390E-01 |
| 39_20190522_1540 | Configuration A; 310 burnup zones (1 per fuel/control block); Enrichment 6%; HFP; all rods out; burnup to 550 days; temperature profile 08 | 1.2212E+00 | 7.4162E+07 | 5.0150E-02 | 1.6523E+08 | 9.6890E-02 |

| | | | | | | |
|---|----------------|---|------------|---|------------|---|
| - | Average | - | 8.0019E+07 | - | 1.6032E+08 | - |
|---|----------------|---|------------|---|------------|---|

Table 8b. k_{eff} -corrected values of the fast ($E > 1 \text{ MeV}$) flux in the pressure vessel at Xe-equilibrium (3 full power days).

| Case ID [##_yyymmdd_HHMM] | Description | k_{eff} (3 full power days) | k_{eff} -corrected Vessel fast flux ($> 1 \text{ MeV}$) average [$\text{cm}^{-2}\text{s}^{-1}$] | Rel. Stand. Dev. | k_{eff} -corrected Vessel fast flux ($> 1 \text{ MeV}$) peak [$\text{cm}^{-2}\text{s}^{-1}$] | Rel. Stand. Dev. |
|------------------------------|--|--------------------------------------|---|------------------|--|------------------|
| 36_20190522_0114 | Configuration A1; 310 burnup zones (1 per fuel/control block); Enrichment 14%; HFP; all rods out; burnup to 550 days; temperature profile 08 | 1.3483E+00 | 8.0223E+07 | 5.0E-2 | 1.5357E+08 | 1.1E-1 |
| 37_20190522_1534 | Configuration A1; 310 burnup zones (1 per fuel/control block); Enrichment 12%; HFP; all rods out; burnup to 550 days; temperature profile 08 | 1.3188E+00 | 8.2159E+07 | 4.8E-2 | 1.6880E+08 | 1.0E-1 |
| 38_20190522_1535 | Configuration A; 310 burnup zones (1 per fuel/control block); Enrichment 9%; HFP; all rods out; burnup to 550 days; temperature profile 08 | 1.2640E+00 | 8.1883E+07 | 5.0E-2 | 1.4923E+08 | 1.1E-2 |
| 39_20190522_1540 | Configuration A; 310 burnup zones (1 per fuel/control block); Enrichment 6%; HFP; all rods out; burnup to 550 days; temperature profile 08 | 1.1705E+00 | 8.0302E+07 | 5.0E-2 | 1.5776E+08 | 1.0E-2 |

| | | | | | | |
|---|----------------|---|------------|---|------------|---|
| - | Average | - | 8.1142E+07 | - | 1.5734E+08 | - |
|---|----------------|---|------------|---|------------|---|

Table 8c. k_{eff} -corrected values of the fast ($E > 1 \text{ MeV}$) flux in the pressure vessel at EOL (550 full power days).

| Case ID [##_yyymmdd_HHMM] | Description | k_{eff} (EOL) | k_{eff} -corrected Vessel fast flux ($> 1 \text{ MeV}$) average [$\text{cm}^{-2}\text{s}^{-1}$] | Rel. Stand. Dev. | k_{eff} -corrected Vessel fast flux ($> 1 \text{ MeV}$) peak [$\text{cm}^{-2}\text{s}^{-1}$] | Rel. Stand. Dev. |
|------------------------------|---|------------------------|--|------------------|---|------------------|
| 36_20190522_0114 | Configuration A1; 310 burnup zones (1 per fuel/control block); Enrichment 14%; HFP; all rods out; burnup to 550 days; temperature profile 08 | 1.0868E+00 | 8.4223E+07 | 5.0E-2 | 1.2748E+08 | 1.2E-1 |
| 37_20190522_1534 | Configuration A1; 310 burnup zones (1 per fuel/control block); Enrichment 12%; HFP; all rods out; burnup to 550 days; temperature profile 08 | 1.0222E+00 | 8.3721E+07 | 4.9E-2 | 1.2880E+08 | 1.1E-1 |
| 38_20190522_1535 | Configuration A; 310 burnup zones (1 per fuel/control block); Enrichment 9%; HFP; all rods out; burnup to 550 days; temperature profile 08 | 8.9776E-01 | 8.9856E+07 | 4.9E-2 | 1.3556E+08 | 1.1E-1 |
| 39_20190522_1540 | Configuration A; 310 burnup zones (1 per fuel/control block); Enrichment 6%; HFP; all rods out; burnup to 550 days; temperature profile 08 | 7.0806E-01 | 8.2483E+07 | 5.1E-2 | 1.2023E+08 | 1.2E-1 |

| | | | | | | |
|---|----------------|---|------------|---|------------|---|
| - | Average | - | 8.5071E+07 | - | 1.2802E+08 | - |
|---|----------------|---|------------|---|------------|---|

Part B - Appendix A - Influence of interchanged temperatures in the reflector

After most of the calculations, presented in this note, had been performed, an error was discovered in the transfer of temperature data from the SPECTRA

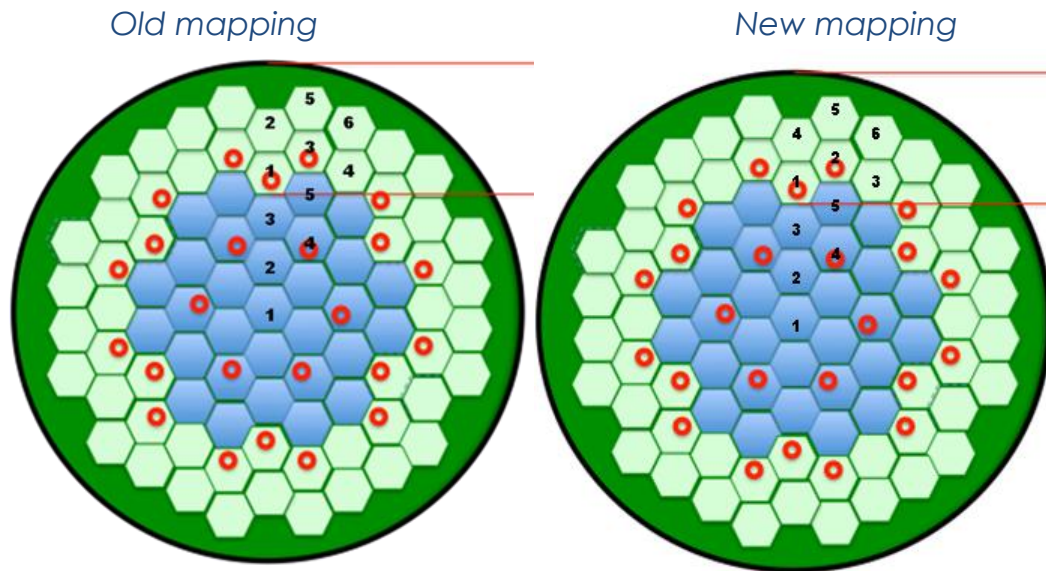


Fig. A.1 Comparison of original (but incorrect; "Old mapping") and the corrected mapping ("New mapping") of temperatures on columns in the radial reflector. Note the mapping in the core (indicated here by "1" to "5", corresponding to "C1" to "C5" in Fig. 2).

thermal hydraulics code to the multi-physics input of the SERPENT model: the temperatures for 2 replaceable reflector columns had been interchanged. Fig. A.1 shows the mapping that was assumed in the calculations up to Case 39 ("Old mapping") and the mapping as it should have been ("New mapping") [13]. In order to assess the impact of this interchange on the results of the SERPENT calculations so far, two additional cases have been run, to be compared with case 34_20190516_1206 (see Table 2; pages 19 - 23):

- Case 40_20190712_1541: Corrected reflector temperature distribution (same temperatures, but "New mapping").
- Case 41_20190712_1649: (Almost) uniform temperature distribution in the radial reflector (vertical distribution for outer permanent reflector was also applied for all replaceable reflector columns, i.e. a radially uniform distribution, which is also approx. 596 K, uniformly distributed).

A comparison (at BOL) was made for:

- k_{eff} ;
- the vertical power distribution, at BOL, for 2 representative columns of fuel blocks in the core ("C1" and "C5");
- the distribution of the fast ($E > 1$ MeV) flux in the pressure vessel.

Comparison of axial power profile

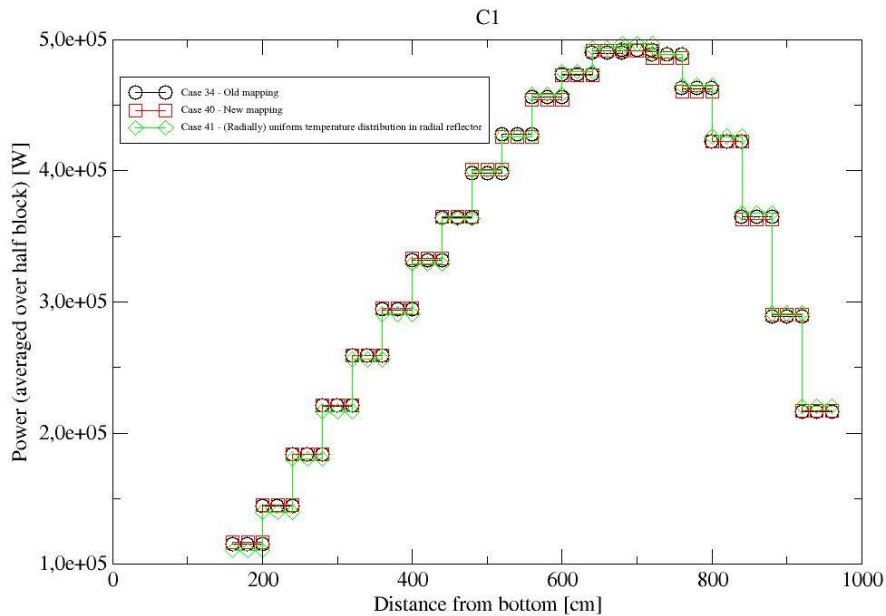


Fig. A.2 Comparison of axial power profiles in central column ("C1") of fuel blocks in the core for different temperature distributions in the radial reflector.

Comparison of axial power profile

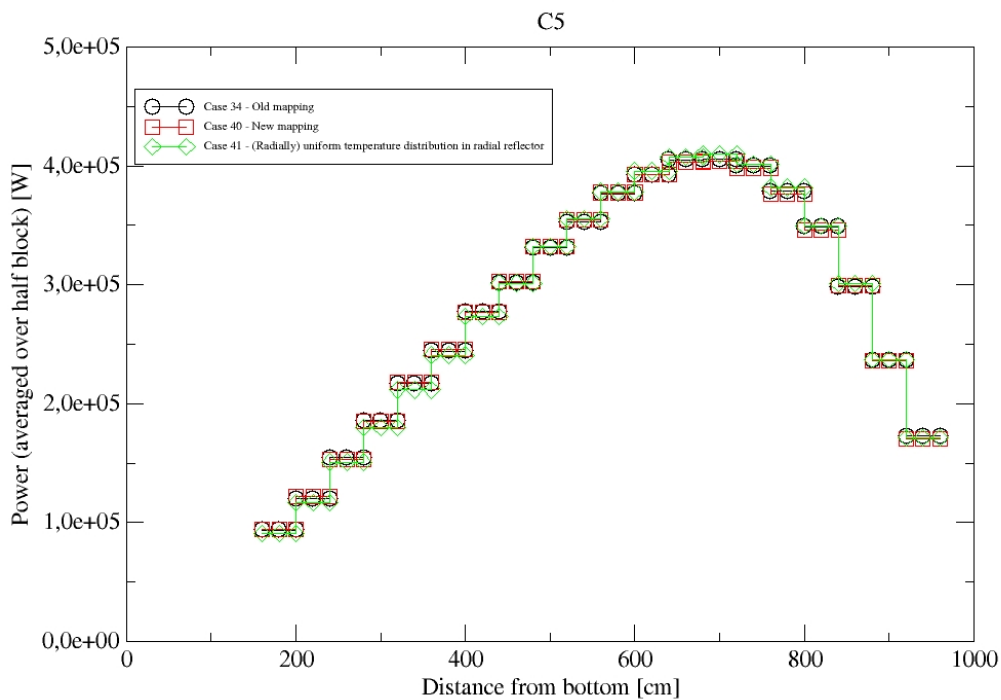


Fig. A.3 Comparison of axial power profiles in representative peripheral column ("C5") of fuel blocks in the core for different temperature distributions in the radial reflector.

Table A.1 shows the values of k_{eff} for cases 34, 40 and 41. If case 40 is taken as the reference (this is the case with the correct temperature distribution in the reflector: "New mapping"), the k_{eff} is only slightly (although statistically

Table A.1 Influence of (erroneous) changes in the temperature distribution in the radial reflector on k_{eff} .

| Case | k_{eff} [-] | Rel. Stand. dev. [-] | Difference [-] |
|---|---------------|----------------------|---|
| 34_20190516_1206 ("Old mapping") | 1.39901 | 8.5E-5 | 2.9E-4 |
| 40_20190712_1541 ("New mapping") | 1.39872 | 8.5E-5 | - (reference; correct temperature distribution) |
| 41_20190712_1649 ("Flat distribution") | 1.39854 | 8.5E-5 | -1.8E-4 |

significant) higher for case 34 (interchanged temperatures: "Old mapping"), whereas the k_{eff} is only slightly (however again statistically significant) lower for case 41 with the uniform temperature distribution in the reflector.

In Figs. A.2 and A.3 a comparison is made for the axial power profiles of the centre ("C1") and representative peripheral ("C5") columns of fuel blocks. Clearly, the influence of the exact temperature distribution in the reflector on the power distribution in the core is very small. Even a nearly uniform temperature distribution in the radial reflector has a very small influence on the power distribution in the core.

Finally, Fig. A.4 shows the comparison of the vertical distribution of the fast ($E > 1$ MeV) flux in the pressure vessel (not corrected for k_{eff}) between Cases

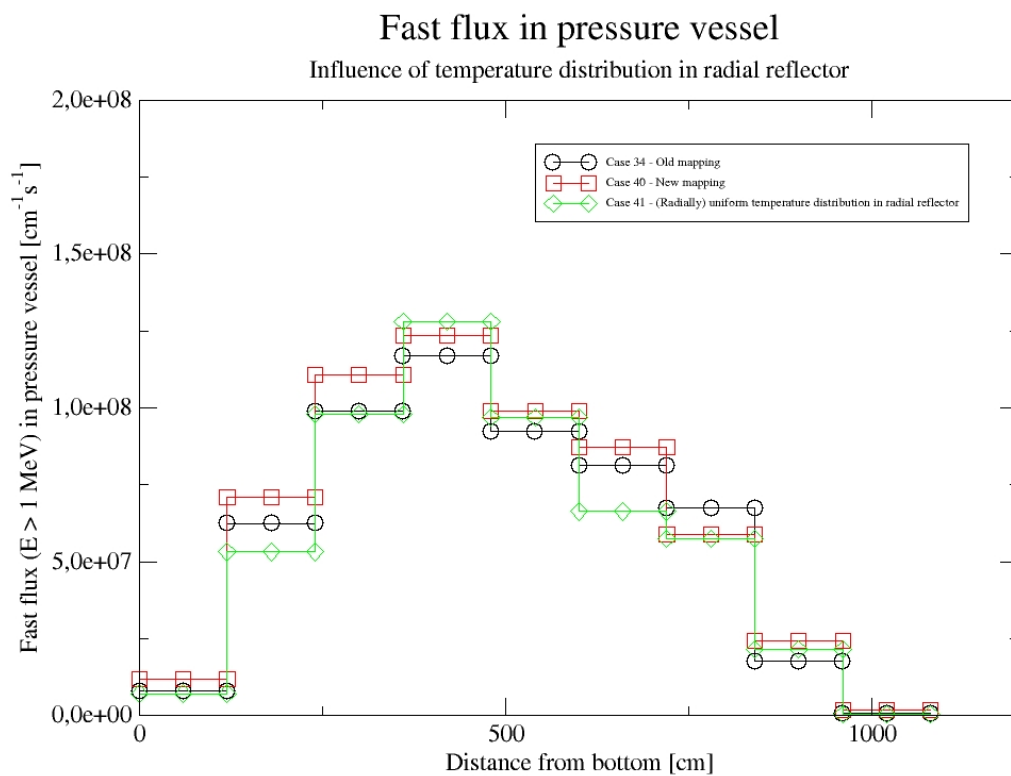


Fig. A.4 Comparison of fast flux distribution in the pressure vessel (not corrected for k_{eff}) between Cases 34, 40 and 41.

34, 40 and 41. A larger influence of the temperature profile in the radial reflector is expected in this case, as can indeed be seen. However, given the uncertainties in the values of the fast flux (approx. 10 % for the highest values, higher for the lower values), the significance of the differences between the 3 curves can be considered as limited.

In summary, it has been shown that the exact distribution of the temperature in the radial reflector is of limited influence on results of neutronics calculations in the core (assuming that the temperature distribution in the core is not changed) and even in the pressure vessel. So, the conclusion stated earlier in this note remain valid.

Part C - Preliminary fuel specification for the GEMINI+ prismatic HTR (conceptual design stage)

Part C provides some additional information concerning the (preliminary) fuel design, which is virtually identical to NUCLIC note N19064 version 02 [1]. An important addition to [1] is the information originating from the AGR (Advanced Gas Reactor) fuel irradiation programme in the USA [2].

[1] J.C. Kuijper, "Preliminary fuel specification for the GEMINI+ prismatic HTR (conceptual design stage) - Status: 16. December 2019", NUCLIC note N19064 version 0.2, 16 December 2019.

[2] M. Feltus, "TRISO FUELS ", Webinar, Gen IV International Forum, 18 December 2019, https://www.gen-4.org/gif/jcms/c_114200/gen-iv-webinar-series-36-madeline-feltus-webinar-presentation-18-december-2019

Introduction

The Euratom Horizon 2020 project GEMINI+ (1. September 2017 - 31. August 2020) focusses on the (pre-) preliminary design of a prismatic High Temperature Gas-Cooled Reactor, with a nominal thermal power of approx. 180 MW, to be primarily used as an industrial heat source in Poland [1]. Some initial assumptions have been given in ref. [2] and although many components are intentionally envisaged to be the same as in (or very similar to those of -) existing designs (see e.g. refs. [3,4,5]), quite some conceptual design work is still to be done on the core as well as other components of the system.

This note focusses on the specification of the fuel to be used in the GEMINI+ HTGR. Although some initial guesses for several parameters (e.g. coated particle dimensions and material densities) have been given or proposed in ref. [2], there are many more items to be specified (see e.g. refs. [6,7,8] for examples of a more extensive HTGR fuel specification). This includes e.g. requirements on the sphericity of the kernels and coated particles and the defective/failure fraction of the coated particles (during manufacturing and as result of operation and accident conditions). Currently we are not yet in the position to provide such a complete fuel specification. It is envisaged to be part of the future basic and detailed design activities for the GEMINI+ reactor. This includes limits/requirements currently still to be determined from core analyses (neutronics and thermal hydraulics, steady state and transient), although some (preliminary) values will be given in this note.

Table 1. GEMINI+ coated particle dimensions (of kernel and coatings) and material densities, including tolerances (German Reference Fuel)[9].

| Layer | Diameter, Thickness [μm] | Density [g/cm ³] |
|--|--|---------------------------------|
| Fuel kernel (UO_x , $x \leq 2.01$) | 500 ± 20 | ≥ 10.4 |
| Buffer layer | 95 ± 18 | ≤ 1.05 |
| Inner PyC layer | 40 ± 10 | 1.9 ± 0.1 |
| SiC layer | 35 ± 4 | ≥ 3.18 |
| Outer PyC layer | 40 ± 10 | 1.9 ± 0.1 |

1. Dimensions and densities

Based on the information from earlier HTGR designs (i.e. the German Reference Fuel) [2,9], the dimensions (incl. tolerances) and material composition and densities for the TRISO coated fuel particles are as given in Table 1. Requirements on initial contamination levels, acceptable deviation from sphericity, etc., will have to be specified at a later stage. Fuel specification and quality requirement data from other HTGR designs may be a good starting point. See e.g. Table 2: Fuel quality and performance limits for the GT-MHR [10].

Table 2. Example: fuel quality and performance limits for the GT-MHR (see [10], page 4-1).

| Parameter | Segment Mean 95% Value | Upper Bound Value |
|--|---------------------------|---------------------------|
| As-manufactured fuel quality | | |
| Heavy metal contamination fraction | $\leq 1.0 \times 10^{-5}$ | $\leq 2.0 \times 10^{-5}$ |
| Missing buffer fraction | $\leq 1.0 \times 10^{-5}$ | $\leq 2.0 \times 10^{-5}$ |
| Missing or permeable inner pyrocarbon | $\leq 4.0 \times 10^{-5}$ | $\leq 1.0 \times 10^{-4}$ |
| SiC coating defect fraction | $\leq 5.0 \times 10^{-5}$ | $\leq 1.0 \times 10^{-4}$ |
| Missing or defective OPyC | $\leq 1.0 \times 10^{-4}$ | $\leq 1.0 \times 10^{-3}$ |
| Fuel performance (allowable core average) | | |
| In-service failure fraction (normal) | $\leq 5.0 \times 10^{-5}$ | $\leq 2.0 \times 10^{-4}$ |
| Incremental failure during accident | $\leq 1.5 \times 10^{-4}$ | $\leq 6.0 \times 10^{-4}$ |

2. Enrichment and particle volume fraction in compact

The **initial enrichment of the fuel is envisaged to be between 9.0 and 14.0 (atom)% in ^{235}U** . As the core neutronics design calculation are currently ongoing (see e.g. ref [11]), it has not been decided yet what the initial enrichment of the fuel will be exactly. Also, it has not been decided yet whether the initial distribution will be uniform or different values of enrichment will be used in different locations in the core.

In this particular prismatic block HTGR design, coated fuel particles are contained in cylindrical graphite compacts of 12.5 mm diameter and 50.0 mm height [2], as was also the case in the earlier designs [3,4,5]. Such a compact will contain between **2500** [11] and **3760** [2] coated particles, i.e. a **coated particle volume fraction of 17 to 25 %**, respectively.

Up to the present day, the neutronics calculations in the GEMINI+ project have been performed with **2500** coated particles per compact [11]. As the core design calculations are currently still ongoing, both the enrichment and

the number of coated particles per compact may change, however within the ranges indicated above.

3. Temperature distribution and failure fraction

The current core analyses consist of neutronics calculations (initial results reported in ref. [11]) and thermal hydraulics calculations (see [12,13] for the initial steady-state thermal hydraulics calculations on “Configuration A”). For the steady-state (full power) situation we aim at obtaining a converged power and temperature distribution, which can already be reached after 3 or 4 iterations (see refs. [11,13] in which the resulting power profile from the neutronics calculation (at the start of the irradiation: BOL, Beginning-Of-Life) is fed into the thermal hydraulics calculation and the temperature profile from the thermal hydraulics calculation is fed back into the neutronics calculation. The thermal hydraulics calculation provides the temperature distribution for steady-state and transient (DLOFC - Depressurised Loss of Forced Cooling - and PLOFC - Pressurised Loss of Forced Cooling) situations. In the latter, the distribution of the decay power drives the evolution of the temperature distribution, when the reactor has become subcritical by control rod insertion and/or increase of temperatures.

As a prediction must be made which fraction of the coated particles is going to fail as a result of such a transient, information is required about the failure fraction curve of the fuel (failed fraction of coated fuel particles as function of temperature). In combination with the performance requirement on the max. allowable failed fraction of coated particles (see e.g. Table 2), this will put limits on the fuel temperature distribution (including peak fuel temperature) during normal operation and during incidents, e.g. a DLOFC. For the moment we assume that an allowable peak temperature for a **PLOFC and DLOFC incident** of **1600 °C** is consistent with the limits on particle failure fraction. For **normal operation**, a maximum fuel temperature of **1250 °C** would be acceptable.

4. Power and Burn up

The initial reactor configuration under study was “Configuration A” [2,11], with a core consisting of 10 layers, each containing 25 fuel blocks and 6 control blocks (i.e. a fuel block with a large (90 mm diameter) hole to accommodate insertion of a control rod into the core). Each fuel block contains 216 channels that can either contain a stack of 15 fuel compacts or a stack of graphite cylinders containing burnable poison. A control block only contains 176 channels for either fuel compacts or burnable poison. In the initial analyses [11] no burnable poison was considered, so all available fuel positions in fuel blocks and control blocks were assumed to be filled with 15 fuel compacts, each containing 2500 coated particles. This amounts to $10 \times (25 \times 216 + 6 \times 174) \times 15 = 966600$ compacts and $966600 \times 2500 = 2.4165 \times 10^9$ coated particles in the reactor core. Given a nominal value of the thermal reactor power of 180 MW [2,11], this results in an **average thermal power of**

290.3 kW per half block (580.6 kW per block), 186.2 W per compact and 0.075 W per coated particle.

Fig. 1 shows the distribution of the 620 half blocks (i.e. 2 power values per fuel block) of “Configuration A, cases 36, 37 and 38” (see ref. [11]) w.r.t. the power. These cases represent the operation from 0 to 550 full power days, assuming that the same converged temperature profile at BOL (Beginning-Of-Life: start of the cycle) for the entire cycle, for enrichment values of 14.3, 12 and 9 %, respectively, at BOL and EOL (End-Of-Life, in this case 550 days). The power range from 0.0 to 600.0 kW has been subdivided into 24 classes of 25 kW width. The graph shows the number of half blocks in the indicated power class. The fact the distribution of half blocks over power classes becomes more peaked at EOL indicates that the actual spatial power distribution at EOL is more uniform than at BOL, although the actually occurring peak powers are still approx. 30 % higher than the average thermal power of 290.3 kW per half block (peaking factor of approx. 1.3). At BOL the peaking factors are 1.7 to 1.8, still for a configuration with all control rods fully

Power distribution - Configuration A - 10 layers in core

Comparison of cases 36, 37 and 38, BOL and EOL - All rods fully out

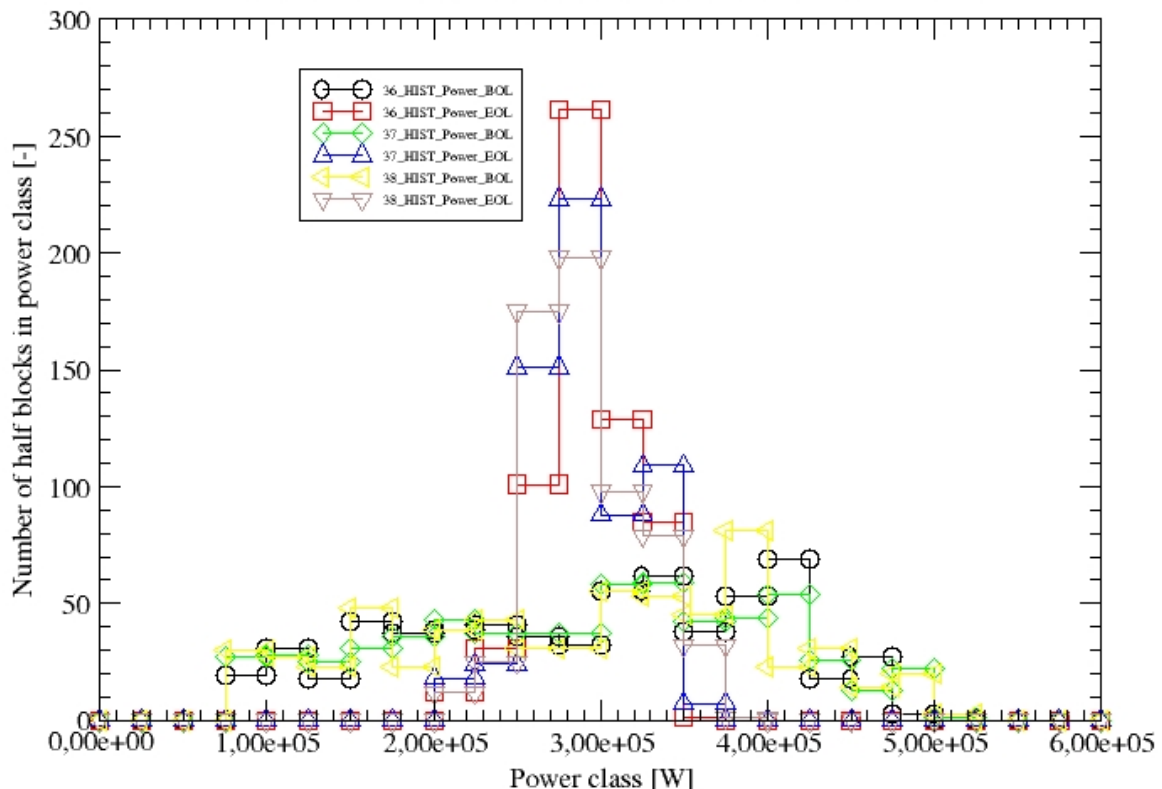


Fig. 1. Power distribution for “Configuration A, cases 36, 37 and 38” [11]. All control rods are fully out of the core. Enrichment values are 14.3 %, 12 % and 9 %, respectively. The actual peak powers are 493.5, 500.6 and 516.5 kW per half block, respectively, at BOL and 354.8, 360.4 and 380.5 kW per half block, respectively, at EOL (550 days).

withdrawn. For configurations with partially or fully inserted control rods, the peaking factors may be even higher [11].

Generally, the 10-layer core exhibits a peaking factor of approximately between 1.2 and 3, depending upon burn up, temperature and control rod insertions [11], so the **maximum peak powers per compact and coated particle** are approximately **559 W** and **0.225 W**, respectively.

Fig. 2 shows the final distribution of the burn up of the 310 fuel blocks in the core of “Configuration A, cases 36, 37 and 38”. The range between 10 and 90 MWd/kg has been subdivided into 16 classes of 5 MWd/kg width. The **average burnup** is virtually the same for the 3 cases, i.e. **68.3 MWd/kg**, as the operation mode (single batch loading scheme), operation time (550 days) and thermal power (180 MW) are identical and the initial heavy metal masses are very close together (the mass density of the UO₂ is identical for the 3 cases, which means a slightly lower heavy metal mass for higher enrichment and therefore a slightly higher burn up expressed in MWd/kg). The spatial distribution of the burn up is also quite similar for the 3 cases: the differences

Burn up distribution - Configuration A - 10 layers in core

Comparison of cases 36, 37 and 38 - All rods fully out

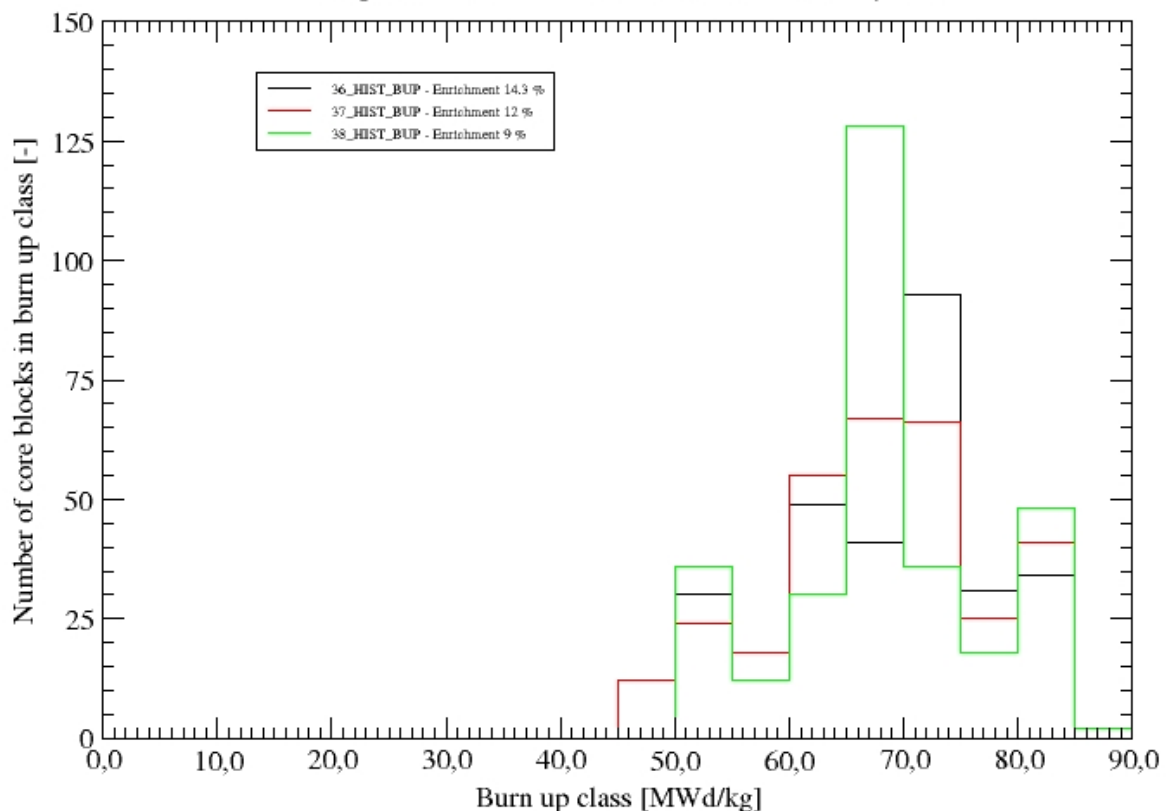


Fig. 2. Burn up distribution (at EOL, 550 days of operation) for “Configuration A, cases 36, 37 and 38” [11]. All control rods are fully out of the core. Enrichment values are 14.3 %, 12 % and 9 %, respectively. The actual peak burn up values are 86.6, 86.7 and 86.1 MWd/kg (averaged over a block).

are somewhat exaggerated in Fig. 2: actual burn up values are close to the class boundaries and slight differences may cause blocks to be assigned to a different (neighbouring) class.

The peak burn up is also very close for the 3 cases: 86.6, 86.7 and 86.1 MWd/kg for cases 36 (14.3 % enrichment), 37 (12 % enrichment) and 38 (9 % enrichment), respectively, averaged over a fuel block. So, the peak burn up value, averaged over a block, is approx. 27 % higher than the average.

For the 11-layer core currently under study the values for power (average per block and peak values) are approximately 10 % lower. Obviously, the power per coated particle will be further decreased if the number of coated particles per compact is increased. The envisaged use of Burnable Poison (BP; replacing 6 - fuel block - or 4 - control block - stacks of 15 compacts each) on the other hand will lower the number of compacts and coated particles, hereby increasing the (average) powers per compact and coated particle.

In Fig. 3 the distribution of the power of 682 (= 11 x 31 x 2) half blocks, at BOL and EOL, is shown for the current 11-layer design, without burnable poison, but with the reflector control rods 200 cm inserted (i.e. 2.5 times the height of 1 block). The range from 0.0 to 600 kW is divided into 24 classes of 25 kW width.

The partial insertion of the reflector rods causes the power in the fuel blocks close to these rods to be lowered, giving raise to the lower power classes to

Power distribution - 11 layers in core - 341 blocks - No BP
Case 42 - Partially (200 cm) inserted reflector rods

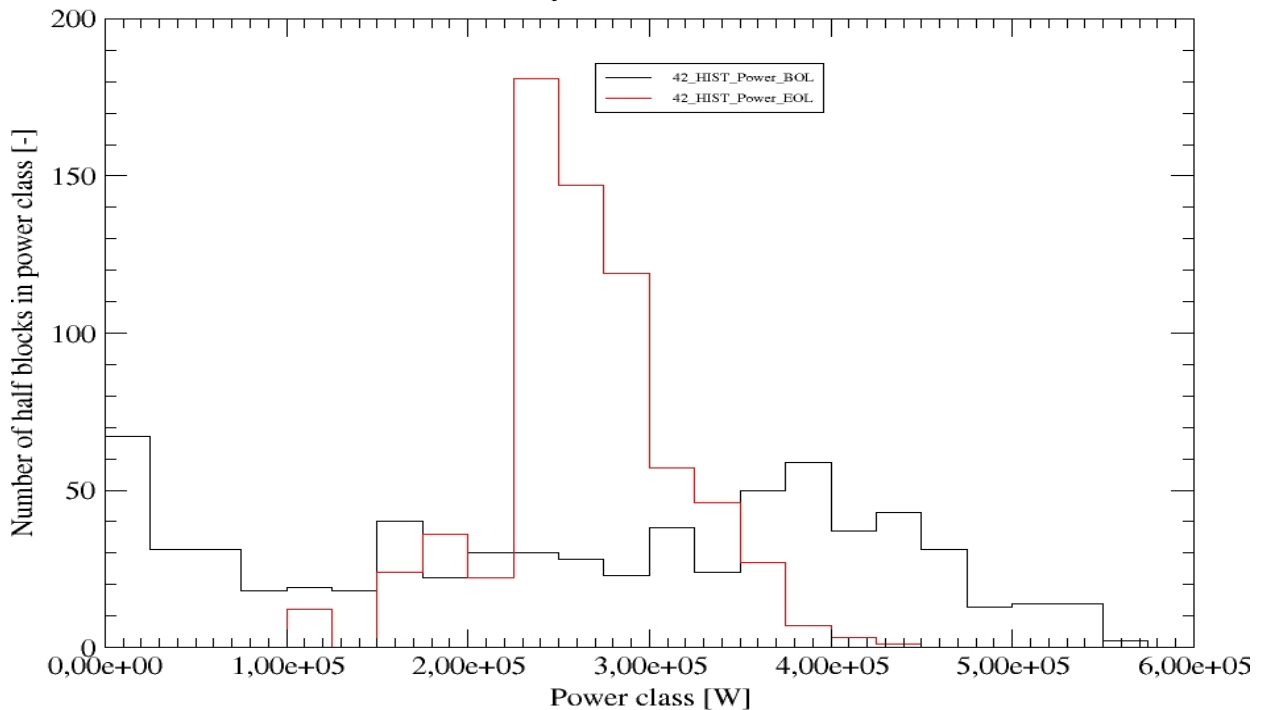


Fig. 3. Power distribution of the 11-layer core with partially inserted reflector control rods, without BP ("Case 42"; enrichment 10 %). The actual peak powers are 563.7 kW per per half block and 427.9 kW per half block at BOL and EOL (550 days), respectively.

be filled, and the power in other locations to be raised, especially at BOL. At BOL, the actual **peak power is 563.7 kW** per half block. With an **average power per half block of 263.9 kW** this means a **peaking factor of 2.14**. At EOL the power distribution has become more uniform (indicated by a peak for the power class between 225 and 250 kW (i.e. just below the average value). At EOL the **peak power has decreased to 427.9 kW** (per half block), i.e. a **peaking factor of 1.62**. If all control rods would have been fully withdrawn, the peaking factors for the 11-layer core would probably be similar to those of the 10-layer core under the same circumstances. However, partially inserted reflector rods approximate better the actual situation under operational conditions.

Fig. 4 shows the final distribution of the burn up of the 341 fuel blocks in the core of the 11-layer core configuration (“Case 42”, 10 % enrichment). The range between 10 and 90 MWd/kg has again been subdivided into 16 classes of 5 MWd/kg width. The average burnup is **62.2 MWd/kg**. The peak burn up is **87.5 MWd/kg**, which is approx. 40 % higher than the average.

From thermal hydraulics analyses it was concluded that a **more uniform power distribution** would be much more favourable from the point of view of safety (much lower peak temperature during DLOFC incident) [13]. One way of achieving such a situation would be the use of Burnable Poison (BP), and possibly a non-uniform initial distribution of the enrichment. The use of BP will

Burn up distribution - 11 layers in core - 341 blocks - No BP Case 42 - Partially (200 cm) inserted reflector rods

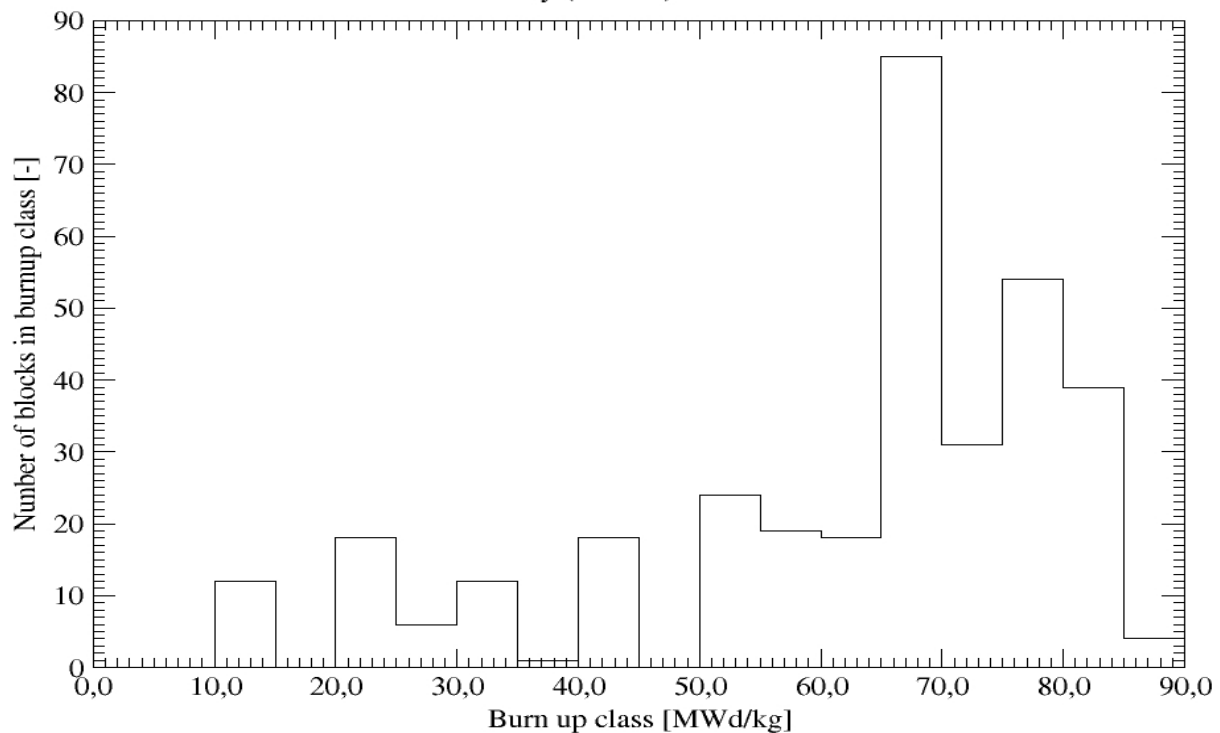


Fig. 4. Burn up distribution for “Case 42” (10 % enrichment) at EOL (550 days of operation). Reflector rods are partially (200 cm) inserted. Actual peak burn up is 87.5 MWd/kg (averaged over a block).

also **reduce considerably the BOL-to-EOL reactivity swing**. This will hopefully enable the use of **only the reflector rods for reactivity control**, opening the possibility to use the positions of the core rods for the reserve shutdown mechanism. A more uniform power distribution will also lead to a more uniform distribution of the burn up at EOL (i.e. lower peak burn up).

In the current implementation of BP, cylinders of B₄C in graphite are being used, replacing 6 stacks of compacts in a fuel block and 4 stacks of compacts in a control block. Full core analyses for these configurations with BP are ongoing.

In **Part A** of this report the latest (**December 2020**) results have been presented on such configurations. Even for “case 214” (“radially optimised” BP parameters) the maximum power per coated particle (averaged over half a block) is still 145 mW at BOL. This is higher than currently achieved/ investigated in recent TRISO fuel irradiation tests in the Advanced Gas Reactor (AGR) fuel development program in the USA [16]. The volume of a compact is 6.136 cm³. So, the power of a single compact filled with 2500 coated particles @ 145 mW would be 362.5 W, corresponding to a power density in the compact of 59.1 W/cm³. In the design of the HTR-PM [17], an average power of 0.6 kW per spherical fuel element (“pebble”; 250 MW thermal power and 420000 pebbles in core) is assumed during operation, with a maximum value of 1.8 kW. This corresponds to an average value of 51 mW per coated particle, and a maximum value of 154 mW. This is even slightly higher than the maximum value found for the GEMINI+ HTGR, while the average power per coated particle is of the same order of magnitude.

It is important to note, from the point of view of available future fuel resources, that the AGR program has narrowed its focus to UCO-type TRISO fuel, as these have exhibited better performance in the initial (irradiation) tests than UO₂ [16]. Changing to UCO-type TRISO fuel is expected to have a negligible impact on the neutronics behaviour of the GEMINI+ HTGR.

So far, we have considered the power profile within (half) a block to be uniform 1 (i.e. same power for all compacts). Although this is not exactly true, for the current studies we focus on flattening the power in the core by trying to make the power per (half) block equal for all blocks, hereby assuming that remaining issues with the within-block power distribution will be dealt with in a later stage.

The current assumption for fuel loading is a **one-batch loading scheme**, in which all fuel is permanently unloaded and replaced by fresh fuel after the desired cycle duration of 550 (equivalent full power) days. This may not be the most favourable refuelling scheme from the point of view of (fuel) economy, but the current focus of the studies is to design a feasible core that meets the safety requirement. In a later stage other (multi-batch) refuelling schemes may (and probably will) be considered. Assuming a linear burn up reactivity model, the attainable average and peak burnup can be expected to increase approximately by a factor $2N/(N+1)$, with **N** the number of batches. Using two batches instead of a single batch will e.g. increase the attainable

burn up by approx. 33 %. However, this will necessitate appropriate additional full core neutronics and thermal hydraulics calculations, taking the specific reload scheme into account. This is not part of the planned activities of GEMINI+ Task 2.4.

6. Conclusions

Given the fact that the core design (neutronics) calculations for the GEMINI+ prismatic HTGR are still ongoing, only a limited set of parameters can currently be provided for the specification of requirements on the fuel. The information currently available concerns the coated particle dimensions and material densities, packing fraction of the coated particles in the compact, ranges of the expected power and burn up and temperature limits.

It is expected that further core neutronics and thermal hydraulics calculations will indeed show that the 11-layer core will stay within the currently assumed fuel temperature limits: 1250 °C in normal operation, 1600 °C in accident (DLOFC) conditions.

Although, to our knowledge, a failure fraction versus temperature curve is not available (yet) for the envisaged fuel, it is expected that it should be possible to obtain these without unexpected surprises. The value ranges of coated particle volume fraction, power per coated particle and burn up can be considered rather benign and well within the acceptable range known from experience. The volume fraction of 17 % can even be considered low for a compact in a prismatic block HTGR.

Further fuel specification parameters (see e.g. [6,7,8,10,15] will have to be established in later design phases.

Finally, it is important to note, from the point of view of available future fuel resources, that the AGR program has narrowed its focus to UCO-type TRISO fuel, as these have exhibited better performance in the initial (irradiation) tests than UO_2 .

References

- [1] European Commission, DG Research & Innovation, Grant Agreement Number - 755478 - GEMINI Plus.
- [2] D. Hittner, "GEMINI+, Task 2.2: Data on block type HTGR core configuration", Report RA0004, Rev. 2, LGI, Paris, France, 29. November 2017.
- [3] AREVA Modular Steam Cycle – High Temperature Gas-Cooled Reactor Development Progress - L. Lommers, F. Shahrokhi, J. Mayer III, F. Southworth, Proceedings of the HTR 2014, Weihai, China, October 27-31, 2014
- [4] Summary Report – SC –HTGR Demonstration Reactor – AREVA Inc. Technical Data Record n° 12 - 9251936 – 001 https://art.inl.gov/INL_ART_TDO/Documents/Advanced_Demonstration_and_Test_Reactor_Options/Study/Attachment_1_AREVA_HTGR_DR.pdf

- [5] ANTARES: The HTR/VHTR project at Framatome ANP - Jean-Claude Gauthier, Gerd Brinkmann, Bernie Copsey, Michel Lecomte – Nuclear Engineering and Design (236, 5-6) 526 (03/2006)
- [6] X. Fu, M. Takahashi, S. Ueta and K. Sawa, “Comparison of HTGR fuel design, manufacture and quality control methods between Japan and China”, Report JAERI-Tech 2002-049, JAERI, Japan, May 2002.
- [7] S. Xu et al., “Research and development of HTR fuel element”, Report CNIC-00573, TSHUNE-0027, INET, Tsinghua University, January 1992.
- [8] M.A. Fütterer et al, “Irradiation of High Temperature Reactor Fuel at VHTR Conditions in the HFR Petten”, Proc. HTR-2004, Beijing, China, 22-24 September 2004.
- [9] C. Pohl, TÜV Rheinland, Germany, Private communication/Email to J.C. Kuijper, 11 November 2019, 14:52.
- [10] General Atomics, “Gas Turbine-Modular Helium Reactor (GT-MHR) Conceptual Design Description Report”, GA Project No.7658, Report 910720, Revision 1, July 1996.
- [11] J.C. Kuijper and D. Muszynski, “Initial SERPENT neutronics calculations on basic HTGR configuration A (no burnable poison) - GEMINI+, WP2, Task 2.4, NUCLIC Note N19060 (DRAFT 02), 4. September 2019.
- [12] M.M. Stempniewicz, “Model of the GEMINI+ Reactor Configuration A - Design-Support Analyses, WP2.4”, 24203/18.148942 Rev. 1, 20/07/2018.
- [13] M.M. Stempniewicz, “GEMINI+ Core Configuration A, - Power from SERPENT, 3-rd Iteration, Design-Support Analyses, WP2.4”, Note NRG-24203/19.153155 Rev. 0, 9 May 2019.
- [14] M. Stempniewicz, NRG, The Netherlands, Private communication/Email to J.C. Kuijper, 12 August 2019, 15:53.
- [15] IAEA-TECDOC-CD-1645, “High Temperature Gas Cooled Reactor Fuels and Materials”, March 2010.
- [16] M. Feltus, “TRISO FUELS “, Webinar, Gen IV International Forum, 18 December 2019, https://www.gen-4.org/gif/jcms/c_114200/gen-iv-webinar-series-36-madeline-feltus-webinar-presentation-18-december-2019.
- [17] “Status report 96 - High Temperature Gas Cooled Reactor - Pebble-Bed Module (HTR-PM)”, Advanced Reactor Information System (ARIS), IAEA, <https://www.iaea.org/resources/databases/advanced-reactors-information-system-aris>.

Part D - Activation

Part D concerns the activation of the replaceable and permanent reflectors, core barrel and pressure vessel, during some operation cycles of 550 days, but also during the 30 to 60 years lifetime of the reactor.

I. INTRODUCTION

The nuclear grade graphite NBG17 is used in the GEMINI+ HTGR system not only in the active core region but also as a surrounding reflector (replaceable reflector and permanent side reflector). The nuclear grade graphite is a pure material but still contains some impurities because of fabrication technology and manufacturing process. The part of the technical specification of NBG17 graphite containing impurity concentrations are presented in Table 1. The last column in Table 1 shows data used in the SERPENT code. The bulk density of graphite NBG17 is 1.89 g/cm³.

The utilization of graphite in the core leads to the generation of different types of radioactive isotopes in this material. The replaceable reflector is replaced after couple fuel cycles (one, two, three). On the other hand, the permanent reflector stays in core for the whole lifetime (60 years). The assessment of activation products and corresponding specific activities are important for irradiated graphite management (replaceable reflector) and later on for decommissioning (permanent reflector).

Table 1. Chemical impurities in nuclear grade graphite NBG17

| Element | | NBG17 graphite, original data [1, 2] | Data used in calculations |
|------------|----|---|---------------------------|
| | | ppm | ppm |
| Iron | Fe | 15 | 15 |
| Chlorine | Cl | < 10 | 10 |
| Nickel | Ni | 1.8 | 1.8 |
| Vanadium | V | 1.8 | 1.8 |
| Boron | B | 0.9 | 0.9 |
| Molybdenum | Mo | 0.15 | 0.15 |
| Indium | In | < 0.14 | 0.14 |
| Uranium | U | < 0.13 | 0.13 |
| Cobalt | Co | < 0.07 | 0.07 |
| Antimony | Sb | < 0.07 | 0.07 |
| Titanium | Ti | < 0.07 | 0.07 |
| Cadmium | Cd | < 0.06 | 0.06 |
| Gold | Au | < 0.05 | 0.05 |
| Thorium | Th | < 0.05 | 0.05 |
| Rhenium | Re | < 0.03 | 0.03 |
| Gadolinium | Gd | < 0.03 | 0.03 |
| Terbium | Tb | < 0.02 | 0.02 |
| Samarium | Sm | < 0.02 | 0.02 |
| Dysprosium | Dy | 0.01 | 0.01 |
| Lithium | Li | < 0.005 | 0.005 |
| Zinc | Zn | < 0.005 | 0.005 |
| Europium | Eu | < 0.002 | 0.002 |
| Nitrogen | N | - | 10 |

Besides the graphite, during the long-term operation the reactor pressure vessel and reactor core barrel are irradiated by a neutron flux. The activation products and their specific activities were also calculated for these materials. The reactor pressure vessel is made of the steel alloy SA508 grade 2. Its chemical composition is shown in Table 2. The density of steel alloy SA508 is 7.833 g/cm³. The reactor core barrel is made of the steel alloy 800H. Its chemical composition is given in the Table 3. The density of steel alloy 800H is 7.94 g/cm³.

Table 2. Chemical composition of steel A508.

| Element | | Steel A508 original data [2] | Data used in calculations |
|------------|----|---------------------------------|---------------------------|
| | | weight % | weight % |
| Carbon | C | ≤0.27 | 0.26 |
| Manganese | Mn | 0.50 – 1.00 | 0.75 |
| Phosphorus | P | ≤0.025 | 0.025 |
| Sulphur | S | ≤0.025 | 0.025 |
| Silicon | Si | ≤0.40 | 0.40 |
| Nickel | Ni | 0.50 – 1.00 | 0.75 |
| Chromium | Cr | 0.25 – 0.45 | 0.35 |
| Molybdenum | Mo | 0.55 – 0.70 | 0.625 |
| Vanadium | V | ≤0.05 | 0.05 |
| Niobium | Ni | ≤0.01 | 0.01 |
| Copper | Cu | ≤0.20 | 0.20 |
| Calcium | Ca | ≤0.015 | 0.015 |
| Boron | B | ≤0.003 | 0.003 |
| Titanium | Ti | ≤0.015 | 0.015 |
| Aluminium | Al | ≤0.025 | 0.025 |
| Iron | Fe | balance | 96.497 (balance) |

Table 3. Chemical composition of steel 800H.

| Element | | Steel 800H original data [2] | Data used in calculations |
|-----------|----|---------------------------------|---------------------------|
| | | weight % | weight % |
| Nickel | Ni | 30.0 – 35.0 | 32.5 |
| Chromium | Cr | 19.0 – 23.0 | 21.0 |
| Iron | Fe | ≥39.5 | 42.4 (balance) |
| Carbon | C | 0.05 – 0.10 | 0.075 |
| Manganese | Mn | 1.50 | 1.5 |
| Copper | Cu | 0.75 | 0.75 |
| Sulphur | S | 0.015 | 0.015 |
| Silicon | Si | 1.0 | 1.0 |
| Aluminium | Al | 0.15 – 0.60 | 0.38 |
| Titanium | Ti | 0.15 – 0.60 | 0.38 |

II. NITROGEN IN NBG17 GRAPHITE

The C14 radionuclide is the greatest concern in the irradiated nuclear graphite [8]. Its concentration arises mainly through the interaction of neutrons with nitrogen according to $N14(n, p)C14$ reaction channel. Isotope N14 is present in the HTGR system and has two origins: impurity in nuclear grade graphite and impurity in reactor coolant. There are a number of pathways for the formation of C14 in irradiated graphite. The main nuclear reactions are $C13(n, \gamma)C14$, $N14(n, p)C14$, $N15(n, d)C14$, $O16(n, 3p)C14$, $O17(n, \alpha)C14$, $U235(n, fission)C14$, and $Pu239(n, fission)C14$ [7, 9].

The technical specification of chemical impurities in nuclear grade graphite NBG17 (Table 1) does not contain any information about nitrogen concentration. Within the GEMINI+ project it was assumed that the NBG17 graphite contains 10 to 100 ppm of nitrogen. The 10 ppm level of nitrogen concentration in the graphite would need a stringent nitrogen management (e.g. refuelling under helium, not air or nitrogen) [1]. Nevertheless, at this stage, for activation calculations the nitrogen concentration of 10 ppm is assumed.

III. SERPENT MODEL AND METHODOLOGY

The Monte Carlo SERPENT code [3] version 2.1.31 in combination with JEFF 3.1.1 nuclear data was used for all neutronics calculations which are presented mainly in this Deliverable D2.8, and others. However, for activation calculations the isotopic composition of each element is required rather than natural composition. The JEFF 3.1.1 library in currently available ACE format does not contain some isotopes, i.e. as C-13, Ti-50, Zn-66, Zn-67, Zn-68, Zn-70, and V-50. Because of that the different library was used, that is ENDF/B-VIII.0 [4, 5].

The neutronics model in SERPENT was built on the most favourable configuration concerning the radial power distribution, that is case 214. For more details see Part A, Section IV. In Part D the model is a little bit elaborated comparing with the one used in Part A. This is because of considering graphite in reflector regions as a burnable material and its division into axial layers.

The goal of activation calculations is to determine the specific activity of selected materials after defined irradiation time together with neutron fluxes and fluences. Those materials are: side replaceable reflector blocks, side permanent reflector, core barrel, and reactor pressure vessel.

In the SERPENT neutronics model the side replaceable reflector is divided radially into two rings. Each ring at a core level is divided axially into layers of 80 cm height (single block height). The side permanent reflector is divided axially into layers of 80 cm height. The top and bottom replaceable reflector are also divided axially into 2 layers each. Finally, the core barrel and the reactor pressure vessel are divided axially into layers of 40 cm height. The division into material zones for burnup/activation calculations is presented in Fig. 1.

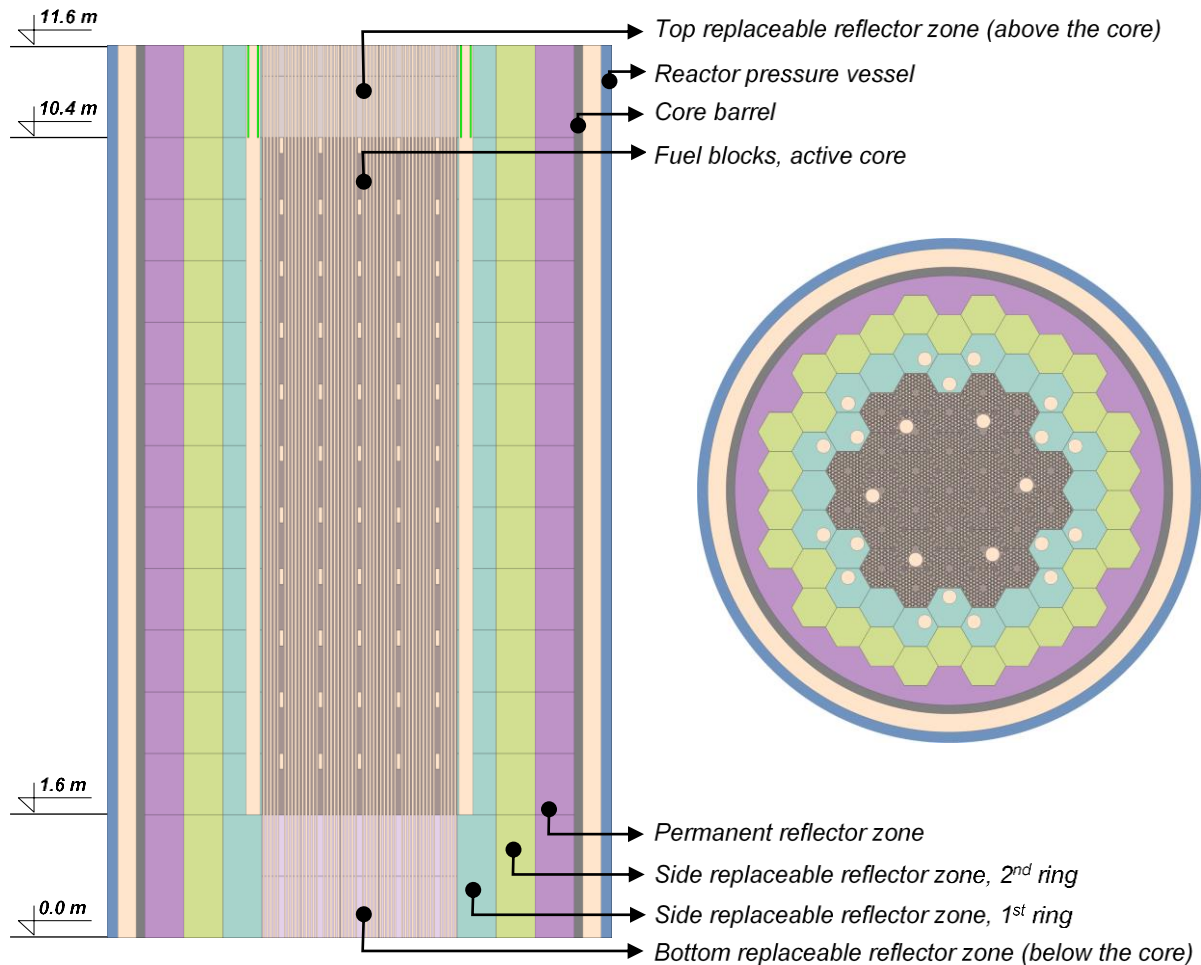


Fig. 1. Horizontal and vertical cross section (not in scale) of SERPENT neutronics model of the GEMINI+ reactor. Division into depletion/activation zones in replaceable reflector and permanent reflector regions.

The SERPENT code allows getting the activation data using two different approaches. One is the depletion mode where the flux changes with the fuel burnup. This approach is reasonable for few fuel cycles because it requires significant computational time to get results with satisfying accuracy. The lifetime of the reactor (some structural materials) is 60 years (~40 fuel cycles). The specific activity assessment of some materials after 60 years of irradiation by using the depletion mode may not be an effective way. Second approach is the activation mode. This is kind of estimation where selected average flux/spectrum distribution over the whole system is used for activation calculations. In this mode cross-sections are not updated after the 1st step. The differences between two modes are presented in next section (Part D, Chapter IV). One of the obstacles in activation mode is that the activation steps cannot be mixed with decay steps (to simulate refuelling period), thus the refuelling period was skipped in the calculations.

For GEMINI+ system a 21 days refuelling period was assumed [6]. The outage period is the same as for General Atomics MHTGR and NGNP 350 MWth

designs. However, for the GEMINI+ reactor the outage period could be reduced because of fewer fuel blocks [6].

IV. SERPENT depletion mode v. activation mode (comparison - one cycle example)

The difference between depletion mode and activation mode in the SERPENT code is described in the previous chapter (Part D, Section III). The activation mode assumes a constant (fixed) neutron flux distribution during activation time. The neutron flux distribution as during middle of life (MOL, $t=250$ days) was used in activation mode. However, in reality the axial neutron flux distribution is not constant, the peak moves with burnup time.

As an example, the axial distribution of fast neutron flux (above 0.1 MeV) in the 1st ring of replaceable reflector is shown in Fig. 2. At the BOL (Begin Of Life; $t=0$ day) the fast neutron flux peak is located in 9th layer of active core (800-880 cm), then moves down to 8th layer (720-800 cm) at MOL (Middle Of Life; $t=250$ days), and finally ends in 3rd layer (320-400 cm) for EOL (End Of Life; $t=550$ days). It is clear that the usage of the constant neutron flux as an average one may lead to overestimation of specific activity in the top layers and underestimation in lower ones. This is particularly important for isotopes of short half-life period. The specific activity distribution (irradiation time 550 days) in 1st ring of replaceable reflector for selected nuclides is shown in Fig. 3.

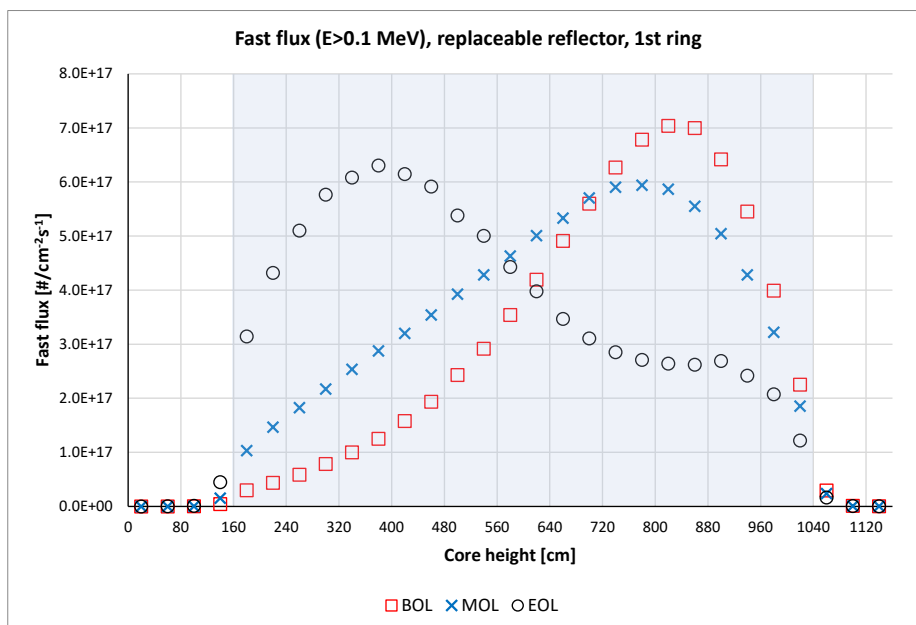


Fig. 2. Depletion mode. Neutron fast flux (above 0.1 MeV) distribution in the 1st ring of replaceable reflector (two neutron detectors per 80 cm; active core between 160 cm and 1040 cm). Relative standard error within the active core height do not exceed 0.95%. BOL – Begin Of Life ($t=0$ day), MOL – Middle Of Life ($t=250$ days), EOL – End Of Life ($t=550$ days).

The difference between activation and depletion mode is especially visible for nuclides of relatively short half-life period, like vanadium V52 ($T_{1/2}=3.75$ min). It is worth mentioning that right after reactor shutdown the share of V52 in the total specific activity is 13.8%. Because of that, the activation mode with MOL flux distribution may give wrong results for nuclides of short half-life periods. Thus, nuclides with relatively short half-life time, that is $T_{1/2}$ below 1 year, has been skipped in this report. However, usage the EOL flux distribution in the activation mode may give better results, but only for short half-life period $T_{1/2}$.

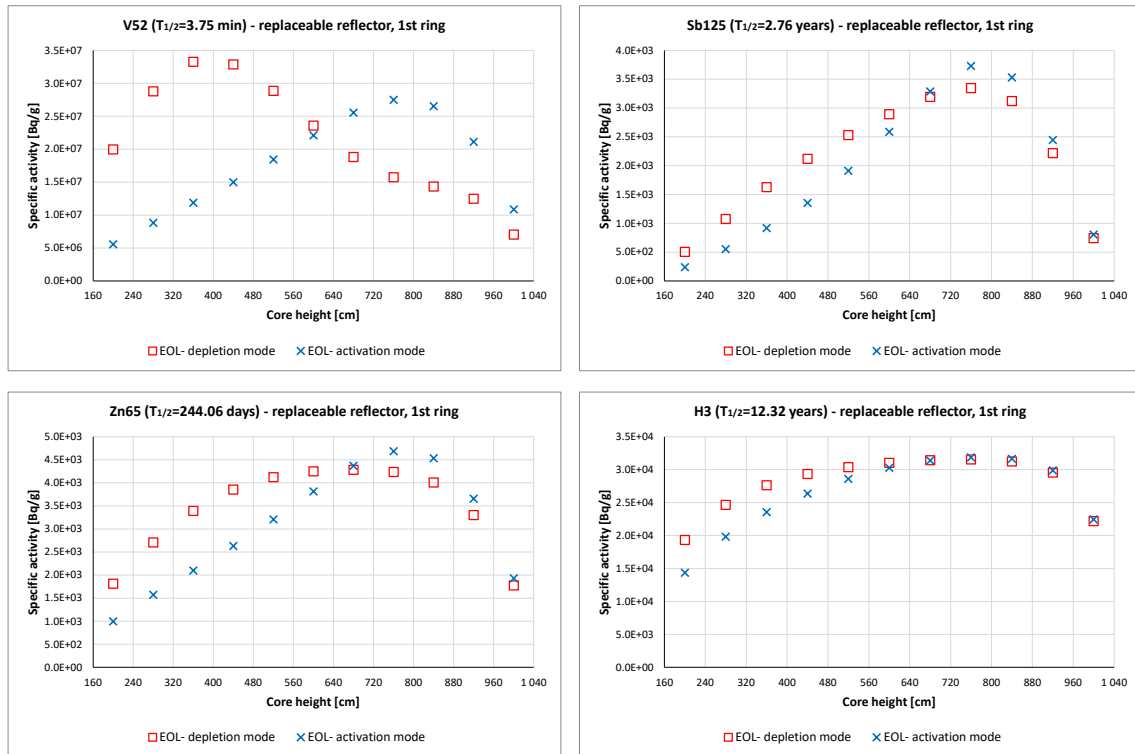


Fig. 3. Specific activity distribution in 1st ring of replaceable reflector for selected nuclides with increasing half-life periods. Comparison between activation mode and depletion mode after one cycle of irradiation 550 days. EOL – End Of Life. Active core is placed between 160 cm and 1040 cm.

Table 4 contains specific activities [Bq/g] in the 1st ring of replaceable reflector for top 15 specific activities of short half-life (1-100 years) period and top 15 of long half-life period (over 100 years). As it was explained before, radionuclides of half-life periods shorter than 1 year was skipped in the calculations. The data are divided into two groups:

- 1) average specific activities in 1st ring of replaceable reflector,
- 2) layer with maximum activity – 8th layer of active core (720-800 cm).

The peak value of specific activities after one cycle (550 days of irradiation) is present in the 8th layer (720-800 cm) regardless of the selected mode in SERPENT: depletion or activation.

Table 4. Specific activity, 1st ring of replaceable reflector, selected radionuclides (top 15 of short lived and top 15 of long lived), no decay (after shutdown).

| Isotope | Half-life time Y – year D - day | Depletion mode | Activation mode | | Depletion mode | Activation mode | |
|---|---------------------------------------|---------------------------------|---------------------------------|----------------|------------------------------------|------------------------------------|----------------|
| | | 1 st ring RR average | 1 st ring RR average | | 1 st ring RR 720-800 cm | 1 st ring RR 720-800 cm | |
| | | Specific activity [Bq/g] | Specific activity [Bq/g] | Relative error | Specific activity [Bq/g] | Specific activity [Bq/g] | Relative error |
| 1 | 2 | 3 | 4 | 5 | 6 | 7 | 8 |
| Short-lived (half-life period: 1 year – 100 years) | | | | | | | |
| Fe55 | 2.74 Y | 1.38E+06 | 1.24E+06 | 10.0% | 1.84E+06 | 1.93E+06 | 4.9% |
| Co60 | 5.27 Y | 1.05E+06 | 9.52E+05 | 9.2% | 1.41E+06 | 1.47E+06 | 4.5% |
| Ru106 | 371.8 D | 6.49E+04 | 6.08E+04 | 6.4% | 9.08E+04 | 1.06E+05 | 16.9% |
| Eu155 | 4.75 Y | 4.51E+04 | 4.25E+04 | 5.8% | 4.84E+04 | 4.86E+04 | 0.3% |
| Eu154 | 8.59 Y | 4.25E+04 | 4.20E+04 | 1.2% | 4.38E+04 | 4.54E+04 | 3.5% |
| H3 | 12.32 Y | 2.80E+04 | 2.64E+04 | 5.9% | 3.16E+04 | 3.19E+04 | 0.9% |
| Pm147 | 2.62 Y | 1.55E+04 | 1.45E+04 | 6.6% | 2.11E+04 | 2.24E+04 | 6.4% |
| Pu241 | 14.29 Y | 1.04E+04 | 1.02E+04 | 1.3% | 1.43E+04 | 1.67E+04 | 17.2% |
| Cs137 | 30.08 Y | 6.63E+03 | 6.17E+03 | 6.8% | 9.55E+03 | 1.04E+04 | 8.8% |
| Sr90 | 28.79 Y | 3.63E+03 | 3.36E+03 | 7.4% | 5.11E+03 | 5.47E+03 | 7.0% |
| Cs134 | 2.07 Y | 3.31E+03 | 3.11E+03 | 6.0% | 5.58E+03 | 6.63E+03 | 18.7% |
| Sb125 | 2.76 Y | 2.12E+03 | 1.94E+03 | 8.6% | 3.34E+03 | 3.73E+03 | 11.4% |
| Kr85 | 10.76 Y | 6.23E+02 | 5.82E+02 | 6.5% | 8.86E+02 | 9.52E+02 | 7.4% |
| Cd109 | 461.4 D | 6.09E+02 | 5.75E+02 | 5.6% | 6.96E+02 | 7.77E+02 | 11.7% |
| Sm151 | 90.0 Y | 4.70E+02 | 4.91E+02 | 4.5% | 4.25E+02 | 4.36E+02 | 2.5% |
| Long-lived (half-life period > 100 years) | | | | | | | |
| Ni63 | 100.1 Y | 2.12E+04 | 1.93E+04 | 9.3% | 2.88E+04 | 2.98E+04 | 3.3% |
| C14 | 5700 Y | 1.39E+04 | 1.26E+04 | 9.4% | 1.91E+04 | 1.98E+04 | 3.5% |
| Cl36 | 3.0E+05 Y | 1.87E+03 | 1.72E+03 | 8.4% | 2.38E+03 | 2.43E+03 | 2.2% |
| Ni59 | 7.6E+04 Y | 1.41E+02 | 1.28E+02 | 9.1% | 1.89E+02 | 1.95E+02 | 2.9% |
| Pu240 | 6561 Y | 8.46E+01 | 7.91E+01 | 6.4% | 1.07E+02 | 1.12E+02 | 4.3% |
| Pu239 | 2.4E+04 Y | 3.48E+01 | 3.80E+01 | 9.1% | 3.46E+01 | 3.99E+01 | 15.3% |
| Ar39 | 269 Y | 8.41E+00 | 7.35E+00 | 12.6% | 1.44E+01 | 1.54E+01 | 7.1% |
| Am241 | 432.6 Y | 5.65E+00 | 5.52E+00 | 2.2% | 9.36E+00 | 8.53E+00 | 8.8% |
| U233 | 1.6E+05 Y | 3.70E+00 | 3.56E+00 | 3.7% | 4.61E+00 | 4.57E+00 | 0.7% |
| Mo93 | 4.0E+03 Y | 1.37E+00 | 1.27E+00 | 7.1% | 1.86E+00 | 1.98E+00 | 6.0% |
| Ho166m | 1.2E+03 Y | 1.21E+00 | 1.22E+00 | 0.7% | 1.33E+00 | 1.42E+00 | 7.0% |
| Tc99 | 2.1E+05 Y | 9.80E-01 | 9.19E-01 | 6.3% | 1.39E+00 | 1.50E+00 | 8.0% |
| Am243 | 7370 Y | 3.78E-01 | 3.84E-01 | 1.7% | 7.87E-01 | 1.04E+00 | 31.6% |
| Be10 | 1.5E+06 Y | 3.24E-01 | 3.20E-01 | 1.2% | 4.34E-01 | 4.90E-01 | 12.9% |
| Zr93 | 1.6E+06 Y | 9.47E-02 | 8.79E-02 | 7.1% | 1.35E-01 | 1.45E-01 | 7.6% |

It is worth mentioning that:

- 1) Specific activities averaged over 1st ring of the replaceable reflector for the activation mode (fixed flux) are consistent ($\pm 10\%$) with data obtained using depletion mode (flux is not fixed);
- 2) Specific activities are the highest in the 8th layer for both activation mode and depletion mode;
- 3) Activation mode overestimates specific activities for the 8th layer comparing with depletion mode;
- 4) The actual maximum values of specific activities per layer for the depletion mode (Table 4, 6th column) are between the calculated maximum value (Table 4, 7th column) and calculated average value (Table 4, 4th column) for activation mode.
- 5) Presented in Table 4 specific activities are right after reactor shutdown (no decay).

V. REPLACEABLE REFLECTOR 1ST AND 2ND RING

Table 5 and Table 6 contain sets of specific activities of top 15 short lived activation products and top 15 long lived ones right after reactor shutdown (no decay time after it). Specific activities are given after 1.5 year of irradiation (one cycle) and after 3 years (two cycles). Additionally, Table 5 contains results obtained in one of the deliverables [1] from former project HTR-N, together with French limits (ANDRA) of acceptance in a surface disposal.

Note that the HTR-N data are for GT-MHR type for Pu-burning (different spectrum), the active core has an annular shape, reactor thermal power is different, and the chemical composition of graphite (impurities) are different, thus these data should be only indicative for GEMINI+ system.

It is worth mentioning that presented in Table 5 specific activities are right after reactor shutdown (no decay). All listed radionuclides have specific activities below ANDRA packages acceptance limits.

Table 5. Specific activity *1st ring of replaceable reflector*, selected radionuclides (top 15 of short lived and top 15 long lived) after 1 and 2 fuel cycles, no decay (after shutdown). Comparison with HTR-N project.

| Isotope | Half-life time Y - year D - day | GEMINI+ project Irradiation time 1.5 year (1 cycle) | | GEMINI+ project Irradiation time 3 years (2 cycles) | | Data from HTR-N project [1] Irradiation time 3 years | |
|---|---------------------------------------|---|---------------------------------------|---|---------------------------------------|---|---|
| | | 1 st ring RR average | 1 st ring RR 720-800 cm | 1 st ring RR average | 1 st ring RR 720-800 cm | Inner RR (20 cm to the fuel assemblies) | ANDRA packages acceptance limits |
| | | Activity [Bq/g] | Activity [Bq/g] | Activity [Bq/g] | Activity [Bq/g] | Activity [Bq/g] | Activity [Bq/g] |
| 1 | 2 | 3 | 4 | 5 | 6 | 8 | 9 |
| Short-lived (half-life period: 1 year – 100 years) | | | | | | | |
| Fe55 | 2.74 Y | 1.24E+06 | 1.93E+06 | 2.05E+06 | 3.19E+06 | 6.10E+05 | 6.10E+09 |
| Co60 | 5.27 Y | 9.52E+05 | 1.47E+06 | 1.66E+06 | 2.51E+06 | 6.50E+05 | 1.30E+08 |
| Ru106 | 371.8 D | 6.07E+04 | 1.06E+05 | 1.08E+05 | 1.78E+05 | 1.62E-02 | 1.20E+08 |
| Eu155 | 4.75 Y | 4.24E+04 | 4.86E+04 | 4.28E+04 | 3.86E+04 | - | - |
| Eu154 | 8.59 Y | 4.20E+04 | 4.54E+04 | 4.06E+04 | 3.51E+04 | 1.37E+04 | 5.80E+07 |
| H3 | 12.32 Y | 2.64E+04 | 3.18E+04 | 3.13E+04 | 3.39E+04 | 1.15E+06 | 1.00E+06 |
| Pm147 | 2.62 Y | 1.44E+04 | 2.24E+04 | 2.44E+04 | 3.46E+04 | 7.75E+00 | 5.80E+08 |
| Pu241 | 14.29 Y | 1.02E+04 | 1.67E+04 | 1.77E+04 | 2.22E+04 | - | - |
| Cs137 | 30.08 Y | 6.17E+03 | 1.04E+04 | 1.43E+04 | 2.33E+04 | 1.10E-03 | 3.30E+05 |
| Sr90 | 28.79 Y | 3.36E+03 | 5.45E+03 | 7.31E+03 | 1.17E+04 | 1.62E-02 | 6.00E+06 |
| Cs134 | 2.07 Y | 3.11E+03 | 6.59E+03 | 1.17E+04 | 2.38E+04 | 5.24E+01 | 1.90E+08 |
| Sb125 | 2.76 Y | 1.94E+03 | 3.71E+03 | 3.74E+03 | 6.95E+03 | 9.01E+03 | 4.10E+08 |
| Cd109 | 461.4 D | 5.82E+02 | 7.76E+02 | 6.68E+02 | 8.41E+02 | - | - |
| Kr85 | 10.76 Y | 5.75E+02 | 9.50E+02 | 1.26E+03 | 2.05E+03 | - | - |
| Sm151 | 90.0 Y | 4.91E+02 | 4.36E+02 | 4.16E+02 | 3.33E+02 | 8.31E+00 | 4.50E+05 |
| Long-lived (half-life period > 100 years) | | | | | | | |
| Ni63 | 100.1 Y | 1.92E+04 | 2.97E+04 | 3.67E+04 | 5.59E+04 | 3.90E+04 | 3.20E+06 |
| C14 | 5700 Y | 1.26E+04 | 1.97E+04 | 2.52E+04 | 3.94E+04 | 4.66E+04 | 9.20E+04 |
| Cl36 | 3.0E+05 Y | 1.71E+03 | 2.43E+03 | 2.62E+03 | 3.37E+03 | 1.30E+03 | 2.40E+04 |
| Ni59 | 7.6E+04 Y | 1.28E+02 | 1.94E+02 | 2.32E+02 | 3.39E+02 | 2.54E+02 | 1.10E+05 |
| Pu240 | 6561 Y | 7.91E+01 | 1.11E+02 | 1.14E+02 | 1.31E+02 | - | - |
| Pu239 | 2.4E+04 Y | 3.80E+01 | 3.99E+01 | 3.93E+01 | 3.85E+01 | - | - |
| Ar39 | 269 Y | 7.34E+00 | 1.54E+01 | 2.91E+01 | 6.08E+01 | - | - |
| Am241 | 432.6 Y | 5.53E+00 | 8.53E+00 | 1.56E+01 | 1.57E+01 | - | - |
| U233 | 1.6E+05 Y | 3.56E+00 | 4.57E+00 | 4.73E+00 | 5.32E+00 | - | - |
| Mo93 | 4.0E+03 Y | 1.27E+00 | 1.97E+00 | 2.52E+00 | 3.89E+00 | 2.19E+00 | 3.80E+04 |
| Ho166m | 1.2E+03 Y | 1.22E+00 | 1.42E+00 | 1.47E+00 | 1.72E+00 | - | - |
| Tc99 | 2.1E+05 Y | 9.18E-01 | 1.50E+00 | 2.02E+00 | 3.19E+00 | 4.27E-01 | 4.40E+04 |
| Am243 | 7370 Y | 3.83E-01 | 1.03E+00 | 3.31E+00 | 7.86E+00 | - | - |
| Be10 | 1.5E+06 Y | 3.20E-01 | 4.89E-01 | 6.40E-01 | 9.79E-01 | 2.90E+00 | 5.10E+03 |
| Zr93 | 1.6E+06 Y | 8.79E-02 | 1.44E-01 | 1.98E-01 | 3.19E-01 | 2.74E-07 | 1.80E+04 |

Table. 6 Specific activity 2nd ring of replaceable reflector, selected radionuclides (top 15 of short lived and top 15 long lived) after 1 and 2 fuel cycles, no decay (after shutdown).

| Isotope | Half-life time Y – year D - day | GEMINI+ project Irradiation time 1.5 year (1 cycle) | | GEMINI+ project Irradiation time 3 years (2 cycles) | |
|---|---|---|--|---|--|
| | | 1 st ring RR <u>average</u> | 1 st ring RR <u>720-800 cm</u> | 1 st ring RR <u>average</u> | 1 st ring RR <u>720-800 cm</u> |
| | | Activity [Bq/g] | Activity [Bq/g] | Activity [Bq/g] | Activity [Bq/g] |
| 1 | 2 | 3 | 4 | 5 | 6 |
| Short-lived (half-life period: 1 year – 100 years) | | | | | |
| Fe55 | 2.74 Y | 7.01E+05 | 1.08E+06 | 1.17E+06 | 1.80E+06 |
| Co60 | 5.27 Y | 5.20E+05 | 7.98E+05 | 9.24E+05 | 1.41E+06 |
| Eu155 | 4.75 Y | 3.11E+04 | 4.18E+04 | 3.95E+04 | 4.45E+04 |
| Eu154 | 8.59 Y | 2.98E+04 | 3.61E+04 | 3.47E+04 | 3.71E+04 |
| H3 | 12.32 Y | 2.02E+04 | 2.66E+04 | 2.73E+04 | 3.22E+04 |
| Ru106 | 371.8 D | 8.88E+03 | 1.56E+04 | 1.66E+04 | 2.82E+04 |
| Pm147 | 2.74 Y | 4.54E+03 | 6.90E+03 | 7.52E+03 | 1.11E+04 |
| Eu152 | 5.27 Y | 1.76E+03 | 3.92E+00 | 1.61E+02 | 1.98E+00 |
| Cs137 | 30.08 Y | 1.62E+03 | 2.60E+03 | 3.48E+03 | 5.55E+03 |
| Sr90 | 28.79 Y | 1.24E+03 | 1.92E+03 | 2.48E+03 | 3.82E+03 |
| Pu241 | 14.29 Y | 8.62E+02 | 1.73E+03 | 2.58E+03 | 4.40E+03 |
| Sm151 | 90.0 Y | 4.61E+02 | 4.35E+02 | 4.19E+02 | 3.73E+02 |
| Cs134 | 2.07 Y | 3.70E+02 | 7.62E+02 | 1.32E+03 | 2.67E+03 |
| Sb125 | 2.76 Y | 2.99E+02 | 5.69E+02 | 6.18E+02 | 1.15E+03 |
| Cd109 | 461.4 D | 2.53E+02 | 3.59E+02 | 3.12E+02 | 4.23E+02 |
| Long-lived (half-life period > 100 years) | | | | | |
| Ni63 | 100.1 Y | 1.11E+04 | 1.70E+04 | 2.15E+04 | 3.27E+04 |
| C14 | 5700 Y | 7.10E+03 | 1.10E+04 | 1.42E+04 | 2.19E+04 |
| Cl36 | 3.0E+05 Y | 1.10E+03 | 1.61E+03 | 1.87E+03 | 2.59E+03 |
| Ni59 | 7.6E+04 Y | 7.59E+01 | 1.15E+02 | 1.43E+02 | 2.14E+02 |
| Pu240 | 6561 Y | 1.62E+01 | 2.74E+01 | 3.47E+01 | 5.18E+01 |
| Pu239 | 2.4E+04 Y | 1.15E+01 | 1.36E+01 | 1.34E+01 | 1.42E+01 |
| Ar39 | 269 Y | 2.33E+00 | 4.78E+00 | 9.26E+00 | 1.90E+01 |
| U233 | 1.6E+05 Y | 1.89E+00 | 2.63E+00 | 2.93E+00 | 3.72E+00 |
| Ho166m | 1.2E+03 Y | 8.30E-01 | 1.00E+00 | 1.00E+00 | 1.13E+00 |
| Mo93 | 4.0E+03 Y | 5.31E-01 | 8.19E-01 | 1.06E+00 | 1.63E+00 |
| Am241 | 432.6 Y | 5.02E-01 | 9.93E-01 | 2.75E+00 | 4.40E+00 |
| Tc99 | 2.1E+05 Y | 2.48E-01 | 3.90E-01 | 5.17E-01 | 8.04E-01 |
| Zr93 | 1.6E+06 Y | 2.84E-02 | 4.44E-02 | 5.89E-02 | 9.16E-02 |
| Be10 | 1.5E+06 Y | 1.52E-02 | 2.42E-02 | 3.04E-02 | 4.84E-02 |
| Cs135 | 2.3E+06 Y | 4.94E-03 | 5.87E-03 | 1.08E-02 | 1.28E-02 |

VI. STRUCTURES WITH LONG IRRADIATION TIME

Some structural materials that stay inside the reactor for the whole lifetime (60 years). These materials are: reactor pressure vessel, reactor core barrel, and permanent side reflector.

VI.A REACTOR PRESSURE VESSEL (STEEL A508)

As it was shown earlier (Fig. 2), in the 1st ring of the replaceable reflector the axial neutron flux distribution during single fuel cycle is not constant. The peak value shifts to the lower half-core at the EOL (550 days). Similar behaviour one can observe in the reactor pressure vessel region (see Fig. 4). The reactor pressure vessel structure is in the very peripheral region of the core thus the impact of the statistical aspects is much more visible.

At MOL (250 days) neutron flux distribution, the peak value of the fast neutron flux ($E > 0.1$ MeV) is $8.74 \cdot 10^8 \text{ cm}^{-2}\text{s}^{-1}$ ($\pm 15\%$). The average value of the fast neutron flux ($E > 0.1$ MeV) at MOL for the whole reactor pressure vessel is $3.9 \cdot 10^8 \text{ cm}^{-2}\text{s}^{-1}$ ($\pm 3.4\%$).

The fast flux in the pressure vessel will give rise to a fast fluence by integration over the entire life of the reactor, i.e. 60 full power years ($\approx 1.89 \cdot 10^9$ s). A very conservative assumption would be the peak fast flux ($8.74 \cdot 10^8 \text{ cm}^{-2}\text{s}^{-1}$) occurring all the time at the same position. This would give a fluence of $1.65 \cdot 10^{18} \text{ cm}^{-2}$ ($\pm 15\%$) at that location. However, the fluence assessed using the average fast flux in the reactor pressure vessel is $7.37 \cdot 10^{17} \text{ cm}^{-2}$ ($\pm 3.4\%$).

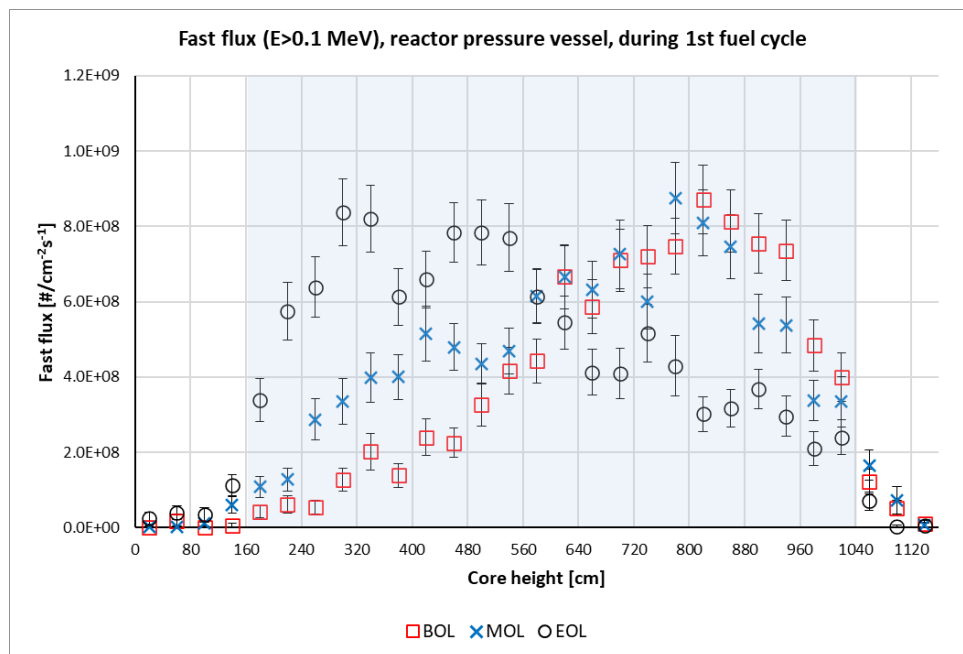


Fig. 4. Depletion mode. Neutron fast flux (above 0.1 MeV) distribution in the reactor pressure vessel (two neutron detectors per 80 cm; active core between 160 cm and 1040 cm). Relative standard error shown on error bars. BOL – Begin Of Life ($t=0$ day), MOL – Middle Of Life ($t=250$ days), EOL – End Of Life ($t=550$ days).

Table 7 Specific activity reactor pressure vessel, selected radionuclides (top importance of short lived and long lived) after 30 and 60 years of irradiation, no decay (after shutdown).

| Isotope | Half-life time Y – year D - day | Irradiation time ~30 years | | Irradiation time ~60 years (reactor lifetime) | |
|---|---------------------------------------|-------------------------------|--------------------------|--|--------------------------|
| | | Average | Peak value 720-800 cm | Average | Peak value 720-800 cm |
| | | Activity [Bq/g] | Activity [Bq/g] | Activity [Bq/g] | Activity [Bq/g] |
| 1 | 2 | 3 | 4 | 5 | 6 |
| Short-lived (half-life period: 1 year – 100 years) | | | | | |
| Fe55 | 2.74 Y | 1.16E+06 | 2.22E+06 | 1.17E+06 | 2.22E+06 |
| Co60 | 5.27 Y | 5.68E+00 | 7.75E+00 | 7.22E+00 | 1.15E+01 |
| H3 | 12.32 Y | 5.91E+00 | 1.05E+01 | 6.99E+00 | 1.24E+01 |
| Nb93m | 16.13 Y | 7.79E-08 | 9.38E-08 | 2.28E-07 | 2.75E-07 |
| Sr90 | 28.79 Y | 1.79E-14 | 1.30E-14 | 5.84E-14 | 4.25E-14 |
| Long-lived (half-life period > 100 years) | | | | | |
| Ni63 | 2.74 Y | 6.02E+03 | 1.15E+04 | 1.09E+04 | 2.08E+04 |
| Ni59 | 5.27 Y | 5.03E+01 | 9.59E+01 | 1.01E+02 | 1.92E+02 |
| Nb94 | 2.03E+4 Y | 8.87E-01 | 1.75E+00 | 1.77E+00 | 3.50E+00 |
| Ca41 | 1.02E+5 Y | 1.51E-01 | 2.87E-01 | 3.02E-01 | 5.73E-01 |
| C14 | 5700 Y | 5.81E-03 | 1.11E-02 | 1.16E-02 | 2.21E-02 |
| Ar39 | 269 Y | 3.09E-04 | 2.38E-04 | 5.94E-04 | 4.59E-04 |
| Be10 | 1.5E+06 Y | 6.55E-06 | 1.05E-05 | 1.31E-05 | 2.09E-05 |
| Zr93 | 1.6E+06 Y | 1.82E-07 | 2.19E-07 | 3.64E-07 | 4.38E-07 |
| Cl36 | 3.0E+05 Y | 5.82E-08 | 1.42E-07 | 2.32E-07 | 5.73E-07 |

Table 7 shows the specific activity of most important radionuclides after long-term irradiation of reactor pressure vessel (steel alloy A508). The results are presented at two timesteps: in the middle of reactor lifetime (~30 years, 20 cycles) and at the end of reactor lifetime (after 60 years). For each timestep two values of specific activity are presented. First is the peak value and second is the average one. The peak value in core barrel occurs in the layer corresponding to 8th fuel layer of active core where the neutron flux is the highest (720-800 cm, see Fig. 1).

The chemical composition of steel alloy A508 in the SERPENT input consists of 44 nuclides and not of 81 as it is for NBG17 graphite. Because of that the list of most important radionuclides is shorter (Table 7). As it was explained earlier (Part D, Section III and IV) radionuclides with half-life period shorter than 1 year are not considered.

It is worth mentioning that presented in Table 7 specific activities are right after reactor shutdown (no decay). All listed radionuclides have specific activities below ANDRA packages acceptance limits. The ANDRA limits for selected radionuclides are listed in Table 5.

VI.B CORE BARREL (STEEL 800H)

Table 8 shows the specific activity of most important radionuclides after long-term irradiation of core barrel (steel alloy 800H). The structure of this Table is analogical and consistent with the one for the reactor pressure vessel (Table 7). The peak value of specific activity in the core barrel occurs also in the layer corresponding to 8th fuel layer of active core where the neutron flux is the highest (720-800 cm, see Fig. 1).

The chemical composition of steel alloy 800H in the SEREPNT input consists of 31 nuclides and not of 81 as it is for NBG17 graphite. Because of that the list of most important radionuclides is shorter (Table 8). As it was explained earlier (Part D, Section III and IV) radionuclides with half-life period shorter than 1 year are not considered.

Table. 8 Specific activity core barrel, selected radionuclides (top importance of short lived and long lived) after 30 and 60 years of irradiation, no decay (after shutdown).

| Isotope | Half-life time Y - year D - day | Irradiation time ~30 years | | Irradiation time ~60 years (reactor lifetime) | |
|---|---------------------------------------|-------------------------------|--------------------------|--|--------------------------|
| | | Average | Peak value 720-800 cm | Average | Peak value 720-800 cm |
| | | Activity [Bq/g] | Activity [Bq/g] | Activity [Bq/g] | Activity [Bq/g] |
| 1 | 2 | 3 | 4 | 5 | 6 |
| Short-lived (half-life period: 1 year – 100 years) | | | | | |
| Fe55 | 2.74 Y | 9.84E+07 | 1.93E+08 | 9.84E+07 | 1.93E+08 |
| Co60 | 5.27 Y | 1.92E+04 | 5.02E+04 | 4.96E+04 | 1.34E+05 |
| H3 | 12.32 Y | 2.67E-03 | 1.61E-06 | 4.59E-03 | 1.86E-05 |
| Long-lived (half-life period > 100 years) | | | | | |
| Ni63 | 100.1 Y | 5.02E+07 | 9.85E+07 | 9.07E+07 | 1.78E+08 |
| Ni59 | 7.6E+04 Y | 4.17E+05 | 8.17E+05 | 8.26E+05 | 1.61E+06 |
| Cl36 | 3.0E+05 Y | 1.26E-03 | 3.33E-03 | 4.99E-03 | 1.31E-02 |
| C14 | 5700 Y | 1.38E-05 | 3.66E-05 | 5.51E-05 | 1.46E-04 |
| Ar39 | 269 Y | 1.64E-09 | 5.31E-09 | 1.29E-08 | 4.18E-08 |
| Be10 | 1.5E+06 Y | 1.69E-10 | 1.30E-10 | 6.77E-10 | 5.21E-10 |

The core barrel after 60 years of irradiation contains two radioactive nuclides of nickel (Ni63 and Ni59) with the specific activity exceeding ANDRA packages acceptance limits. It is worth mentioning that presented in Table 8 specific activities are right after reactor shutdown (no decay). The ANDRA limits for selected radionuclides are listed in Table 5.

The limit for Ni63 is 3.20E+06 Bq/g. The average specific activity (after shutdown) of Ni63 in core barrel after 60 years of irradiation is 9.07E+07 Bq/g (peak value is 1.78E+08 Bq/g).

The limit for Ni59 is $1.10E+05$ Bq/g. The average specific activity (after shutdown) of Ni59 in core barrel after 60 years of irradiation is $1.10E+05$ Bq/g (peak value is $1.61E+06$ Bq/g).

All the other listed radionuclides have specific activities below ANDRA packages acceptance limits.

The short-lived radionuclide Fe55 reaches its equilibrium state after 10 years of irradiation. Radioactive Fe55 is generated as a result of neutron activation of stable iron by (n,γ) nuclear reaction: $Fe54(n,\gamma)Fe55$ and $56Fe56(n,2n)Fe55$. Its half-life time is 2.74 years.

VI.C PERMANENT REFLECTOR (GRAPHITE NGB17)

Table 9 shows the specific activity of most important radionuclides after long-term irradiation of permanent reflector (graphite NGB17). The structure of this Table is analogical and consistent with the one for the reactor pressure vessel and core barrel (Tables 7 and 8). The peak value of specific activity in the core barrel occurs also in the layer corresponding to 8th fuel layer of active core where the neutron flux is the highest (720-800 cm, see Fig. 1).

The permanent reflector after 60 years of irradiation contains only one radionuclide C14 with the specific activity exceeding ANDRA packages acceptance limits. It is worth mentioning that presented in Table 9 specific activities are right after reactor shutdown (no decay). The ANDRA limits for selected radionuclides are listed in Table 5.

The limit for C14 is $9.20E+04$. The average specific activity (after shutdown) of C14 in core barrel after 60 years of irradiation is $8.62E+04$ Bq/g with the peak value is $1.31E+05$ Bq/g.

It is worth mentioning that the peak value is a result of fixed flux in the SERPENT activation mode (see Part D, Chapter IV and Fig. 2) and may be a conservative approach. Nevertheless, the average value is very close to the ANDRA limit for C14.

The interaction of neutrons with nitrogen according to $N14(n,p)C14$ is the main reaction channel for C14 generation. It must be noted that a low value (10 ppm) of nitrogen as impurity in graphite was assumed in calculations. All the other listed radionuclides have specific activities below ANDRA packages acceptance limits.

Table. 9 Specific activity *permanent reflector*, selected radionuclides (top 15 of short lived and top 15 long lived) after 30 and 60 years of irradiation, no decay (after shutdown).

| Isotope | Half-life time Y - year D - day | Irradiation time ~30 years | | Irradiation time ~60 years (reactor lifetime) | |
|---|---------------------------------------|-------------------------------|--------------------------|--|--------------------------|
| | | Average | Peak value 720-800 cm | Average | Peak value 720-800 cm |
| | | Activity [Bq/g] | Activity [Bq/g] | Activity [Bq/g] | Activity [Bq/g] |
| 1 | 2 | 3 | 4 | 5 | 6 |
| Short-lived (half-life period: 1 year – 100 years) | | | | | |
| Fe55 | 2.74 Y | 6.66E+05 | 1.01E+06 | 6.55E+05 | 9.86E+05 |
| Co60 | 5.27 Y | 7.21E+05 | 1.03E+06 | 5.72E+05 | 7.50E+05 |
| H3 | 12.32 Y | 3.15E+04 | 3.29E+04 | 3.20E+04 | 3.30E+04 |
| Eu155 | 4.75 Y | 2.81E+04 | 2.49E+04 | 1.70E+04 | 1.03E+04 |
| Eu154 | 8.59 Y | 2.56E+04 | 2.06E+04 | 1.53E+04 | 7.73E+03 |
| Cs137 | 30.08 Y | 7.21E+03 | 1.12E+04 | 1.11E+04 | 1.70E+04 |
| Sr90 | 28.79 Y | 5.09E+03 | 7.73E+03 | 7.45E+03 | 1.13E+04 |
| Ru106 | 371.8 D | 5.46E+03 | 8.68E+03 | 5.66E+03 | 8.70E+03 |
| Cs134 | 2.07 Y | 2.35E+03 | 4.55E+03 | 4.45E+03 | 8.40E+03 |
| Pu241 | 14.29 Y | 3.68E+03 | 4.72E+03 | 4.42E+03 | 4.94E+03 |
| Pm147 | 2.74 Y | 3.85E+03 | 5.73E+03 | 3.96E+03 | 5.85E+03 |
| Kr85 | 10.76 Y | 6.25E+02 | 9.64E+02 | 7.20E+02 | 1.09E+03 |
| Cm244 | 18.11 Y | 5.29E+01 | 1.45E+02 | 4.60E+02 | 1.15E+03 |
| Pu238 | 87.7 Y | 1.47E+02 | 2.02E+02 | 3.04E+02 | 2.79E+02 |
| Sb125 | 2.76 Y | 2.70E+02 | 4.39E+02 | 2.70E+02 | 4.24E+02 |
| Long-lived (half-life period > 100 years) | | | | | |
| Ni63 | 100.1 Y | 5.46E+04 | 7.96E+04 | 8.64E+04 | 1.20E+05 |
| C14 | 5700 Y | 4.33E+04 | 6.60E+04 | 8.62E+04 | 1.31E+05 |
| Cl36 | 3.0E+05 Y | 3.21E+03 | 3.57E+03 | 3.17E+03 | 2.67E+03 |
| Ni59 | 7.6E+04 Y | 3.54E+02 | 4.85E+02 | 5.30E+02 | 6.62E+02 |
| Ar39 | 269 Y | 8.29E+01 | 1.67E+02 | 3.17E+02 | 6.35E+02 |
| Pu240 | 6561 Y | 5.09E+01 | 6.04E+01 | 5.98E+01 | 6.25E+01 |
| Am241 | 432.6 Y | 2.49E+01 | 2.35E+01 | 3.69E+01 | 2.53E+01 |
| Pu239 | 2.4E+04 Y | 9.78E+00 | 9.77E+00 | 9.72E+00 | 9.55E+00 |
| Mo93 | 4.0E+03 Y | 3.05E+00 | 4.61E+00 | 5.90E+00 | 8.83E+00 |
| Am243 | 7370 Y | 8.28E-01 | 1.90E+00 | 4.07E+00 | 8.29E+00 |
| U233 | 1.6E+05 Y | 3.89E+00 | 4.04E+00 | 3.92E+00 | 3.77E+00 |
| Tc99 | 2.1E+05 Y | 1.29E+00 | 1.92E+00 | 2.40E+00 | 3.50E+00 |
| Ho166m | 1.2E+03 Y | 1.24E+00 | 1.40E+00 | 1.39E+00 | 1.47E+00 |
| Zr93 | 1.6E+06 Y | 1.61E-01 | 2.46E-01 | 3.21E-01 | 4.87E-01 |
| Cs135 | 2.3E+06 Y | 6.18E-02 | 7.88E-02 | 1.24E-01 | 1.58E-01 |

VII. CONCLUSIONS

- The activation mode in the SERPENT code has been successfully used for activity calculations and compared with the depletion mode.
- For the replaceable side reflector (1st and 2nd ring) specific activities of the most important radionuclides right after reactor shutdown (no decay) are below ANDRA packages acceptance limits.
- At MOL (250 days) neutron flux distribution, the peak value of the fast neutron flux ($E > 0.1$ MeV) is $8.74 \cdot 10^8$ cm⁻²s⁻¹ ($\pm 15\%$). The average value of the fast neutron flux at MOL for the whole reactor pressure vessel is $3.9 \cdot 10^8$ cm⁻²s⁻¹ ($\pm 3.4\%$). The peak value gives a fluence of $1.65 \cdot 10^{18}$ cm⁻² ($\pm 15\%$) at that location. The average fast flux in the reactor pressure vessel is $7.37 \cdot 10^{17}$ cm⁻² ($\pm 3.4\%$).
- The specific activities of listed radionuclides right after reactor shutdown (no decay) are below ANDRA packages acceptance limits (even the peak values).
- The core barrel after 60 years of irradiation contains two radioactive nuclides of nickel (Ni63 and Ni59) with the specific activity exceeding ANDRA packages acceptance limits. All the other listed radionuclides have specific activities below acceptance limits.
- The permanent reflector after 60 years of irradiation contains only one radionuclide C14 with the specific activity (peak value) exceeding ANDRA packages acceptance limits. N14(n, p)C14 is the main reaction channel for C14 generation. It must be noted that a low value (10 ppm) of nitrogen as impurity in graphite was assumed in calculations. All the other listed radionuclides have specific activities below acceptance limits.

Recommendations for follow-up activities:

- Activity calculations with higher concentration of nitrogen in graphite NBG17.
- Assessment of the short-lived radionuclides (half-life period < 1 year). May be useful for management of the replaceable reflector.
- Management of the 1st and 2nd ring of the side replaceable reflector. Assessment of the lifetime of replaceable reflector (two or more cycles).
- Activity calculations for the top and bottom replaceable reflector.

References

- [1] Werner VON LENSEA et al., Gemini Plus – Deliverable D2.13: Decommissioning and Waste Management of GEMINI system, 2020.
- [2] Dominique Hittner – GEMINI+ report, Task 2.2: Data on block type HTGR core configuration.
- [3] Jaakko Leppänen. Serpent – a Continuous-energy Monte Carlo Reactor Physics Burnup Calculation Code, VTT Technical Research Centre of Finland. (June 18, 2015).
- [4] <https://www.nndc.bnl.gov/endl/b8.0/>
- [5] Release of ENDF/B-VIII.0-Based ACE Data Files, LA-UR-18-24034 Jeremy Lloyd Conlin, Wim Haeck, Denise Neudecker, D. Kent Parsons, and Morgan

C. White Nuclear Data Team, XCP-5, Los Alamos National Laboratory, May 23, 2018.

[6] Deliverable D2.7: Final GEMINI+ Safety Options Report, page 102.

[7] Evgeny V. Bepala et al, About chemical form and binding energy of ^{14}C in irradiated graphite of uranium-graphite nuclear reactors, DOI 10.3897/nucet.4.29855.

[8] IAEA 2010, TECDOC-1647 - Progress in Radioactive Graphite Waste Management.

[9] Rita Plukienė et. al., Modelling of Impurity Activation in the RBMK Reactor Graphite Using MCNPX, NUCLEAR SCIENCE and TECHNOLOGY, Vol. 2, pp.421-426 (2011).

Part E – Review and update

Part E contains the review comments to version 0.0 of this report [1], as well as the responses by the authors. This has also been reported separately in NUCLIC note N21060 [2].

[1] J.C. Kuijper, D. Muszynski, “Core design neutronics for the GEMINI+ HTGR – GEMINI+ Deliverable D2.8”, NUCLIC report R20060, version 0.0, NUCLIC, Schagen, The Netherlands, 19 January 2021.

[2] J.C. Kuijper, D. Muszynski, “Response to review comments D2.8 (Report R20060/version 0.0)”, NUCLIC note N21060, NUCLIC, Schagen, The Netherlands, 17 February 2021.

Introduction

Version 0.0 of NUCLIC report R20060 (GEMINI+ draft deliverable D2.8, 19 January 2021 [1]) was distributed for review to GEMINI+ WP2 partners and others (J. Lillington, C. Pohl, G. Brinkmann, F. Sharokhi, M.H. Kim, W. von Lensa, M. Davies, F. Southworth, M.M. Stempniewicz) 20 January 2021. By 5 February 2021, review comments have (only) been received from Dr. C.K. Jo (KAERI). This part contains the response from the authors to these comments. These have also been reported in a separate note [2]. When necessary, modifications have also been made to Parts A – D, to arrive to the current/final version of this report.

Response to review comments

| Item/page commented on | Comment | Reviewer | Response |
|------------------------|--|-----------------|---|
| Page 13 | How do you considered the axial burnup difference in a block? I think this approach can not consider the axial burnup difference. | C.K. Jo (KAERI) | Within a block the axial burn-up distribution was not taken into account. The difference in burn-up between different blocks in the same column on the other hand was taken into account in the calculations, and this was considered to be sufficient in the current stage of the project. In fact, it is rather easy to enter an axial subdivision of the block, or the compact stack, into the model, or even to consider every compact in a block separately, however, at the expense of considerable additional computing resources. This will be considered for future stages of the project. |
| Page 16 | During the fuel depletion, the temperature distribution are changed with power shape change. Then, it needs to consider the temperature changes with burnup. | C.K. Jo (KAERI) | In general this is true for HTGR core physics calculations. However, as is stated in the GEMINI+ grant agreement, it was originally not the intention to apply this in the project. In our opinion it is also not absolutely necessary in this stage of the design, which is -concerning neutronics- focussed on demonstrating feasibility. In a sense, the currently applied approximation provides a kind of "worst case" analysis for the final burn-up distribution (and related power distribution), as the "mitigating" influence (lower power and temperature peaks) of the adapting temperature distribution on the power- as well as the temperature distribution (see e.g. Part A, Fig. 5 and Section 6.2 of [3]) is not taken into account. This being said, for the future stages of the project, it is intended to include thermal hydraulic feedback in the neutronics analyses, for improved accuracy. For this, a simplified T/H feedback module for |

| | | | |
|----------------------|---|--------------------|--|
| | | | <p>the SERPENT code is being developed by NCBJ and NUCLIC. The parameters of this simplified model will be tuned to the more comprehensive models, as e.g. implemented in SPECTRA.</p> |
| Page 20/ Table 3a | <p>When two control rods are withdrawn, k_{eff} is decreased compared with All (CR, RR) rods in case. What's the reason? Please check with the Table 3b.</p> | C.K. Jo (KAERI) | <p>Further checking revealed that the k_{eff} value in Part A, Table 3a for 1 CR and 1 RR withdrawn was calculated for HZP instead of CZP. The corresponding row has been removed from Table 3A, as it does not concern the CZP state.</p> |
| Page 23 | <p>If the control rods are operated to make core criticality, the axial power shape are changed by inserting the rods from the core top. The RR in side reflector can affect the radial power shape in C3 & C5 block. In order to discuss the power and burnup distribution, it needs to consider at the state of core critical.</p> | C.K. Jo (KAERI) | <p>This is a correct observation. In the envisaged operation mode, it is the intention to fully withdraw the core rods before the reactor is made critical. Also it is intended to avoid partially inserted reflector rods as much as possible to limit the disturbance of the axial power shape (see Part A, Section VIII). Obviously, this is not entirely possible. Keeping the reactor exactly critical during the burn-up calculation, would require additional iterations (control rod insertion search), which would require considerable additional computing resources. Also see next remark.</p> |
| Page 35 | <p>It needs to find the operational control rod position to make core criticality with temperature feedback. And, it also needs to calculate the depletion of boron in control rod in time.</p> <p>Also, it have to consider the impurities in graphite which is affected the k-effective.</p> <p>It needs to check the maximum fuel temperature at the steady-state.</p> | C.K. Jo (KAERI) | <p>Indeed it would be desirable to perform the depletion calculation from BOL to EOL, keeping the k_{eff} exactly equal to 1, also taking into account thermal-hydraulic feedback (and keeping track of the maximum fuel temperature). Besides thermal hydraulic feedback calculation (see earlier remark above), this would require criticality search iterations at every burn-up step, requiring considerably more computing resources. So, in the current stage of the project we settled for showing that the exactly critical state is at least within reach of the control rod system at each point in time between BOL and EOL.</p> <p>Depletion of the boron in the control rods could indeed have been taken into account (again at the expense of additionally required computing resources). However, in the current stage of the project we assumed that control rods either contain a sufficient amount of boron, or be replaced regularly.</p> <p>Impurities in the NBG-17 (see Part D) have also been taken into account in the model, although a low value (10 ppm) of nitrogen was assumed</p> |

| | | | |
|----------|--|-----------------|---|
| | | | <i>in the graphite. Calculations are currently ongoing, assuming 100 ppm of nitrogen.</i> |
| Page 101 | <i>Ar-18 activation calculation in reactor cavity are recommended.</i> | C.K. Jo (KAERI) | <i>In the current neutronics model, only the pressure vessel and internals have been taken into account. Extending the model to include the reactor cavity could (and should) be part of future activities.</i> |

References

- [1] J.C. Kuijper, D. Muszynski, "Core design neutronics for the GEMINI+ HTGR – GEMINI+ Deliverable D2.8", NUCLIC report R20060, version 0.0, NUCLIC, Schagen, The Netherlands, 19 January 2021.
- [2] J.C. Kuijper, D. Muszynski, "Response to review comments D2.8 (Report R20060/version 0.0)", NUCLIC note N21060, NUCLIC, Petten, The Netherlands, 17 February 2021.
- [3] M.M. Stempniewicz, "Thermal-Hydraulic Model of the GEMINI+ HTR Plant – Safety Analysis, WP1.6", NRG report 24203/19.153415, NRG, Petten, The Netherlands, 31 May 2019.